Eur. Phys. J. C (2024) 84:779
https://doi.org/10.1140/epjc/s10052-024-12925-0

THE EUROPEAN PHYSICAL JOURNAL C

Regular Article - Experimental Physics

Constraints on anomalous Higgs boson couplings from its production and decay using the WW channel in proton–proton collisions at $\sqrt{s} = 13$ TeV

CMS Collaboration*

CERN, 1211 Geneva 23, Switzerland

Received: 1 March 2024 / Accepted: 16 May 2024

Abstract A study of the anomalous couplings of the Higgs boson to vector bosons, including *CP*-violation effects, has been conducted using its production and decay in the WW channel. This analysis is performed on proton–proton collision data collected with the CMS detector at the CERN LHC during 2016–2018 at a center-of-mass energy of 13 TeV, and corresponds to an integrated luminosity of 138 fb^{-1}. The different-flavor dilepton (eμ) final state is analyzed, with dedicated categories targeting gluon fusion, electroweak vector boson fusion, and associated production with a W or Z boson. Kinematic information from associated jets is combined using matrix element techniques to increase the sensitivity to anomalous effects at the production vertex. A simultaneous measurement of four Higgs boson couplings to electroweak vector bosons is performed in the framework of a standard model effective field theory. All measurements are consistent with the expectations for the standard model Higgs boson and constraints are set on the fractional contribution of the anomalous couplings to the Higgs boson production cross section.

1 Introduction

After the discovery of the Higgs boson (H) by the ATLAS and CMS Collaborations in 2012 [1–3], the CMS [4–11] and ATLAS [12–18] experiments set constraints on the spin-parity properties of the Higgs boson and its couplings with gluons and electroweak (EW) gauge bosons, denoted here as Hgg and HVV, respectively. The Higgs boson quantum numbers are consistent with the standard model (SM) expectation $J^{PC} = 0^{++}$, but the possibility of small, anomalous couplings is not yet ruled out. In beyond-the-SM (BSM) theories, interactions with the Higgs boson may occur through several anomalous couplings, which lead to new tensor structures in the interaction terms that can be both *CP*-even or *CP*-odd. The *CP*-odd anomalous couplings between the Higgs boson and BSM particles may generate *CP* violation in the interactions of the Higgs boson.

In this paper, we study the tensor structure of the Hgg and HVV couplings, and we search for several anomalous effects, including *CP* violation, using the different-flavor dilepton (eμ) final state from H → WW decays. The Higgs boson production processes include gluon fusion (ggH), EW vector boson fusion (VBF), and associated production with a W or Z boson (VH). Higgs boson production and decay processes are sensitive to certain anomalous contributions, which can be described by higher-dimensional operators in an effective field theory (EFT) [19] that can modify the kinematic distributions of the Higgs boson decay products and the particles from associated production.

Each production process of the Higgs boson is identified using its kinematic features, and events are assigned to corresponding production categories. The matrix element likelihood approach (MELA) [20–24] is employed to construct observables that are optimal for the measurement of anomalous couplings, or EFT operators, at the production vertex. These and other decay-based variables are used to explore all kinematic features of the events, giving the analysis sensitivity to simultaneous anomalous effects at the Higgs boson production and decay vertices. Fully simulated signal samples that include anomalous couplings incorporate the detector response into the analysis.

The analysis is based on the proton–proton (pp) collision data collected at the CERN LHC from 2016 to 2018, at a center-of-mass energy of 13 TeV, corresponding to an integrated luminosity of 138 fb^{-1}. This paper builds on a previous analysis conducted by the CMS Collaboration in the H → WW channel [25], which focused on measuring the Higgs boson production cross sections and coupling parameters in the so-called κ framework [26]. We follow a formalism used in previous CMS analyses of anomalous couplings in Run 1 and Run 2 [4–11,27,28], focusing on the case where the Higgs boson is produced on-shell. The coupling parame-

* e-mail: cms-publication-committee-chair@cern.ch (corresponding author)

Published online: 05 August 2024

ters are extracted using the signal strength and the fractional contributions of the couplings to the cross section. A general study of the HVV interaction is performed with four anomalous couplings analyzed individually. Through SU(2) x U(1) symmetry considerations, the anomalous HVV couplings are reduced in number to three and analyzed simultaneously. The primary HVV coupling measurements are performed in terms of cross section fractions with additional interpretations in terms of EFT couplings included. A study of the Hgg interaction is also performed in terms of a *CP*-odd anomalous coupling cross section fraction.

This paper is organized as follows. The phenomenology of anomalous couplings is discussed in Sect. 2. Section 3 gives a brief overview of the CMS apparatus. Data sets and Monte Carlo (MC) simulation samples are discussed in Sect. 4. The event reconstruction and selection are outlined in Sects. 5 and 6, respectively. Methods to estimate backgrounds are given in Sect. 7. In Sect. 8, we discuss the kinematic variables associated with Higgs boson production and decay. Sources of systematic uncertainties are presented in Sect. 9. The results are presented and discussed in Sect. 10. Finally, a summary is given in Sect. 11. Tabulated results are provided in the HEPData record for this analysis [29].

2 Phenomenology

In this analysis, we investigate anomalous coupling effects in gluon fusion or electroweak Higgs boson production, as well as in its decay to WW pairs. A detailed discussion of the theoretical considerations can be found in Refs. [22,24,28]. The interaction of the spin-zero Higgs boson with two spin-one gauge bosons V_1V_2, such as WW, ZZ, Zγ, $\gamma\gamma$, or gg, can be parametrized by the scattering amplitude

$$A(\mathrm{HV_1V_2}) \sim \left[a_1^{\mathrm{VV}} + \frac{\kappa_1^{\mathrm{VV}} q_{\mathrm{V1}}^2 + \kappa_2^{\mathrm{VV}} q_{\mathrm{V2}}^2}{\left(\Lambda_1^{\mathrm{VV}}\right)^2} \right] m_{\mathrm{V1}}^2 \epsilon_{\mathrm{V1}}^* \epsilon_{\mathrm{V2}}^* + \frac{1}{v} a_2^{\mathrm{VV}} f_{\mu\nu}^{*(1)} f^{*(2),\mu\nu} + \frac{1}{v} a_3^{\mathrm{VV}} f_{\mu\nu}^{*(1)} \tilde{f}^{*(2),\mu\nu}, \quad (1)$$

where $q_{\mathrm{V}i}$ and $\epsilon_{\mathrm{V}i}$ are the spin-one gauge boson four-momentum and polarization vectors, m_{V1} is the pole mass of the boson, $f^{(i),\mu\nu} = \epsilon_{\mathrm{V}i}^{\mu} q_{\mathrm{V}i}^{\nu} - \epsilon_{\mathrm{V}i}^{\nu} q_{\mathrm{V}i}^{\mu}$ and $\tilde{f}_{\mu\nu}^{(i)} = \frac{1}{2}\epsilon_{\mu\nu\rho\sigma} f^{(i),\rho\sigma}$ (with $\epsilon_{\mu\nu\rho\sigma}$ the Levi-Civita symbol), Λ_1^{VV} is the scale of BSM physics, and v is the Higgs field vacuum expectation value.

The only leading tree-level contributions in the scattering amplitude are $a_1^{\mathrm{ZZ}} \neq 0$ and $a_1^{\mathrm{WW}} \neq 0$; other a_1 coupling parameters (Zγ, $\gamma\gamma$, gg) do not contribute because the pole mass vanishes. Additional ZZ and WW couplings are considered anomalous contributions. Anomalous terms arising in the SM via loop effects are typically small and are not yet accessible experimentally. The BSM contributions, however, could yield larger coupling parameters. Among the anomalous contributions, considerations of symmetry and gauge invariance require $\kappa_1^{\mathrm{ZZ}} = \kappa_2^{\mathrm{ZZ}}$, $\kappa_1^{\gamma\gamma} = \kappa_2^{\gamma\gamma} = 0$, $\kappa_1^{\mathrm{gg}} = \kappa_2^{\mathrm{gg}} = 0$, and $\kappa_1^{\mathrm{Z}\gamma} = 0$ [24]. The presence of *CP*-odd a_3^{VV} couplings together with any of the other couplings (all of them *CP*-even), will result in *CP* violation. We reduce the number of independent parameters by assuming that $a_2^{\gamma\gamma}$, $a_3^{\gamma\gamma}$, $a_2^{\mathrm{Z}\gamma}$ and $a_3^{\mathrm{Z}\gamma}$ are constrained in direct decays of $\mathrm{H} \to \gamma\gamma$ and Zγ, therefore fixing them to be zero. The a_2^{gg} term results from loop effects in the SM.

The relationship between the ZZ and WW couplings is mostly relevant for VBF production. There are no kinematic differences between the ZZ and WW fusion processes; therefore, it is not possible to disentangle the couplings. One possibility is to set the ZZ and WW couplings to be equal, $a_i = a_i^{\mathrm{ZZ}} = a_i^{\mathrm{WW}}$, leaving four HVV anomalous couplings to be measured: a_2, a_3, $\kappa_1/(\Lambda_1)^2$, and $\kappa_2^{\mathrm{Z}\gamma}/(\Lambda_1^{\mathrm{Z}\gamma})^2$. The $a_1^{\mathrm{ZZ}} = a_1^{\mathrm{WW}}$ relationship also appears under custodial symmetry. This approach provides a general test of the Higgs boson Lagrangian tensor structure and a search for *CP* violation in HVV interactions. In an alternative approach, the SU(2) $\times$ U(1) symmetry reduces the number of independent HVV anomalous couplings to three (a_2, a_3, and $\kappa_1/(\Lambda_1)^2$) through the introduction of the following coupling parameter relationships [19] :

$$a_1^{\mathrm{WW}} = a_1^{\mathrm{ZZ}}, \quad (2)$$

$$a_2^{\mathrm{WW}} = c_{\mathrm{w}}^2 a_2^{\mathrm{ZZ}}, \quad (3)$$

$$a_3^{\mathrm{WW}} = c_{\mathrm{w}}^2 a_3^{\mathrm{ZZ}}, \quad (4)$$

$$\frac{\kappa_1^{\mathrm{WW}}}{(\Lambda_1^{\mathrm{WW}})^2} = \frac{1}{c_{\mathrm{w}}^2 - s_{\mathrm{w}}^2} \left(\frac{\kappa_1^{\mathrm{ZZ}}}{(\Lambda_1^{\mathrm{ZZ}})^2} - 2 s_{\mathrm{w}}^2 \frac{a_2^{\mathrm{ZZ}}}{m_{\mathrm{Z}}^2} \right), \quad (5)$$

$$\frac{\kappa_2^{\mathrm{Z}\gamma}}{(\Lambda_1^{\mathrm{Z}\gamma})^2} = \frac{2 s_{\mathrm{w}} c_{\mathrm{w}}}{c_{\mathrm{w}}^2 - s_{\mathrm{w}}^2} \left(\frac{\kappa_1^{\mathrm{ZZ}}}{(\Lambda_1^{\mathrm{ZZ}})^2} - \frac{a_2^{\mathrm{ZZ}}}{m_{\mathrm{Z}}^2} \right), \quad (6)$$

where c_{w} and s_{w} are the cosine and sine of the weak mixing angle, respectively, and m_{Z} is the Z boson mass. With this approach, there is a linear relationship between the scattering amplitude couplings and the SM EFT (SMEFT) couplings in the Higgs basis [19]:

$$\delta c_{\mathrm{z}} = \frac{1}{2} a_1^{\mathrm{ZZ}} - 1, \quad (7)$$

$$c_{\mathrm{zz}} = -\frac{2 s_{\mathrm{w}}^2 c_{\mathrm{w}}^2}{e^2} a_2^{\mathrm{ZZ}}, \quad (8)$$

$$\tilde{c}_{\mathrm{zz}} = -\frac{2 s_{\mathrm{w}}^2 c_{\mathrm{w}}^2}{e^2} a_3^{\mathrm{ZZ}}, \quad (9)$$

$$c_{z\Box} = \frac{m_Z^2 s_w^2}{e^2} \frac{\kappa_1^{ZZ}}{(\Lambda_1^{ZZ})^2}, \tag{10}$$

where e is the electron charge. The amplitude couplings may also be related to the SMEFT Warsaw basis [19,30] couplings through the following translation [28,31] :

$$\delta a_1^{ZZ} = \frac{v^2}{\Lambda^2}\left(2c_{H\Box} + \frac{6e^2}{s_w^2}c_{HWB} + \left(\frac{3c_w^2}{2s_w^2} - \frac{1}{2}\right)c_{HD}\right), \tag{11}$$

$$\kappa_1^{ZZ} = \frac{v^2}{\Lambda^2}\left(-\frac{2e^2}{s_w^2}c_{HWB} + \left(1 - \frac{1}{2s_w^2}\right)c_{HD}\right), \tag{12}$$

$$a_2^{ZZ} = -2\frac{v^2}{\Lambda^2}\left(s_w^2 c_{HB} + c_w^2 c_{HW} + s_w c_w c_{HWB}\right), \tag{13}$$

$$a_3^{ZZ} = -2\frac{v^2}{\Lambda^2}\left(s_w^2 c_{H\tilde{B}} + c_w^2 c_{H\tilde{W}} + s_w c_w c_{H\tilde{W}B}\right), \tag{14}$$

where Λ is the UV cutoff of the theory (set to 1 TeV), and δa_1^{ZZ} is a correction to the SM value of a_1^{ZZ}. Further discussion on the EFT operators corresponding to the couplings considered here may be found in Chapter 2.2 of Ref. [19]. The assumed constraints on $a_2^{\gamma\gamma}$, $a_3^{\gamma\gamma}$, $a_2^{Z\gamma}$ and $a_3^{Z\gamma}$ imply that only one of the three coupling parameters c_{HW}, c_{HWB}, and c_{HB} is independent; the same is also true for their *CP*-odd counterparts $c_{H\tilde{W}}$, $c_{H\tilde{W}B}$, and $c_{H\tilde{B}}$. Therefore, we have four independent HVV couplings in both the Higgs and Warsaw basis. All the EFT couplings are expected to be zero in the SM.

We thus adopt two approaches to the HVV coupling study. In Approach 1, we use the $a_i^{ZZ} = a_i^{WW}$ relationship and individually analyze each of the four anomalous couplings. In Approach 2, we enforce the SU(2) x U(1) relationships from Eqs. (2–6) and analyze the three independent anomalous couplings both individually and simultaneously. Approach 1 may be considered to follow the relationships from Eqs. (2–5) in the limiting case $c_w = 1$.

It is convenient to measure the fractional contribution of the anomalous couplings to the Higgs boson cross section rather than the anomalous couplings themselves. For the anomalous HVV couplings, the effective fractional cross sections f_{ai} are defined as

$$f_{ai} = \frac{|a_i|^2 \sigma_i}{\sum_j |a_j|^2 \sigma_j} \text{sign}\left(\frac{a_i}{a_1}\right), \tag{15}$$

where $\sum_j$ sums over all the coupling parameters considered, including a_1, and σ_i is the cross section for the process corresponding to $a_i = 1$ and $a_{j\neq i} = 0$. Many systematic uncertainties cancel out in the ratio, and the physical range is conveniently bounded between -1 and $+1$. Our primary measurements are performed in terms of cross section fractions, with additional interpretations in terms of the SMEFT Higgs and Warsaw basis couplings also included. For consistency with previous CMS measurements, the σ_i coefficients used to define the fractional cross sections correspond to the $gg \to H \to VV \to 2e2\mu$ process [28]. The numerical values are given in Table 1 as calculated using the JHUGEN simulation [20–23]. Two sets of values are shown corresponding to the different coupling relationships adopted in Approach 1 and 2.

Table 1 The cross sections (σ_i) of the anomalous contributions (a_i) relative to the SM value (σ_1) used to define the fractional cross sections f_{ai} for the Approach 1 and 2 coupling relationships. For the κ_1 and $\kappa_2^{Z\gamma}$ couplings, the numerical values $\Lambda_1 = \Lambda_1^{Z\gamma} = 100$ GeV are chosen to keep all coefficients of similar order of magnitude

f_{ai}	a_i	Approach 1 σ_i/σ_1	Approach 2 σ_i/σ_1
f_{a2}	a_2	0.361	6.376
f_{a3}	a_3	0.153	0.153
$f_{\Lambda 1}$	κ_1	0.682	5.241
$f_{\Lambda 1}^{Z\gamma}$	$\kappa_2^{Z\gamma}$	1.746	–

It has been shown that the angular correlations of the associated jets in the ggH + 2 jets process are sensitive to anomalous Hgg coupling effects at the production vertex [32]. The quark-quark initiated process, $qq \to qqH$, corresponds to the gluon scattering topology sensitive to anomalous effects. For the anomalous Hgg coupling, the effective fractional cross section can be defined as

$$f_{a3}^{ggH} = \frac{\left|a_3^{gg}\right|^2 \sigma_3^{gg}}{\left|a_2^{gg}\right|^2 \sigma_2^{gg} + \left|a_3^{gg}\right|^2 \sigma_3^{gg}} \text{sign}\left(\frac{a_3^{gg}}{a_2^{gg}}\right). \tag{16}$$

The σ_3^{gg} and σ_2^{gg} cross sections correspond to $a_3^{gg} = 1, a_2^{gg} = 0$ and $a_2^{gg} = 1, a_3^{gg} = 0$, respectively, and are equal. With this analysis it is not possible to distinguish the top quark, bottom quark, and heavy BSM particle contributions in the gluon fusion loop. As such, the Hgg coupling is treated as an effective coupling with heavy degrees of freedom integrated out.

3 The CMS detector

The CMS apparatus [33] is a multipurpose, nearly hermetic detector, designed to identify electrons, muons, photons, and (charged and neutral) hadrons [34–37]. A global reconstruction "particle-flow" (PF) algorithm [38] combines the information provided by the all-silicon inner tracker and by the crystal electromagnetic and brass-scintillator hadron calorimeters, operating inside a 3.8 T superconducting solenoid, with data from gas-ionization muon detectors interleaved with the solenoid return yoke, to build τ lep-

tons, jets, missing transverse momentum, and other physics objects [39–41].

Events of interest are selected using a two-tiered trigger system [42,43]. The first level (L1), composed of custom hardware processors, uses information from the calorimeters and muon detectors to select events at a rate of around 100 kHz within a fixed latency of about 4 μs [42]. The second level, known as the high-level trigger (HLT), consists of a farm of processors running a version of the full event reconstruction software optimized for fast processing, and reduces the event rate to around 1 kHz before data storage [43]. A more detailed description of the CMS detector, together with a definition of the coordinate system and kinematic variables, can be found in Ref. [33].

4 Data sets and simulation

The data sets included in this analysis were recorded with the CMS detector in 2016, 2017, and 2018, and correspond to integrated luminosities of 36.3, 41.5, and 59.7 fb^{-1}, respectively [44–46]. The collision events must fulfill HLT selection criteria that require the presence of one or two leptons satisfying isolation and identification requirements. For the 2016 data set, the single-electron trigger has a transverse momentum (p_{T}) threshold of 25 GeV for electrons with pseudorapidity $|\eta| < 2.1$ and 27 GeV for $2.1 < |\eta| < 2.5$, whereas the single-muon trigger has a p_{T} threshold of 24 GeV for $|\eta| < 2.4$. For the 2017 (2018) data set, the p_{T} threshold is 35 (32) GeV for the single-electron trigger (covering $|\eta| < 2.5$) and 27 (24) GeV for the single-muon trigger ($|\eta| < 2.4$). The dilepton eμ trigger has p_{T} thresholds of 23 and 12 GeV for the leading and subleading leptons, respectively, with the same coverage in pseudorapidity for electrons and muons as above. During the first part of data taking in 2016, a lower p_{T} threshold of 8 GeV for the subleading muon was used.

Monte Carlo event generators are used to model the signal and background processes. For each process, three independent sets of simulated events, corresponding to the three years of data taking, are used. This approach includes year-dependent effects in the CMS detector, data taking, and event reconstruction. All simulated events corresponding to a given data set share the same set of parton distribution functions (PDFs), underlying event (UE) tune, and parton shower (PS) configuration. The PDF sets used are NNPDF 3.0 [47,48] for 2016 and NNPDF 3.1 [49] for 2017 and 2018. The CUETP8M1 [50] tune is used to describe the UE in 2016 simulations, whereas the CP5 [51] tune is adopted in 2017 and 2018 simulated events. The MC samples are interfaced with PYTHIA 8.226 [52] in 2016, and 8.230 in 2017 and 2018, for the modeling of UE, PS, and hadronization. Standard Model Higgs boson production through ggH, VBF, and VH is simulated at next-to-leading order (NLO) accuracy in quantum chromodynamics (QCD), including finite quark mass effects, using POWHEG v2 [53–59]. The MINLO HVJ [58] extension of POWHEG v2 is used for the simulation of WH and quark-induced ZH production, providing NLO accuracy for the VH + 0- and 1-jet processes. For ggH production, the simulated events are weighted to match the NNLOPS [60,61] prediction in the hadronic jet multiplicity (N_{jet}) and Higgs boson p_{T} distributions. The weighting is based on p_{T} and N_{jet} as computed in the simplified template cross section scheme 1.0 [62]. The MINLO HJJ [63] generator, which provides NLO accuracy for $N_{\mathrm{jet}} \geq 2$, is also used for ggH production. The associated production processes with top quarks ($\mathrm{t\bar{t}H}$) and bottom quarks ($\mathrm{b\bar{b}H}$) are simulated with POWHEG v2 and MADGRAPH5_aMC@NLO v2.2.2 [64], respectively, and have a negligible contribution in the analysis phase space. All SM Higgs boson samples are normalized to the cross sections recommended in Ref. [19]. The Higgs boson mass in the event generation is assumed to be 125 GeV, while a value of 125.38 GeV [65] is used for the calculation of cross sections and branching fractions. The decay to a pair of W bosons and subsequently to leptons or hadrons is performed using the JHUGEN v5.2.5 generator in 2016, and v7.1.4 in 2017 and 2018, for ggH, VBF, and quark-induced ZH samples. The Higgs boson and W boson decays are performed using PYTHIA 8.212 for the other signal simulations.

The ggH, VBF, and VH Higgs boson events with HVV anomalous couplings are generated with JHUGEN at LO accuracy. With respect to the $\kappa_2^{Z\gamma}/(\Lambda_1^{Z\gamma})^2$ coupling parameter discussed in Sect. 2, the sign convention of the photon field is determined by the sign in front of the gauge fields in the covariant derivative. In this analysis, we define the covariant derivative $D_\mu = \partial_\mu - \mathrm{i}e\sigma^i W_\mu^i/(2s_w) + \mathrm{i}eB_\mu/(2c_w)$ following the convention in JHUGEN [31]. The JHUGEN and POWHEG SM Higgs boson simulations were compared after parton showering and no significant differences in the distributions of kinematic observables were found. We adopt the JHUGEN simulation to describe the kinematic features in all production modes with HVV anomalous couplings. The expected yields are scaled to match the SM theoretical predictions [19] for inclusive cross sections and the POWHEG SM prediction of relative event yields in the event categorization based on associated particles. Simulation of the ggH + 2 jets process with Hgg anomalous couplings is done using MINLO X0JJ [66] at NLO in QCD. A large number of signal samples with various anomalous couplings were generated. The MELA package [20–24] contains a library of matrix elements from JHUGEN for different Higgs boson signal hypotheses. Matrix elements from different coupling signal hypotheses, but with the same production mechanism, are used to reweight the generated signal events. This procedure is used in the construction of the predictions for the different coupling components and their interference, allow-

ing us to cover all points in the signal model phase space with sufficient statistical precision.

Background events are produced using several simulations. The quark-initiated nonresonant WW process is simulated with POWHEG v2 [67] at NLO accuracy for inclusive production. A reweighting is performed to match the diboson p_T spectrum computed at NNLO+NNLL QCD accuracy [68,69]. The MCFM v7.0 [70–72] generator is used to simulate gluon-induced WW production at LO accuracy, with the normalization chosen to match the NLO cross section [73]. Nonresonant EW production of WW pairs with two additional jets is simulated at LO accuracy with MADGRAPH5_aMC@NLO v2.4.2 using the MLM matching and merging scheme [74]. Top quark pair production ($t\bar{t}$) and single top quark processes, including tW, s- and t-channel contributions, are simulated with POWHEG v2 [75–77]. A reweighting of the top quark and antiquark p_T spectrum at parton level is performed for the $t\bar{t}$ simulation in order to match the NNLO and next-to-next-to-leading logarithm (NNLL) QCD predictions, including also the NLO EW contribution [78].

The Drell–Yan (DY) production of a charged-lepton pair is simulated with MADGRAPH5_aMC@NLO v2.4.2 at NLO accuracy with up to two additional partons, using the FxFx matching and merging scheme [79]. Production of a W boson associated with an initial state radiation photon ($W\gamma$) is simulated with MADGRAPH5_aMC@NLO v2.4.2 at NLO accuracy with up to 1 additional parton, using the FxFx jet merging. Diboson processes containing at least one Z boson or a virtual photon (γ^*) with a mass as low as 100 MeV are generated with POWHEG v2 [67] at NLO accuracy. Production of a W boson in association with a γ^* ($W\gamma^*$) for masses below 100 MeV is simulated by PYTHIA 8.212 in the parton showering of $W\gamma$ events. Triboson processes with inclusive decays are also simulated at NLO accuracy with MADGRAPH5_aMC@NLO v2.4.2.

For all processes, the detector response is simulated using a detailed description of the CMS detector, based on the GEANT4 toolkit [80]. The distribution of additional pp interactions within the same or nearby bunch crossings (pileup) in the simulation is reweighted to match that observed in data. The efficiency of the trigger system is evaluated in data on a per lepton basis using dilepton events consistent with the Z boson decay. The overall efficiencies of the trigger selections used in the analysis are obtained as the average of the per-lepton efficiencies weighted by their probability. The resulting efficiencies are applied directly on simulated events.

5 Event reconstruction

The identification and measurement of the properties of individual particles (PF candidates) in an event is achieved in the PF algorithm by combining information from various subdetectors. Electrons are identified and their momenta are measured in the pseudorapidity interval $|\eta| < 2.5$ by combining tracks in the silicon tracker with spatially compatible energy deposits in the electromagnetic calorimeter. Muons are identified and their momenta are measured in the pseudorapidity range $|\eta| < 2.4$ by matching tracks in the muon system and the silicon tracker. For better rejection of nonprompt leptons, increasing the sensitivity of the analysis, leptons are required to be isolated and well reconstructed using a set of criteria based on the quality of the track reconstruction, shape of calorimetric deposits, and energy flux in the vicinity of the particle's trajectory [34,35]. In addition, a selection based on a dedicated multivariate analysis (MVA) tagger developed for the CMS $t\bar{t}H$ analysis [81] is added in all channels for muon candidates.

Multiple pp interaction vertices are identified from tracking information by use of the adaptive vertex fitting algorithm [82]. The primary pp interaction vertex is taken to be the vertex corresponding to the hardest scattering in the event, evaluated using tracking information alone, as described in Section 9.4.1 of Ref. [83]. Leptons are required to be associated to the primary vertex using transverse and longitudinal impact parameter criteria [34,35].

Hadronic jets are clustered from PF candidates using the infrared- and collinear-safe anti-k_T algorithm with distance parameters of 0.4 (AK4) and 0.8 (AK8). The jet momentum is determined as the vectorial sum of all particle momenta in the jet. The AK8 jets considered are required to be reconstructed within the silicon tracker acceptance ($|\eta| < 2.4$), whereas AK4 jets are reconstructed in the range $|\eta| < 4.7$. For AK4 jets, contamination from pileup is suppressed using charged-hadron subtraction which removes charged PF candidates originating from vertices other than the primary interaction vertex. The residual contribution from neutral particles originating from pileup vertices is removed by means of an event-by-event jet-area-based correction to the jet four-momentum [84]. For AK8 jets, the pileup-per-particle identification algorithm (PUPPI) [85] is used to mitigate the effect of pileup at the reconstructed-particle level, making use of local shape information, event pileup properties, and tracking information. Additional selection criteria are applied to remove jets potentially dominated by instrumental effects or reconstruction failures [84].

The AK8 jets are used to reconstruct hadronic V boson decays in a single merged jet when the decay products are highly collimated. This approach targets boosted W or Z bosons originating from the VH production mode. Such Lorentz-boosted V decays are identified using the ratio of the 2- to 1-subjettiness [86], τ_2/τ_1, and the groomed jet mass m_J. The groomed mass is calculated after applying a modified mass drop algorithm [87,88], known as the soft-drop algorithm [89], with parameters $\beta = 0$, $z_{cut} = 0.1$, and

$R_0 = 0.8$. The algorithm also identifies two hard subjets within the AK8 jet.

We refer to the identification of jets likely originating from bottom quarks as b tagging [90,91]. For each AK4 jet in the event, a score is calculated through a multivariate combination of different jet properties, making use of boosted decision trees and deep neural networks. A jet is considered b-tagged if its associated score exceeds a threshold, tuned to achieve a certain tagging efficiency as measured in $\mathrm{t\bar{t}}$ events. The chosen working point corresponds to about 90% efficiency for bottom quark jets and to a mistagging rate of about 10% for light-flavor or gluon jets and of about 50% for charm quark jets.

The missing transverse momentum vector $\vec{p}_{\mathrm{T}}^{\,\mathrm{miss}}$ is computed as the negative vector sum of the transverse momenta of all the PF candidates in an event, and its magnitude is denoted as $p_{\mathrm{T}}^{\mathrm{miss}}$ [41]. The PUPPI algorithm is applied to reduce the pileup dependence of the $\vec{p}_{\mathrm{T}}^{\,\mathrm{miss}}$ observable by computing the $\vec{p}_{\mathrm{T}}^{\,\mathrm{miss}}$ from the PF candidates weighted by their probability to originate from the primary interaction vertex [41].

6 Event selection

The analysis is performed using $\mathrm{H} \to \mathrm{WW}$ candidate events in the eμ final state. For an event to be selected, the transverse momenta of the leading lepton $p_{\mathrm{T}}^{\ell 1}$ and the subleading lepton $p_{\mathrm{T}}^{\ell 2}$ must be greater than 25 and 13 GeV, respectively. The $p_{\mathrm{T}}^{\ell 2}$ threshold in the case of a muon is lowered to 10 GeV for the 2016 data set because of the lower threshold in the corresponding HLT algorithm. Events containing additional leptons with $p_{\mathrm{T}} > 10$ GeV are discarded. The dilepton system is required to have an invariant mass $m_{\ell\ell}$ greater than 12 GeV and transverse momentum $p_{\mathrm{T}}^{\ell\ell}$ above 30 GeV. A requirement on the missing transverse momentum of $p_{\mathrm{T}}^{\mathrm{miss}} > 20$ GeV is implemented. We define transverse mass discriminating variables $m_{\mathrm{T}}^{\mathrm{H}}$ and $m_{\mathrm{T}}^{\ell 2}$ as

$$m_{\mathrm{T}}^{\mathrm{H}} = \sqrt{2 p_{\mathrm{T}}^{\ell\ell} p_{\mathrm{T}}^{\mathrm{miss}} [1 - \cos \Delta\Phi(\vec{p}_{\mathrm{T}}^{\,\ell\ell}, \vec{p}_{\mathrm{T}}^{\,\mathrm{miss}})]}, \quad (17)$$

$$m_{\mathrm{T}}^{\ell 2} = \sqrt{2 p_{\mathrm{T}}^{\ell 2} p_{\mathrm{T}}^{\mathrm{miss}} [1 - \cos \Delta\Phi(\vec{p}_{\mathrm{T}}^{\,\ell 2}, \vec{p}_{\mathrm{T}}^{\,\mathrm{miss}})]}, \quad (18)$$

and select events with $m_{\mathrm{T}}^{\mathrm{H}} > 60$ GeV and $m_{\mathrm{T}}^{\ell 2} > 30$ GeV. The $m_{\mathrm{T}}^{\mathrm{H}}$ requirement suppresses the $\mathrm{DY} \to \tau\tau$ background process and avoids overlap with the $\mathrm{H} \to \tau\tau$ analysis [11]. To ensure orthogonality with a future off-shell $\mathrm{H} \to \mathrm{WW}$ analysis we require $m_{\mathrm{T}}^{\mathrm{H}} < 125$ GeV. In addition, the region $76.2 < m_{\ell\ell} < 106.2$ GeV is excluded to avoid overlap with the off-shell $\mathrm{H} \to \mathrm{ZZ} \to 2\ell 2\nu$ analysis [10]. These requirements will simplify a future combination of Higgs boson decay final states. Finally, events with any b-tagged jets with $p_{\mathrm{T}} > 20$ GeV are vetoed. These base selection criteria are summarized in Table 2.

Table 2 Summary of the base selection criteria

Variable	Selection
Number of leptons	2 (eμ of opposite charge)
$p_{\mathrm{T}}^{\ell 1}$	> 25 GeV
$p_{\mathrm{T}}^{\ell 2}$	> 13 GeV (10 GeV for 2016 data)
$m_{\ell\ell}$	12–76.2 GeV or > 106.2 GeV
$p_{\mathrm{T}}^{\ell\ell}$	> 30 GeV
$p_{\mathrm{T}}^{\mathrm{miss}}$	> 20 GeV
$m_{\mathrm{T}}^{\ell 2}$	> 30 GeV
$m_{\mathrm{T}}^{\mathrm{H}}$	60–125 GeV
N_{jet}(bjets)	0

Table 3 Summary of the ggH, VBF, and VH production channels used for the HVV coupling study

Variable	ggH	VBF	Resolved VH	Boosted VH
N_{jet}(V jets)	0	0	0	> 0
N_{jet}(AK4 jets)	0 and 1	2	2	–
m_{jj}	–	> 120 GeV	60–120 GeV	–

For the HVV coupling analysis, exclusive selection criteria, which are based on the associated jet activity in the event, are applied that target the ggH, VBF, and VH production processes. The AK4 (AK8) jets considered are required to have $p_{\mathrm{T}} > 30$ (200) GeV. In the ggH channel, zero or one AK4 jet is required in the event. For the VBF and Resolved VH channels, we require two AK4 jets with dijet masses of $m_{\mathrm{jj}} > 120$ GeV and $60 < m_{\mathrm{jj}} < 120$ GeV, respectively. The Boosted VH channel requires the presence of a V-tagged AK8 jet (V jet); such jets have a groomed mass in the region $65 < m_{\mathrm{J}} < 105$ GeV and satisfy the requirement $\tau_2/\tau_1 < 0.4$. In the other channels, a V jet veto is implemented to ensure orthogonality. These production channels for the HVV coupling study are summarized in Table 3.

As the production vertex of the ggH + 2 jets process is sensitive to anomalous Hgg coupling effects, we use a 2-jet ggH channel that follows the VBF selection described above for the Hgg coupling analysis. The HWW decay vertex is not sensitive to anomalous Hgg effects, and so decay-based variables are not studied in this channel. This permits a relatively tight selection of $m_{\ell\ell} < 55$ GeV which is beneficial for background suppression. The 0- and 1-jet ggH channels are also included to constrain the ggH signal strength. All channels included for the Hgg coupling study are summarized in Table 4.

Control regions (CRs) are defined using the base selection criteria together with a set of alternative requirements sum-

Table 4 Summary of ggH channel selections used for the Hgg coupling study

Variable	ggH	2-jet ggH
N_{jet} (AK4 jets)	0 and 1	2
m_{jj}	–	> 120 GeV
$m_{\ell\ell}$	–	< 55 GeV

Table 5 Summary of the ττ, top quark, and WW control region requirements

Variable	ττ	Top quark	WW
$m_{\ell\ell}$	40–80 GeV	> 50 GeV	> 106.2 GeV
m_{T}^{H}	< 60 GeV	–	60–125 GeV
$m_{\text{T}}^{\ell 2}$	–	> 30 GeV	> 30 GeV
N_{jet} (b jets)	0	> 0	0

marized in Table 5. They are used to validate the background description and to estimate the number of background events in the signal region (SR). A dedicated ττ CR targets events from the DY process $\text{Z} \rightarrow \tau\tau$ with τ leptons decaying leptonically to produce the eμ final state. Also a top quark CR is defined to enhance events with one or more top quarks decaying to a W boson and bottom quark. Splitting events according to the number of associated jets, separate ττ and top quark CRs are defined for the 0-, 1- and 2-jet SRs. An additional CR with an enhanced contribution from the nonresonant WW background is used in the 2-jet SR. All CRs are used in the final data fit to constrain the DY, top quark, and WW background normalizations.

Additional ττ, top quark, and WWCRs are defined requiring a V jet. These CRs are used to validate the background description in the Boosted VH channel. However, they generally do not have a sufficient number of events to significantly constrain the background normalizations in the final fit to the data. As such, we rely on the 2-jet CRs to determine the normalizations to be used in the Boosted VH channel. Agreement between data and the background prediction in the V jet CRs is observed when using normalizations determined in the 2-jet CRs.

7 Background estimation

The nonprompt-lepton backgrounds originating from leptonic decays of heavy quarks, hadrons misidentified as leptons, and electrons from photon conversions are suppressed by identification and isolation requirements imposed on electrons and muons. In this analysis, the nonprompt-lepton background primarily originates from W+jets events and is estimated from data, as described in detail in Ref. [92]. The procedure involves measuring the rate at which a nonprompt lepton passing a loose selection further passes a tight selection (misidentification rate) and the corresponding rate for a prompt lepton to pass this selection (prompt rate). The misidentification rate is measured in a data sample enriched in multijet events, whereas the prompt rate is measured using a tag-and-probe method [93] in a data sample enriched in DY events. The nonprompt-lepton background estimation is validated with data in a CR enriched with W+jets events, in which a pair of same-sign leptons is required.

The backgrounds from top quark processes and nonresonant WW production are estimated using a combination of MC simulations and the dedicated CRs described in the previous section. The normalisations of these backgrounds are left as free parameters in the fit, keeping different parameters for each jet multiplicity region. The top quark background normalization is measured from the observed data in the top quark enriched CRs. A separate normalization parameter is included for the quark-induced and gluon-induced WW backgrounds. For the 2-jet regions, the WW enriched CR is used to constrain the WW background normalisation parameters. In the 0- and 1-jet channels, these parameters are constrained directly in the signal regions, which span the high $m_{\ell\ell}$ phase space enriched in WW events.

The $\text{DY} \rightarrow \tau\tau$ background process is estimated with a data-embedding technique [94]. As for the top quark and WW backgrounds, the DY normalization is left unconstrained in the data fit. The $\text{DY} \rightarrow \tau\tau$ enriched CR described in Sect. 6 is used to constrain the free normalization parameters in the 0-, 1-, 2-jet regions. The data-embedded samples cover the events that pass the eμ triggers, which represent the vast majority of the selected events. The remaining $\text{DY} \rightarrow \tau\tau$ events, which enter the analysis through the single-lepton triggers (≈5% of the total), are estimated using MC simulation.

The WZ and $\text{W}\gamma^*$ background contributions are simulated as described in Sect. 4, and a data-to-simulation scale factor is derived in a three-lepton CR, as described in Ref. [92]. The contribution of the $\text{W}\gamma$ process may also be a background because of photon conversions in the detector material. This process is estimated using MC simulation and validated using data in a CR requiring events with a leading μ and a trailing e with same sign and a separation in $\Delta R = \sqrt{\Delta\phi^2 + \Delta\eta^2}$ (where ϕ is the azimuthal angle in radians) smaller than 0.5. Triple vector boson production is a minor background in all channels and is estimated using MC simulation.

8 Observables and kinematic discriminants

In this paper, we search for anomalous HVV and Hgg coupling effects by studying:

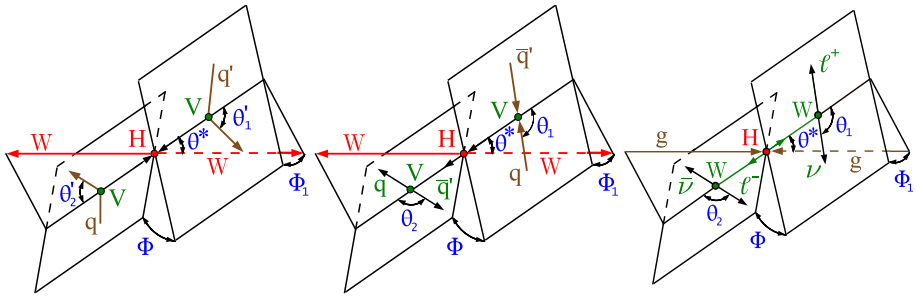

Fig. 1 Topologies of the Higgs boson production and decay for vector boson fusion $qq' \to qq'H$ (left), $q\bar{q}' \to VH$ (center), and gluon fusion with decay $gg \to H \to 2\ell 2\nu$ (right). For the electroweak production topologies, the intermediate vector bosons and their decays are shown in green and the $H \to WW$ decay is marked in red. For the $gg \to H \to 2\ell 2\nu$ topology, the W boson leptonic decays are shown in green. In all cases, the incoming particles are depicted in brown and the angles characterizing kinematic distributions are marked in blue. Five angles fully characterize the orientation of the production and decay chain and are defined in the suitable rest frames

1. the two quark jets from VBF and VH production (HVV coupling);
2. the $H \to WW$ decay products (HVV coupling); and
3. the two quark jets from ggH + 2 jets production (Hgg coupling).

The VBF, VH, and ggH production and decay topologies relevant for the HVV coupling are illustrated in Fig. 1.

When combined with the momentum transfer of the vector bosons, the five angles illustrated for VBF/VH production provide complete kinematic information for production and decay of the Higgs boson. The illustration for Higgs boson production via ggH in association with two jets is identical to the VBF diagram, except for replacing the intermediate vector bosons by gluons. Full production kinematic information is extracted for VBF, VH, and ggH + 2 jets candidate events using discriminants built from the matrix element calculations of the MELA package. The MELA approach is designed to reduce the number of observables to a minimum, while retaining all essential information. To form the production-based MELA kinematic discriminants, we use jets to reconstruct the four-momentum of the associated production particles. The presence of two neutrinos in the final state means it is not possible to reconstruct the four-momentum of all the Higgs boson decay products. Therefore, decay-based kinematic discriminants built from matrix elements are not used in this analysis. Instead, we rely on kinematic variables related to the measured final state of the Higgs boson decay. The strategies used for each of the topologies listed above are now discussed in more detail.

8.1 Kinematic features of two quark jets in VBF and VH channels

Kinematic distributions of associated particles in VBF and VH production are sensitive to the anomalous HVV couplings of the Higgs boson.

As illustrated in Fig. 1, a set of seven observables can be defined for the VBF and VH production topologies: $\Omega = \{\theta_1^{(\prime)}, \theta_2^{(\prime)}, \theta^*, \Phi, \Phi_1, q_1^2, q_2^2\}$, with q_1^2 and q_2^2 the squared four-momenta of the vector bosons [22]. Three types of discriminants are defined using the full kinematic description characterized by Ω. The first type of discriminant is designed to separate signal and background Higgs boson production processes:

$$\mathcal{D}_{\text{sig}} = \frac{\mathcal{P}_{\text{sig}}(\Omega)}{\mathcal{P}_{\text{sig}}(\Omega) + \mathcal{P}_{\text{bkg}}(\Omega)}, \tag{19}$$

where the probability density $\mathcal{P}$ for a specific process is calculated from the matrix elements provided by the MELA package. The second type of discriminant separates the anomalous coupling BSM process from that of the SM:

$$\mathcal{D}_{\text{BSM}} = \frac{\mathcal{P}_{\text{BSM}}(\Omega)}{\mathcal{P}_{\text{BSM}}(\Omega) + \mathcal{P}_{\text{SM}}(\Omega)}. \tag{20}$$

Throughout this document the generic BSM label is generally replaced by the specific anomalous coupling state targeted. For the a_3 *CP*-odd and a_2 *CP*-even coupling parameters, we use, respectively, $\mathcal{D}_{0-}$ and $\mathcal{D}_{0+}$, whereas for the Λ_1 coupling parameters we use $\mathcal{D}_{\Lambda_1}$ and $\mathcal{D}_{\Lambda_1}^{Z\gamma}$. The third type of discriminant isolates the interference contribution:

$$\mathcal{D}_{\text{int}} = \frac{\mathcal{P}^{\text{int}}_{\text{SM-BSM}}(\Omega)}{\mathcal{P}_{\text{SM}}(\Omega) + \mathcal{P}_{\text{BSM}}(\Omega)}, \tag{21}$$

where $\mathcal{P}^{\text{int}}_{\text{SM-BSM}}$ is the interference part of the probability distribution for a process with a mixture of the SM and BSM contributions. The *CP* label is generally used for the a_3 coupling parameter, as the BSM signal in this case is a pseudoscalar and the interference discriminant is a *CP*-sensitive observable. The $\mathcal{P}$ values are normalized to give the same integrated cross sections in the relevant phase space of each process. Such normalization leads to a balanced distribution of events in the range between 0 and 1 for $\mathcal{D}_{\text{sig}}$ and $\mathcal{D}_{\text{BSM}}$, and between -1 and $+1$ for $\mathcal{D}_{\text{int}}$.

The selected events are split into three main production channels: VBF, Resolved VH, and Boosted VH. In the first two channels, the four-momenta of the two AK4 jets assigned as the associated particles are used in the MELA probability calculation. For the Boosted VH category, we use the four-momentum of the two subjets of the V-tagged AK8 jet. An estimate of the Higgs boson four-momentum is also required for the probability calculation. This can not be measured directly since the final state contains two neutrinos. As such, we construct a proxy Higgs boson four-momentum in the following manner. The p_{x} and p_{y} of the dineutrino system are estimated from the $\vec{p}_{\mathrm{T}}^{\,\mathrm{miss}}$ in a given event. The corresponding p_z is then set to equal that of the dilepton system, which is based on the observed correlation between these variables at the generator level for simulated signals. Finally, the mass of the dineutrino system is set equal to the mean value of the generator-level dineutrino mass. The resulting four-momentum can then be combined with that of the measured dilepton system to create a proxy Higgs boson four-momentum. We note that the MELA probability calculation for the production vertices is largely based on the kinematic features of the associated particles, so the reconstruction of the proxy Higgs boson has a relatively small effect on the final discriminants. As an illustrative example of the MELA based discriminants used in this analysis, Fig. 2 shows the $\mathcal{D}_{0-}$ discriminant in the VBF and Resolved VH production channels for a number of different signal hypotheses. The discriminants are designed to target the dominant signal production process in a given channel.

In the VBF channel, a $\mathcal{D}_{\mathrm{VBF}}$ discriminant is constructed, following Eq. (19), where $\mathcal{P}_{\mathrm{sig}}$ corresponds to the probability for the VBF production hypothesis, and $\mathcal{P}_{\mathrm{bkg}}$ corresponds to that of gluon fusion production in association with two jets. The discriminant is also suitable for separating SM backgrounds from the VBF signal process. In the Resolved and Boosted VH channels, the corresponding discriminants do not give a significant level of separation with respect to ggH production or SM backgrounds. This is due to the relatively tight selection criteria, which limit the phase space to VH-like events. Hence, these discriminants are not included in the VH channels.

The $\mathcal{D}_{CP}$ discriminant is sensitive to the sign of the interference between the *CP*-even SM and *CP*-odd BSM states. An asymmetry between the number of events detected with positive and negative $\mathcal{D}_{CP}$ values is expected for mixed *CP* states. Therefore, a forward-backward categorization (forward defined as $\mathcal{D}_{CP} > 0$ and backward as $\mathcal{D}_{CP} < 0$) is used to analyze the *CP*-odd couplings. Similarly, $\mathcal{D}_{\mathrm{int}}$ gives sensitivity to the sign of the interference between the SM and a_2 HVV BSM states. A forward-backward $\mathcal{D}_{\mathrm{int}}$ categorization is also included. The value of $\mathcal{D}_{\mathrm{int}}$ used to define the categories is chosen to symmetrize the SM Higgs boson expectation. In the case of the Λ_1 measurements, the interference discriminants were shown to be highly correlated with the $\mathcal{D}_{\mathrm{BSM}}$ discriminants and so are not considered.

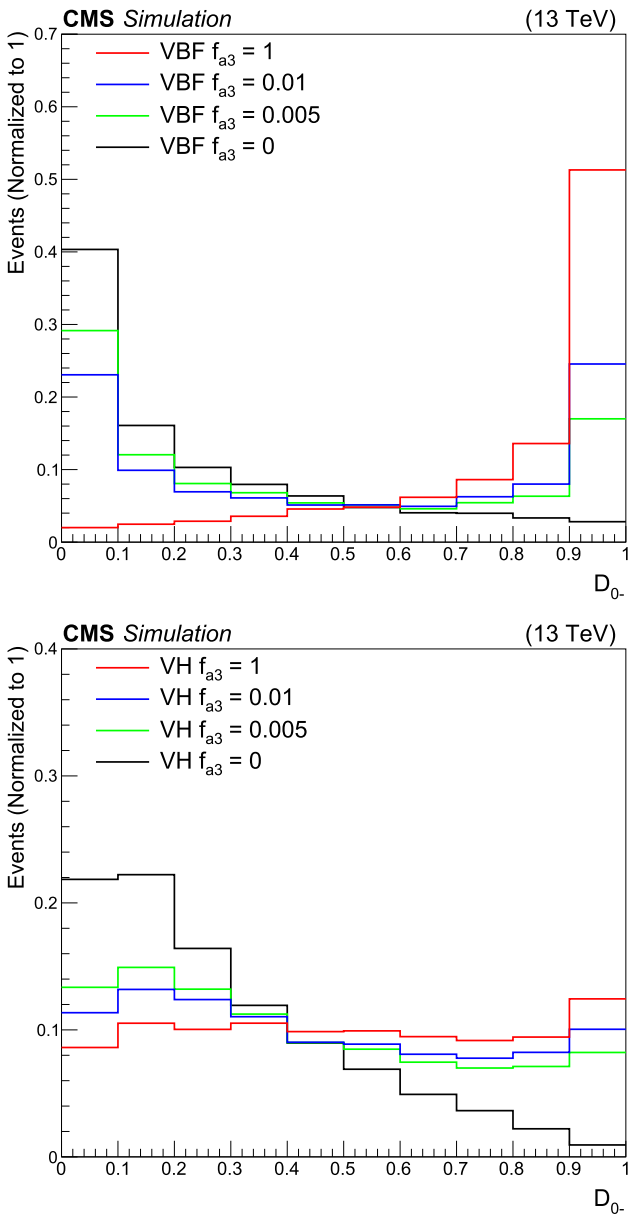

Fig. 2 The $\mathcal{D}_{0-}$ discriminant in the VBF (upper) and Resolved VH (lower) production channels for a number of VBF (upper) and VH (lower) signal hypotheses. Pure a_1 ($f_{a3} = 0$) and a_3 ($f_{a3} = 1$) HVV signal hypotheses are shown along with two mixed coupling hypotheses ($f_{a3} = 0.005$ and $f_{a3} = 0.01$). All distributions are normalized to unity

We now discuss the categorization and construction of the final multidimensional discriminants used for the two HVV coupling approaches defined in Sect. 2. The binning of the final discriminants was optimized to ensure sufficient statistical precision in the predictions of all bins, while retaining

the kinematic information required to discriminate between the SM and anomalous coupling signal hypotheses.

8.1.1 VBF/ VH analysis strategy for Approach 1

In Approach 1, each of the four anomalous HVV coupling parameters (a_2, a_3, $\kappa_1/(\Lambda_1)^2$, and $\kappa_2^{Z\gamma}/(\Lambda_1^{Z\gamma})^2$) are analyzed separately. For this purpose, we construct a multidimensional discriminant for each of the four anomalous couplings in the VBF, Resolved VH, and Boosted VH channels.

In the VBF channel, we use two bins of the production discriminant $\mathcal{D}_{\text{VBF}}$, corresponding to low and high purity, using a bin boundary of 0.75. The $m_{\ell\ell}$ variable, which is sensitive to anomalous effects at the H $\rightarrow$ WW decay vertex, is included with two bins in the range 12–76.2 GeV. A bin boundary of 45 GeV is chosen based on the expected signal shape changes induced by anomalous effects. Finally, one of the $\mathcal{D}_{\text{BSM}}$ discriminants is included with ten equally sized bins. Depending on the anomalous coupling under study this discriminant may be $\mathcal{D}_{0+}$, $\mathcal{D}_{0-}$, $\mathcal{D}_{\Lambda_1}$ or $\mathcal{D}_{\Lambda_1}^{Z\gamma}$.

For the VH channels, the $m_{\ell\ell}$ and $\mathcal{D}_{\text{BSM}}$ observables are used to build 2D kinematic discriminants. The $m_{\ell\ell}$ bins are the same as for the VBF channel. In the Resolved VH channel, we use four $\mathcal{D}_{\text{BSM}}$ bins of equal size. For the Boosted VH case, three variable bins with boundaries of 0.6 and 0.8 are used, a large first bin is chosen because relatively little signal is expected at low values of $\mathcal{D}_{\text{BSM}}$. A distinct multidimensional discriminant is constructed for each anomalous coupling hypothesis in the VH channels.

For the a_3 coupling parameter, a forward-backward categorization of events based on $\mathcal{D}_{CP}$ is implemented. In the case of the a_2 coupling parameter, $\mathcal{D}_{\text{int}}$ is largely correlated with $\mathcal{D}_{0+}$ in the VH channels. Therefore, a forward-backward $\mathcal{D}_{\text{int}}$ categorization is implemented only in the VBF channel. Figures 3, 4 and 5 show the discriminants used in the final fit to the data for the a_2, a_3, $\kappa_1/(\Lambda_1)^2$, and $\kappa_2^{Z\gamma}/(\Lambda_1^{Z\gamma})^2$ Approach 1 coupling studies in the VBF and VH channels. A summary of the observables used in the HVV Approach 1 analysis may be found in Table 6.

8.1.2 VBF/ VH analysis strategy for Approach 2

In Approach 2, we use one categorization strategy and build one multidimensional discriminant in each channel to target all the HVV coupling parameters ($a_2, a_3, \kappa_1/(\Lambda_1)^2$) simultaneously. In the VBF channel, the $\mathcal{D}_{CP}$ and $\mathcal{D}_{\text{int}}$ discriminants are used to create four interference categories. Both $\mathcal{D}_{\text{VBF}}$ and $m_{\ell\ell}$ are used as for Approach 1. All three $\mathcal{D}_{\text{BSM}}$ discriminants that target the a_2, a_3 and $\kappa_1/(\Lambda_1)^2$ coupling parameters are included. However, the number of bins we implement is limited by the number of simulated events. Also the $\mathcal{D}_{\text{BSM}}$ discriminants are significantly correlated and so have similar performance for all couplings. Therefore, we use the *CP*-odd discriminant $\mathcal{D}_{0-}$ and just one of the *CP*-even discriminants, $\mathcal{D}_{0+}$, both with three bins and bin boundaries of 0.1 and 0.9. A dedicated rebinning strategy is applied to the $[\mathcal{D}_{0-}, \mathcal{D}_{0+}]$ distribution merging bins dominated by the SM Higgs boson prediction or with low precision in the background prediction. In the VH channels, just two categories using $\mathcal{D}_{CP}$ are defined and the discriminant is built using $m_{\ell\ell}$ as for Approach 1. Again, both $\mathcal{D}_{0-}$ and $\mathcal{D}_{0+}$ are chosen for the final discriminant. For the Resolved VH channel, we use three bins with boundaries of 0.25 and 0.75, whereas for the Boosted VH case we use two bins with a boundary of 0.8. The same rebinning strategy described for the VBF channel is applied to both Resolved and Boosted VH multidimensional discriminants. Table 6 includes a summary of the observables used in the HVV Approach 2 analysis.

8.2 Kinematic features of H $\rightarrow$ WW decay products in 0- and 1-jet ggH channels

Similar to the SM H $\rightarrow$ WW analysis [25], we use $m_{\ell\ell}$ and m_{T} to build 2D discriminants in the 0- and 1-jet ggH channels. The distributions have nine bins for $m_{\ell\ell}$ in the range 12–200 GeV and six bins for m_{T} in the range 60–125 GeV. The bin widths vary and are optimized to achieve good separation between the SM Higgs boson signal and backgrounds, as well as between the different anomalous coupling signal hypotheses. In particular, a finer binning with respect to the SM H $\rightarrow$ WW analysis is implemented in regions where anomalous effects are most significant. Figure 6 shows the $[m_{\text{T}}, m_{\ell\ell}]$ distributions in the 0- and 1-jet ggH channels. The same $[m_{\text{T}}, m_{\ell\ell}]$ discriminant is used to study all HVV anomalous couplings for both Approach 1 and 2.

8.3 Kinematic features of two quark jets in 2-jet ggH channel

For the Hgg coupling, we adopt a similar approach to the VBF *CP* study, where the *CP*-odd a_3 HVV coupling parameter is included. In this case, the optimal observables are $\mathcal{D}_{0-}^{\text{ggH}}$ and $\mathcal{D}_{CP}^{\text{ggH}}$, targeting the *CP*-odd a_3 Hgg coupling parameter. A forward-backward categorization is implemented using $\mathcal{D}_{CP}^{\text{ggH}}$, and the $\mathcal{D}_{\text{VBF}}$ and $\mathcal{D}_{0-}^{\text{ggH}}$ observables are used to build 2D discriminants. The $m_{\ell\ell}$ variable is not considered in this case because it is not sensitive to anomalous Hgg effects. For $\mathcal{D}_{\text{VBF}}$, the bin boundary is relaxed to 0.5 to ensure sufficient ggH events are accepted in the more VBF-like bin. For $\mathcal{D}_{0-}$, eight (five) bins are used in the more (less) VBF-like bin with larger bin sizes at the extremes of the distribution to ensure sufficient precision in the background and signal predictions. The 0- and 1-jet channels discussed previously are also included in this study to constrain the ggH signal

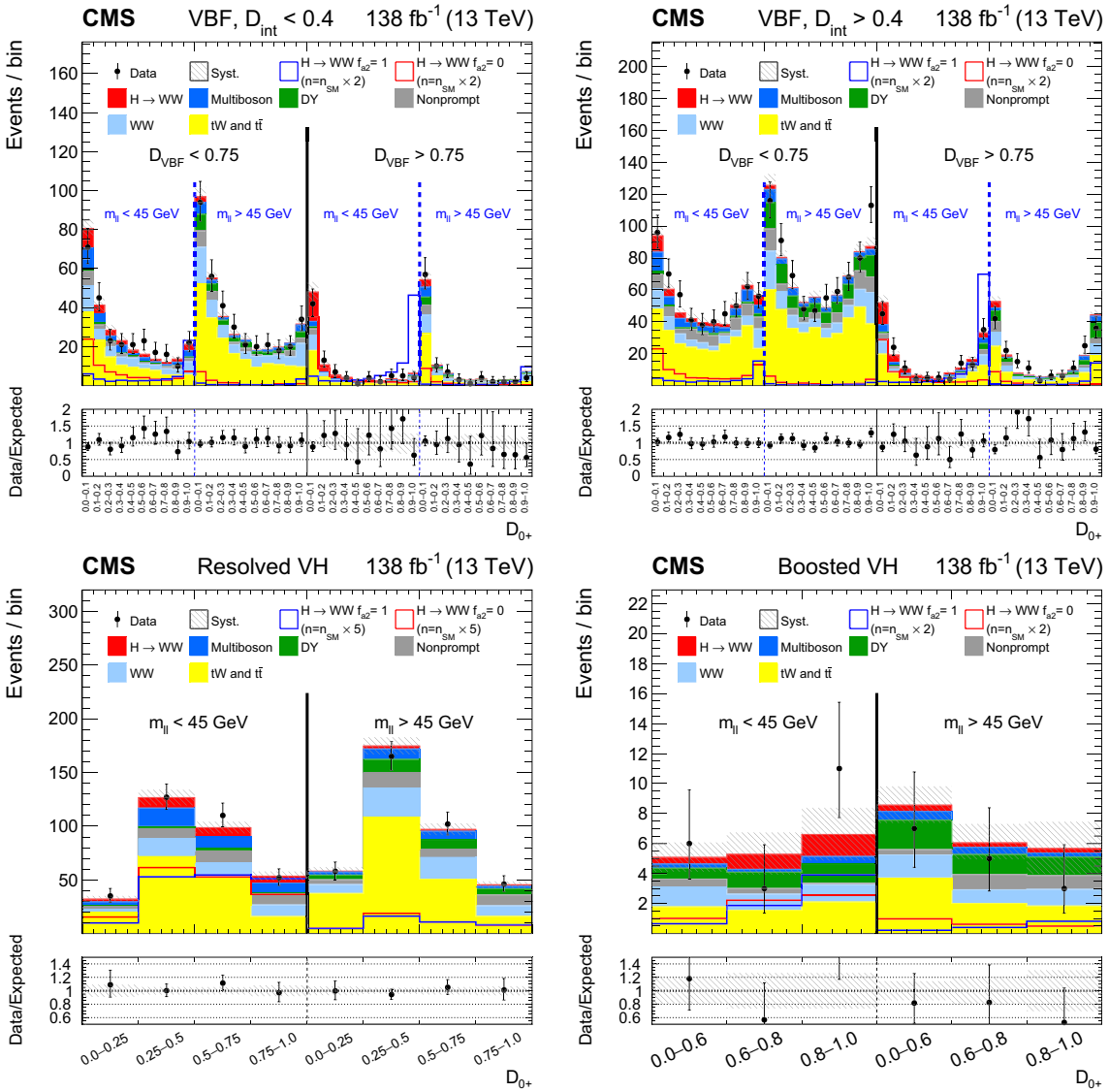

Fig. 3 Observed and predicted distributions after fitting the data for $[\mathcal{D}_{\text{VBF}}, m_{\ell\ell}, \mathcal{D}_{0+}]$ in the VBF channel (upper), and for $[m_{\ell\ell}, \mathcal{D}_{0+}]$ in the Resolved VH (lower left) and Boosted VH (lower right) channels. For the VBF channel, the $\mathcal{D}_{\text{int}} < 0.4$ (left) and $\mathcal{D}_{\text{int}} > 0.4$ (right) categories are shown. The predicted Higgs boson signal is shown stacked on top of the background distributions. For the fit, the a_1 and a_2 HVV coupling contributions are included. The corresponding pure a_1 ($f_{a2} = 0$) and a_2 ($f_{a2} = 1$) signal hypotheses are also shown superimposed, their yields correspond to the predicted number of SM signal events scaled by an arbitrary factor to improve visibility. The uncertainty band corresponds to the total systematic uncertainty. The lower panel in each figure shows the ratio of the number of events observed to the total prediction

strength. The $[\mathcal{D}_{\text{VBF}}, \mathcal{D}_{0-}^{\text{ggH}}]$ distributions used to analyze the Hgg a_3 anomalous coupling in the 2-jet ggH channel are shown in Fig. 7. A summary of the observables used in the Hgg analysis is given in Table 6.

9 Systematic uncertainties

The signal extraction is performed using binned templates to describe the various signal and background processes. Systematic uncertainties that change the normalization or shape of the templates are included. All the uncertainties are modeled as nuisance parameters that are profiled in the maximum likelihood fit described in Sect. 10. The systematic uncertainties arise from both experimental or theoretical sources.

9.1 Experimental uncertainties

The following experimental systematic uncertainties are included in the final fit to data:

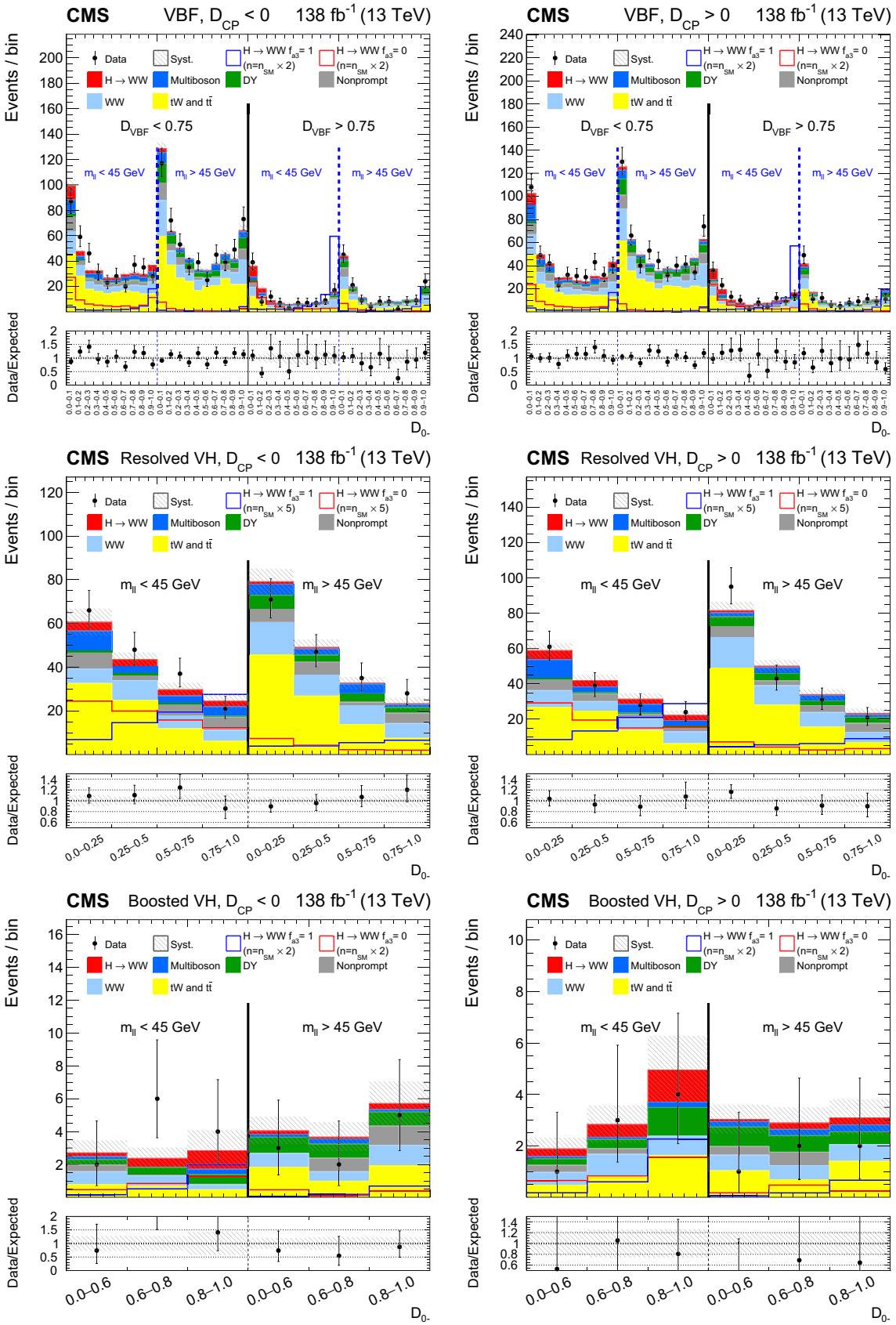

Fig. 4 Observed and predicted distributions after fitting the data for $[\mathcal{D}_{\text{VBF}}, m_{\ell\ell}, \mathcal{D}_{0-}]$ in the VBF channel (upper), and for $[m_{\ell\ell}, \mathcal{D}_{0-}]$ in the Resolved VH (middle) and Boosted VH (lower) channels. For each channel, the $\mathcal{D}_{CP} < 0$ (left) and $\mathcal{D}_{CP} > 0$ (right) categories are shown. For the fit, the a_1 and a_3 HVV coupling contributions are included. More details are given in the caption of Fig. 3

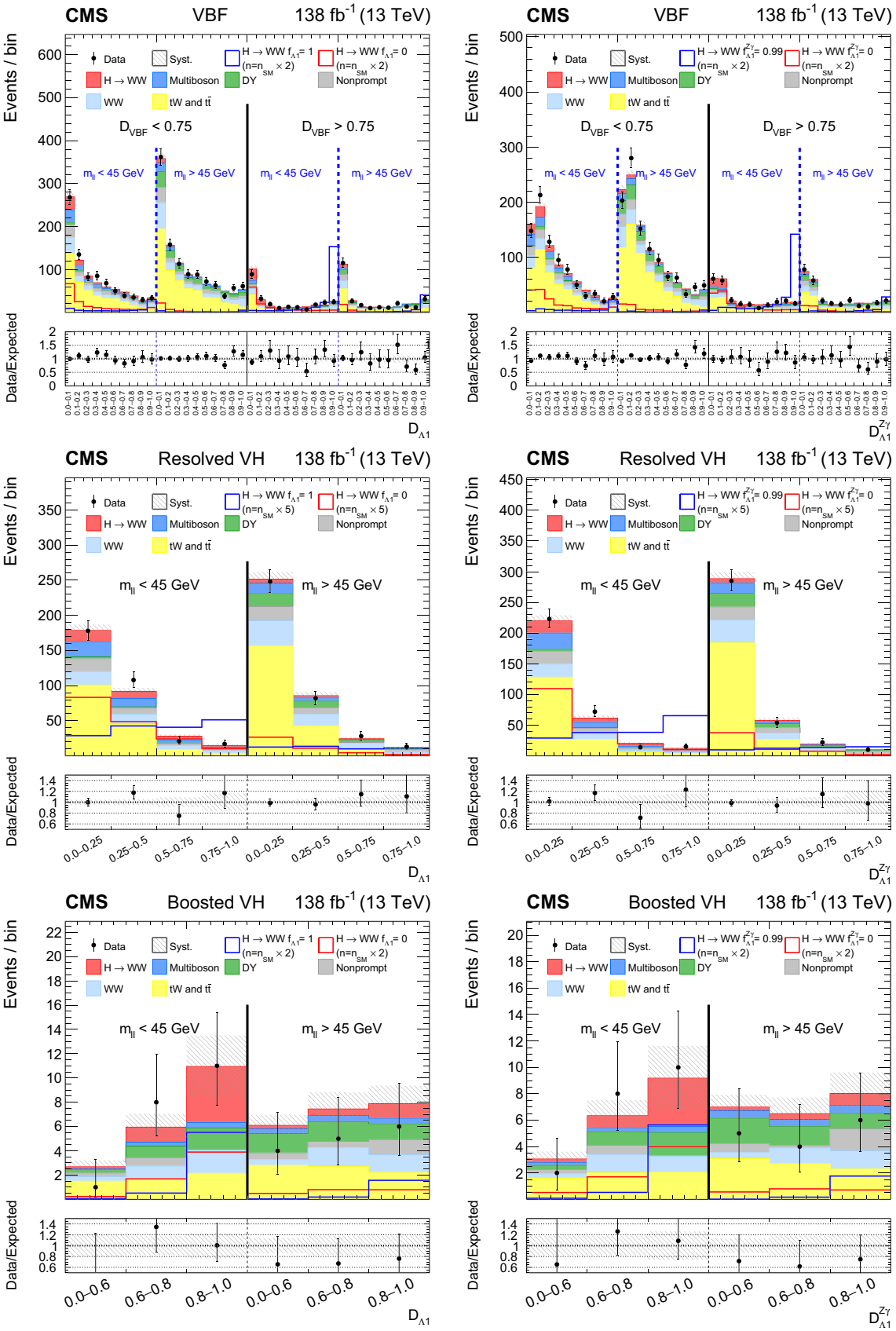

Fig. 5 Observed and predicted distributions after fitting the data for $[\mathcal{D}_{\text{VBF}}, m_{\ell\ell}, \mathcal{D}_{\Lambda 1}]$ (upper left) and $[\mathcal{D}_{\text{VBF}}, m_{\ell\ell}, \mathcal{D}_{\Lambda 1}^{Z\gamma}]$ (upper right) in the VBF channel, and for $[m_{\ell\ell}, \mathcal{D}_{\Lambda 1}]$ (left) and $[m_{\ell\ell}, \mathcal{D}_{\Lambda 1}^{Z\gamma}]$ (right) in the Resolved VH (middle) and Boosted VH (lower) channels. For the fits, the a_1 and $\kappa_1/(\Lambda_1)^2$ (left) or a_1 and $\kappa_2^{Z\gamma}/(\Lambda_1^{Z\gamma})^2$ (right) HVV coupling contributions are included. More details are given in the caption of Fig. 3

Table 6 The kinematic observables used for the interference based categorization and for the final discriminants used in the fits to data to study the HVV and Hgg couplings. For each of the anomalous HVV couplings in Approach 1, we have a dedicated analysis in the VBF and VH channels. In Approach 2, we use one analysis to target all anomalous HVV couplings simultaneously

Analysis	Channel	Categorization	Final discriminant
HVV	VBF (a_2)	$\mathcal{D}_{\text{int}}$	$[\mathcal{D}_{\text{VBF}}, m_{\ell\ell}, \mathcal{D}_{0+}]$
Approach 1	VBF (a_3)	$\mathcal{D}_{CP}$	$[\mathcal{D}_{\text{VBF}}, m_{\ell\ell}, \mathcal{D}_{0-}]$
	VBF (κ_1)	–	$[\mathcal{D}_{\text{VBF}}, m_{\ell\ell}, \mathcal{D}_{\Lambda 1}]$
	VBF ($\kappa_2^{\text{Z}\gamma}$)	–	$[\mathcal{D}_{\text{VBF}}, m_{\ell\ell}, \mathcal{D}_{\Lambda_1}^{\text{Z}\gamma}]$
	VH (a_2)	–	$[m_{\ell\ell}, \mathcal{D}_{0+}]$
	VH (a_3)	$\mathcal{D}_{CP}$	$[m_{\ell\ell}, \mathcal{D}_{0-}]$
	VH (κ_1)	–	$[m_{\ell\ell}, \mathcal{D}_{\Lambda 1}]$
	VH ($\kappa_2^{\text{Z}\gamma}$)	–	$[m_{\ell\ell}, \mathcal{D}_{\Lambda_1}^{\text{Z}\gamma}]$
	0- and 1-jet ggH	–	$[m_{\text{T}}, m_{\ell\ell}]$
HVV	VBF	$\mathcal{D}_{CP}$, $\mathcal{D}_{\text{int}}$	$[\mathcal{D}_{\text{VBF}}, m_{\ell\ell}, \mathcal{D}_{0-}, \mathcal{D}_{0+}]$
Approach 2	VH	$\mathcal{D}_{CP}$	$[m_{\ell\ell}, \mathcal{D}_{0-}, \mathcal{D}_{0+}]$
	0- and 1-jet ggH	–	$[m_{\text{T}}, m_{\ell\ell}]$
Hgg	2-jet ggH	$\mathcal{D}_{CP}^{\text{ggH}}$	$[\mathcal{D}_{\text{VBF}}, \mathcal{D}_{0-}^{\text{ggH}}]$
	0- and 1-jet ggH	–	$[m_{\text{T}}, m_{\ell\ell}]$

– The total uncertainty associated with the measurement of the integrated luminosity for 2016, 2017, and 2018 is 1.2% [44], 2.3% [45], and 2.5% [46], respectively. This uncertainty is partially correlated among the three data sets, resulting in an overall uncertainty of 1.6%.
– The systematic uncertainty in the trigger efficiency is determined by varying the tag lepton selection criteria and the Z boson mass window used in the tag-and-probe method. It affects both the normalization and the shape of the signal and background distributions, and is kept uncorrelated among data sets. The total normalization uncertainty is less than 1%.
– The tag-and-probe method is also used to determine the lepton identification and isolation efficiency. Corrections are applied to account for any discrepancy in the efficiencies measured in data and simulation. The corresponding systematic uncertainty is about 1% for electrons and 2% for muons.
– The uncertainties in the determination of the lepton momentum scale mainly arise from the limited data sample used for their estimation. The impact on the normalization of the signal and background templates ranges between 0.6–1.0% for the electron momentum scale and is about 0.2% for the muon momentum scale. They are treated as uncorrelated among the three data-taking years.
– The jet energy scale uncertainty is modeled by implementing eleven independent nuisance parameters corresponding to different jet energy correction sources, six of which are correlated among the three data sets. Their effects vary in the range of 1–10%, mainly depending on the jet multiplicity in the analysis phase space. Another source of uncertainty arises from the jet energy resolution smearing applied to simulated samples to match the p_{T} resolution measured in data. The effect varies in a range of 1–5%, depending on the jet multiplicity and is uncorrelated among the data sets. These uncertainties are included for both AK4 and AK8 jets. In addition, the m_{J} scale and resolution, and V tagging corrections with their corresponding uncertainties are included for V-tagged AK8 jets. These variables are calibrated in a top quark–antiquark sample enriched in hadronically decaying W bosons [95].
– The effects of the unclustered energy scale, jet energy scale, and lepton p_{T} scales are included for the calculation of the missing transverse momentum. The resulting normalization systematic uncertainty is 1–10% and is treated as uncorrelated among the years.
– Both the normalization and shape of the signal and background templates are affected by the jet pileup identification uncertainty. The effect is below 1%.
– The uncertainty associated with the b tagging efficiency is modeled by seventeen nuisance parameters out of which five are of a theoretical origin and are correlated among the three data sets. The remaining set of four parameters per data set are treated as uncorrelated as they arise from the statistical accuracy of the efficiency measurement [90].
– Estimation of the nonprompt-lepton background is affected by the limited size of the data sets used for the misidentification rate measurements. It is also affected by the difference in the flavor composition of jets misidentified as leptons between the misidentification rate measurement region (enriched in multijet events) and the signal phase space. The effects on the nonprompt-lepton background estimation range between a few percent to about 10% depending on the SR and are treated as nui-

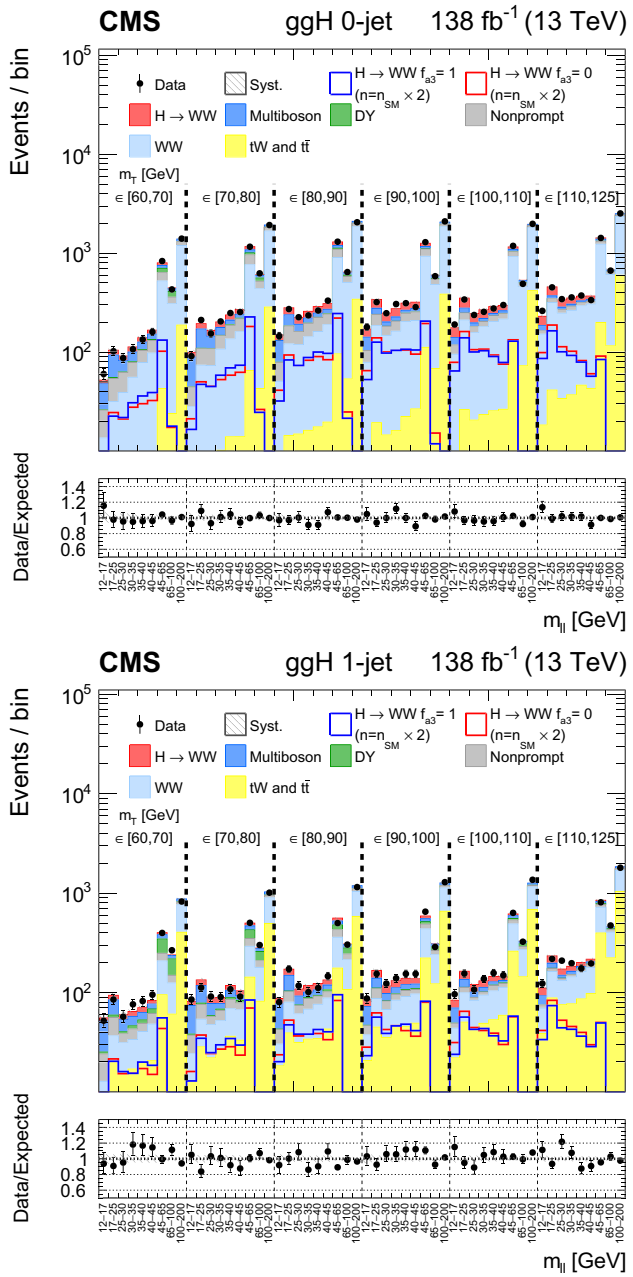

Fig. 6 Observed and predicted distributions after fitting the data for $[m_{\mathrm{T}}, m_{\ell\ell}]$ in the 0- (upper) and 1-jet (lower) ggH channels. For the fit, the a_1 and a_3 HVV coupling contributions are included. More details are given in the caption of Fig. 3

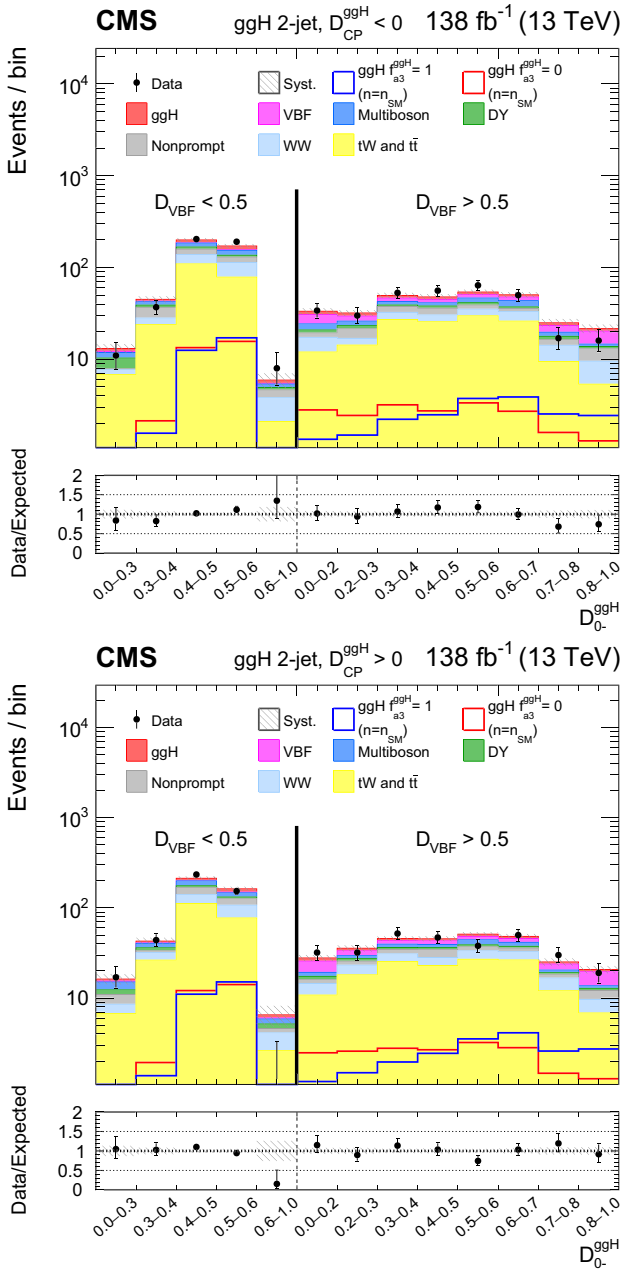

Fig. 7 Observed and predicted distributions after fitting the data for $[\mathcal{D}_{\mathrm{VBF}}, \mathcal{D}_{0-}^{\mathrm{ggH}}]$ in the 2-jet ggH channel. Both the $\mathcal{D}_{\mathrm{CP}}^{\mathrm{ggH}} < 0$ (upper) and $\mathcal{D}_{\mathrm{CP}}^{\mathrm{ggH}} > 0$ (lower) categories are shown. In this case, the VBF and ggH signals are shown separately. For the fit, the a_2^{gg} and a_3^{gg} coupling contributions are included. The corresponding pure a_2^{gg} ($f_{a3}^{\mathrm{ggH}} = 0$) and a_3^{gg} ($f_{a3}^{\mathrm{ggH}} = 1$) signal hypotheses are also shown superimposed, their yields correspond to the predicted number of SM signal events. More details are given in the caption of Fig. 3

sance parameters uncorrelated between electrons and muons and among the three data sets. A normalization uncertainty of 30% [92] is assigned to fully cover for any discrepancies with respect to data in a W+jets CR and is treated as uncorrelated among data sets.

– The statistical uncertainties due to the limited number of simulated events are also included for all bins of the background distributions used to extract the results [96].

9.2 Theoretical uncertainties

Multiple theoretical uncertainties are considered and are correlated among data sets, unless stated otherwise:

– The uncertainties related to the choice of PDF and α_S have a minor effect on the shape of the distributions. Therefore, only normalization effects related to the event acceptance and to the cross section are included. However, these uncertainties are not considered for the backgrounds that have their normalization constrained through data in dedicated CRs. For the Higgs boson signal processes, these uncertainties are calculated by the LHC Higgs cross section working group [19].
– The theoretical uncertainties arising from missing higher-order corrections in the cross section calculations are also included. Background simulations are reweighted to the alternative scenarios corresponding to renormalization μ_R and factorization μ_F scales varied by factors 0.5 or 2 and the envelopes of the varied templates are taken as the one standard deviations. For background processes that have their normalization constrained through data in dedicated CRs, we consider only the shape effect of the uncertainties coming from the missing higher-order corrections. The WWnonresonant background has the uncertainties derived by varying μ_R, μ_F, and the resummation scale. For the ggH and VBF signal processes, the effects of the missing higher-order corrections on the overall cross section are decoupled into multiple sources according to the recipes described in Ref. [19].
– The uncertainty due to the pileup modeling was included for the main simulated background processes (DY, WW, top quark) as well as the ggH and VBF signals. The effect is determined by varying the total inelastic pp cross section (69.2 mb [97,98]) within the assigned 5% uncertainty.
– The PS modeling mainly affects the jet multiplicity, causing migration of events between categories that results in template shape changes. Associated uncertainties are evaluated by reweighting events with varied PS weights computed with PYTHIA 8.212. The effect on the signal strength is found to be below 1%.
– Uncertainties associated with UE modeling are evaluated by varying the UE tune parameters used in the MC sample generation. Systematic uncertainties are correlated between the 2017 and 2018 data sets since they share the same UE tunes, whereas for 2016 the uncertainty is considered uncorrelated. The UE uncertainty has a minimal effect on the template shapes and affects the normalization by about 1.5%.
– A 15% uncertainty is applied to the relative fraction of the gg-induced component in nonresonant WW production [99]. The relative fraction between single top quark and $t\bar{t}$ processes is assigned a systematic uncertainty of 8% [100]. Additional process-specific (DY, VZ, $V\gamma$, $V\gamma^*$) uncertainties, related to corrections to account for possible discrepancies between data and simulation, are assigned and are correlated among data sets.

10 Results

The optimization and validation of the analysis were performed using simulation and data in CRs. The data in the SRs were examined once all details of the analysis were finalized. For the final results, we perform a binned maximum likelihood fit to the data combining all channels and data-taking periods. The statistical approach was developed by the ATLAS and CMS Collaborations in the context of the LHC Higgs Combination Group [101]. The likelihood function is defined for candidate events as:

$$\mathcal{L}(\text{data}|\mu_{\text{ggH}}, \mu_{\text{EW}}, f_{ai}, \theta) = \prod_{\text{j}} \text{Poisson}(n_{\text{j}}|s_{\text{j}}(\mu_{\text{ggH}}, \mu_{\text{EW}}, f_{ai}, \theta) + b_{\text{j}}(\theta))\, p(\tilde{\theta}|\theta), \tag{22}$$

where j runs over all bins and n_{j} is the observed number of data events in each bin. Total signal and background expectations in each bin are represented by s_{j} and b_{j}, respectively. The individual signal and background processes considered in each category are described using binned templates of multidimensional discriminants as described in Sect. 8. Each signal process is parametrized as a linear combination of terms originating from the SM, and anomalous couplings and their interference. The signal expectation depends on the parameters μ_{ggH}, μ_{EW}, and f_{ai}, and is constrained by the data fit. Both the signal and background expectations are functions of θ, which represents the full set of nuisance parameters corresponding to the systematic uncertainties. The CRs described in Sect. 6 are included in the fit in the form of single bins, representing the number of events in each CR.

The μ_{ggH} and μ_{EW} parameters correspond to the Higgs boson signal strength modifiers for the ggH and VBF/VH signals, respectively. Signal yields for the VBF and VH processes are related to each other because the same HVV couplings enter both in production and decay of the Higgs boson. The ggH signal is initiated predominantly by the top fermion couplings and is unrelated to the VBF and VH production mechanisms. As the signal strength modifiers are free parameters in the fit, the overall signal event yield is not used to discriminate between alternative signal hypotheses. The f_{ai} parameter corresponds to the anomalous coupling cross section fraction and determines the shape of the signal expectation. The cross section fraction for the SM coupling is simply taken as $1-|f_{ai}|$. In Approach 1, the SM and just one anomalous HVV coupling are included, and each f_{ai} is thus studied independently. Depending on the particular anomalous coupling under investigation, f_{ai} may represent f_{a2}, f_{a3}, $f_{\Lambda 1}$, or $f_{\Lambda 1}^{\text{Z}\gamma}$. For Approach 2, the SM and three anomalous HVV couplings are included. In this case, f_{ai} represents f_{a2}, f_{a3} and $f_{\Lambda 1}$, which are studied simultaneously. It is explicitly required that $|f_{a2}| + |f_{a3}| + |f_{\Lambda 1}| \leq 1$ to avoid probing an

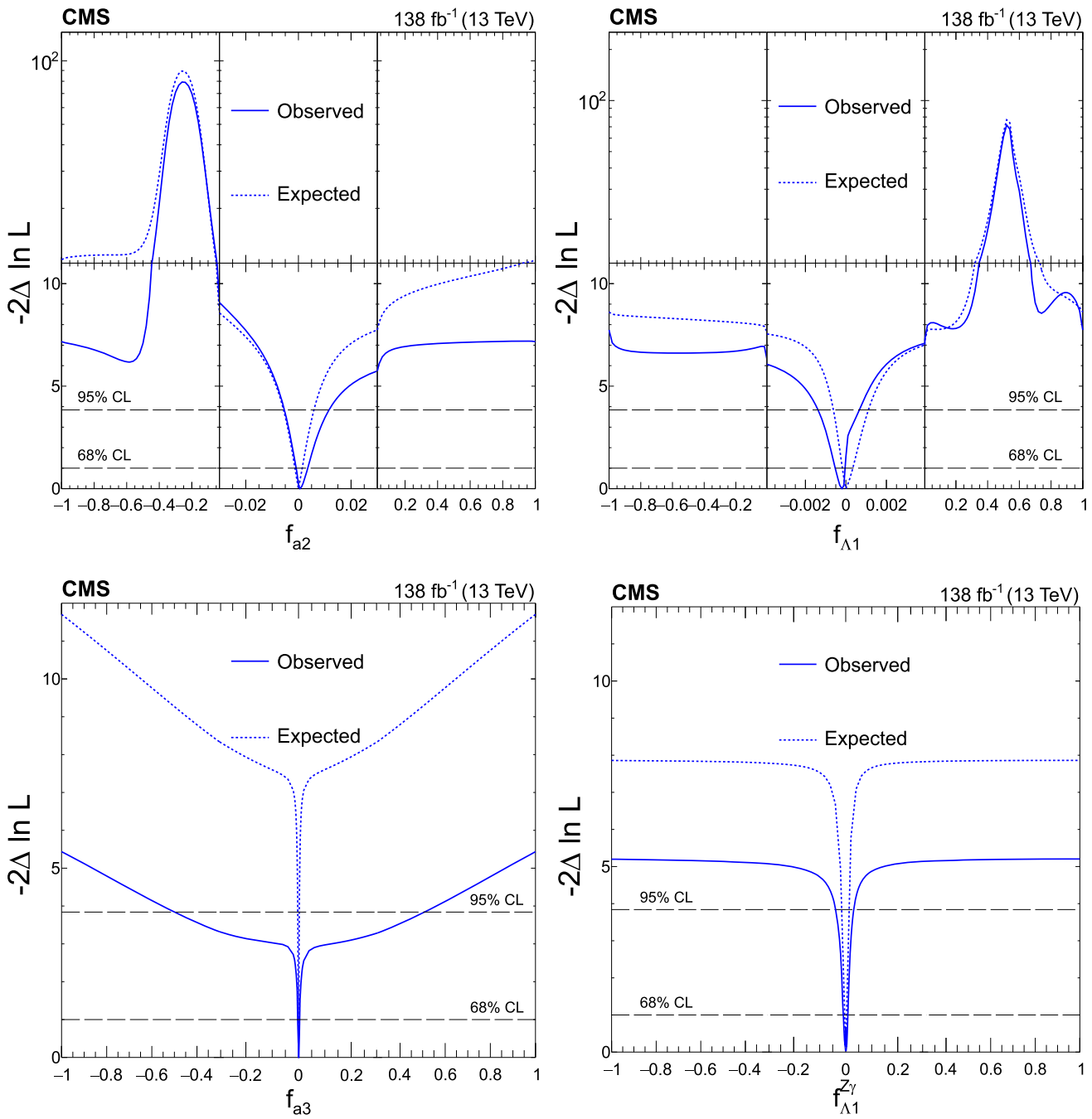

Fig. 8 Expected (dashed) and observed (solid) profiled likelihood on f_{a2} (upper left), $f_{\Lambda 1}$ (upper right), f_{a3} (lower left), and $f_{\Lambda 1}^{Z\gamma}$ (lower right) using Approach 1. In each case, the signal strength modifiers are treated as free parameters. The dashed horizontal lines show the 68 and 95% CL regions. Axis scales are varied for f_{a2} and $f_{\Lambda 1}$ to improve the visibility of important features

unphysical parameter space. Finally, there is just one anomalous coupling corresponding to f_{a3}^{ggH} to consider for the Hgg vertex. For this study, we also include the effect of the *CP*-odd HVV anomalous coupling on the VBF process. This is achieved by including f_{a3} as a free parameter in the fit. The $p(\tilde{\theta}|\theta)$ are the probability density functions (PDFs) for the observed values of the nuisance parameters, $\tilde{\theta}$, obtained from calibration measurements. The systematic uncertainties that affect only the normalizations of the signal and background processes are treated as PDFs following a log-normal distribution, whereas shape-altering systematic uncertainties are treated as Gaussian PDFs [101].

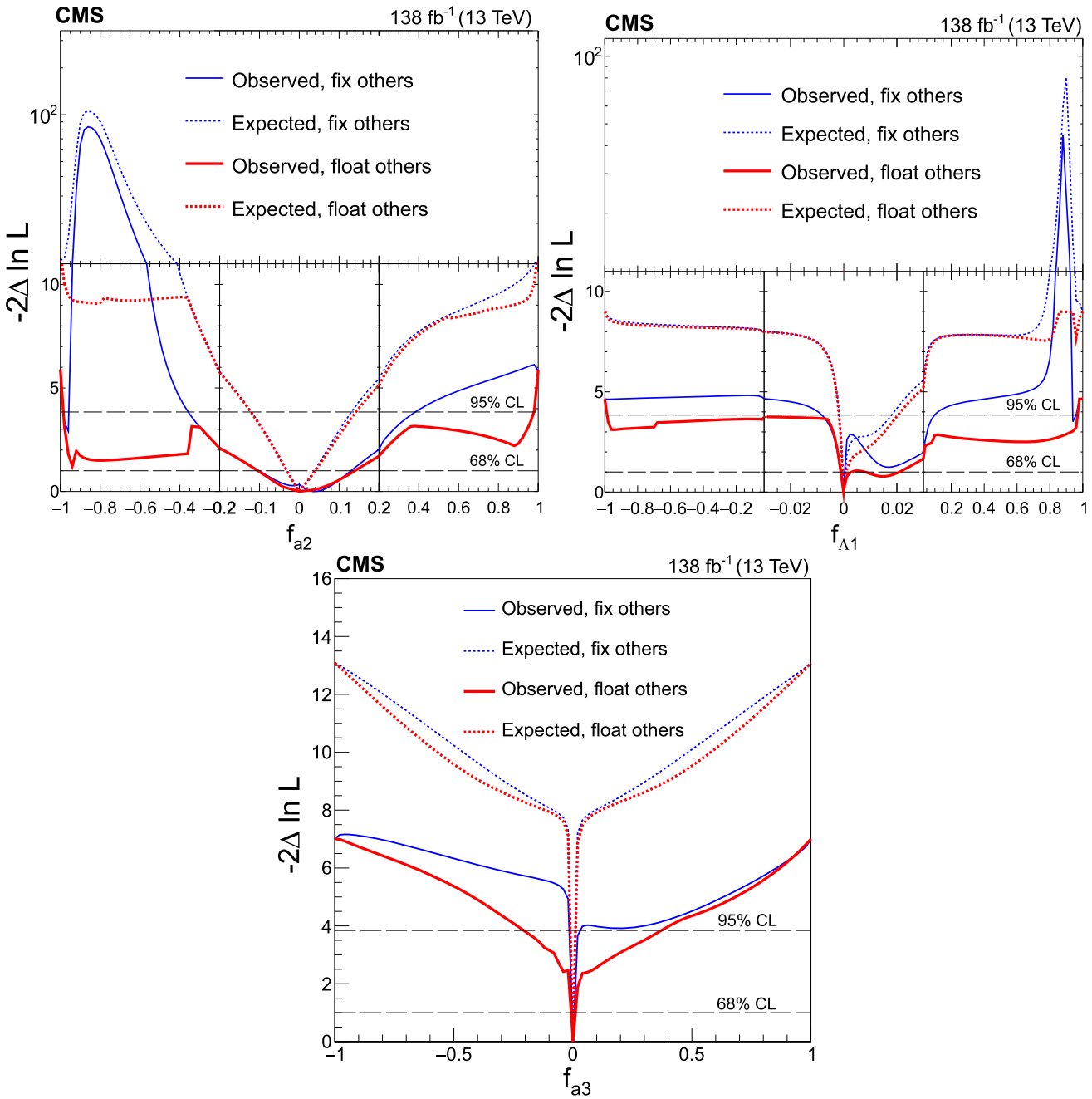

Fig. 9 Expected (dashed) and observed (solid) profiled likelihood on f_{a2} (upper left), $f_{\Lambda 1}$ (upper right) and f_{a3} (bottom) using Approach 2. The other two anomalous coupling cross section fractions are either fixed to zero (blue) or left floating in the fit (red). In each case, the signal strength modifiers are treated as free parameters. The dashed horizontal lines show the 68 and 95% CL regions. Axis scales are varied for f_{a2} and $f_{\Lambda 1}$ to improve the visibility of important features

Additional interpretations in terms of the SMEFT Higgs and Warsaw basis coupling parameters are also considered using Eqs. (7–10) and Eqs. (11–14), respectively. In each case, four independent couplings are studied simultaneously and the effect of the couplings on the total width of the Higgs boson is taken into account. For the f_{ai} measurements, this effect is absorbed by the signal strength modifiers. A parameterization of the partial widths of the main Higgs boson decay modes as a function of the couplings is used to determine the effect on the Higgs boson width [24,28].

The likelihood is maximized with respect to the signal modifier parameters and with respect to the nuisance parameters. Confidence level (CL) intervals are determined from profile likelihood scans of the respective parameters. The allowed 68% and 95% CL intervals are defined using the set of parameter values at which the profile likelihood function

Table 7 Summary of constraints on the anomalous HVV and Hgg coupling parameters with the best fit values and allowed 68 and 95% CL (in square brackets) intervals. For Approach 1, each f_{ai} is studied independently. For Approach 2, each f_{ai} is shown separately with the other two cross section fractions either fixed to zero or left floating in the fit. In each case, the signal strength modifiers are treated as free parameters

Analysis	f_{ai}		Observed ($\times 10^{-3}$)	Expected ($\times 10^{-3}$)
HVV	f_{a2}	Best fit	0.5	0.0
Approach 1		68% CL	[−0.8, 3.5]	[−1.4, 1.3]
		95% CL	[−5.7, 12.0]	[−5.2, 6.1]
	f_{a3}	Best fit	0.9	0.0
		68% CL	[−2.7, 4.1]	[−0.7, 0.7]
		95% CL	[−553.0, 561.0]	[−2.8, 2.9]
	$f_{\Lambda 1}$	Best fit	−0.2	0.0
		68% CL	[−0.5, 0.0]	[−0.2, 0.5]
		95% CL	[−1.4, 0.7]	[−0.6,1.4]
	$f_{\Lambda 1}^{Z\gamma}$	Best fit	3.0	0.0
		68% CL	[−11.0, 9.1]	[−5.0, 3.8]
		95% CL	[−55.0, 42.0]	[−14.0, 11.0]
HVV	f_{a2}	Best fit	38.0	0.0
Approach 2		68% CL	[−112.2, 129.3]	[−30.9, 37.5]
(Fix others)		95% CL	[−376.6, 430.0]∪[−989.2, −826.3]	[−126.1, 136.8]
	f_{a3}	Best fit	0.8	0.0
		68% CL	[−0.8, 3.5]	[−0.8, 1.1]
		95% CL	[−7.6, 58.8]	[−3.4, 4.3]
	$f_{\Lambda 1}$	Best fit	−0.15	0.0
		68% CL	[−1.21, 0.16]	[−0.4, 0.4]
		95% CL	[−19.5, 118.5]∪[909.9, 964.1]	[−1.7, 18.9]
HVV	f_{a2}	Best fit	−1.0	0.0
Approach 2		68% CL	[−104.1, 139.9]	[−31.1, 39.8]
(Float others)		95% CL	[−986.4, 981.2]	[−127.5, 148.7]
	f_{a3}	Best fit	0.34	0.0
		68% CL	[−0.69, 3.4]	[−1.0, 1.2]
		95% CL	[−201.3, 361.5]	[−4.3, 5.3]
	$f_{\Lambda 1}$	Best fit	−0.1	0.0
		68% CL	[−1.08, 3.78]∪[7.2, 20.7]	[−0.4, 0.9]
		95% CL	[−994.8, 993.9]	[−1.9, 21.4]
Hgg	f_{a3}^{ggH}	Best fit	−34	0
		68% CL	[−721, 383]	[−1000, 1000]
		95% CL	[−1000, 1000]	[−1000, 1000]

$-2\Delta \ln \mathcal{L} = 1.00$ and 3.84 [102], respectively, for which exact coverage is expected in the asymptotic limit [103]. The likelihood value at a given f_{ai} is determined by the shape of the signal hypothesis and the relative signal event yields between categories. Expected results are obtained using the Asimov data set [104] constructed using the SM values of the signal modifier parameters.

For Approach 1, where we assume $a_i^{ZZ} = a_i^{WW}$, the expected and observed f_{a2}, f_{a3}, $f_{\Lambda 1}$, and $f_{\Lambda 1}^{Z\gamma}$ likelihood scans are shown in Fig. 8. Significant interference effects for negative values of f_{a2}, around −0.25, and positive values of $f_{\Lambda 1}$, around 0.5, are evident. Relatively large changes in the signal shape with respect to the SM are predicted at these values. Also evident are narrow minima around $f_{ai} = 0$. The anomalous coupling terms in Eq. (1) have a q_i^2 dependence, which can be larger at the VBF/VH production vertex than at the Higgs decay vertex. This causes the cross section and the shape of the VBF/VH signal hypothesis to change rapidly

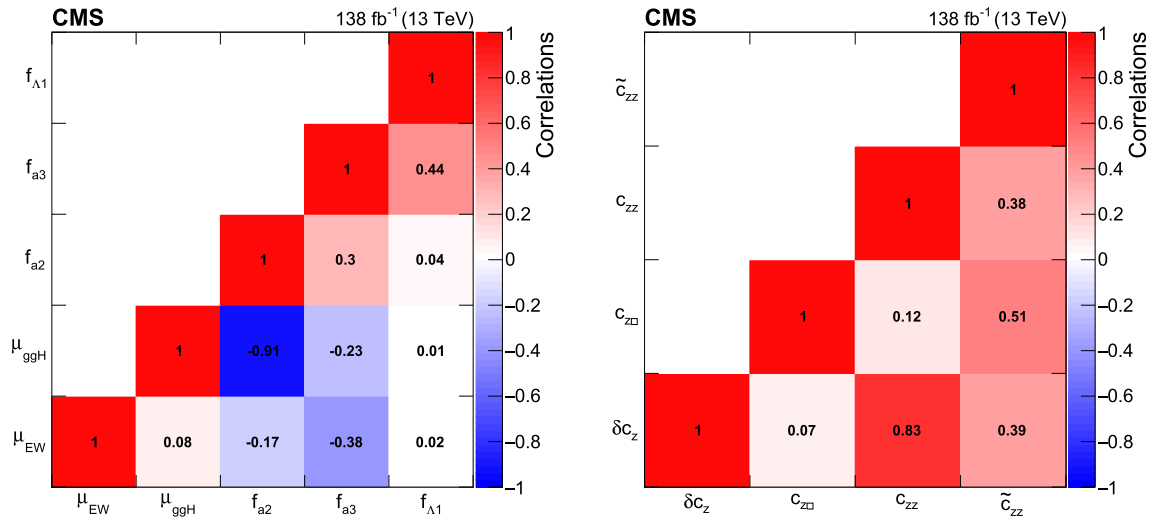

Fig. 10 The observed correlation coefficients between HVV anomalous coupling cross section fractions and signal strength modifiers (left) and between SMEFT Higgs basis coupling parameters (right)

with f_{ai}. For $f_{\Lambda 1}^{Z\gamma}$, there are no anomalous effects at the Higgs decay vertex and so the only structure present is the narrow minimum related to the VBF/VH production vertex. The axis scales are varied to improve the visibility of important features for f_{a2} and $f_{\Lambda 1}$. For Approach 2, where the SU(2) x U(1) coupling relationships from Eqs. (2–6) are adopted, the expected and observed f_{a2}, f_{a3} and $f_{\Lambda 1}$ likelihood scans are shown in Fig. 9. The results are shown for each f_{ai} separately with the other two f_{ai} either fixed to zero or left floating in the fit. The measured values of the signal strength parameters correspond to $\mu_{\mathrm{EW}} = 0.9^{+0.19}_{-0.24}$ and $\mu_{\mathrm{ggH}} = 0.9^{+0.38}_{-0.20}$ when all parameters float simultaneously. It is notable that the observed $-2\Delta \ln \mathcal{L}$ profile values are generally lower than expected. This is consistent with a downward statistical fluctuation in the number of VBF and VH events. The lowest μ_{EW} value measured is 0.82 for the Approach 1 f_{a3} fit which can be compared with the highest value of 0.97 for the corresponding $f_{\Lambda 1}$ fit. In each case, the uncertainty in μ_{EW} is about 20% and as such all fitted values are consistent with both the SM and each other. More generally, all anomalous HVV coupling parameter measurements are consistent with the expectations for the SM Higgs boson. The p-value compatibility of the full Approach 2 fit, where all signal parameters float simultaneously, with the SM is 91%. A summary of constraints on the anomalous HVV coupling parameters with the best fit values and allowed 68% and 95% CL intervals are shown in Table 7. The most stringent constraints on the HVV anomalous coupling cross section fractions are at the per mille level. Some constraints are less stringent than expected due to the fitted values of μ_{EW} being lower than the SM expectation. The observed correlation coefficients between HVV anomalous coupling cross section fractions and signal strength modifiers are displayed in Fig. 10.

For the SMEFT Higgs basis interpretation, the expected and observed constraints on the δc_z, $c_{z\Box}$, c_{zz}, and $\tilde{c}_{zz}$ coupling parameters are shown in Fig. 11. Table 8 presents a summary of the constraints on the couplings whereas Fig. 10 reports the observed correlation coefficients between them. For the Warsaw basis interpretation, the expected and observed constraints on the $c_{H\Box}$, c_{HD}, c_{HW}, c_{HWB}, c_{HB}, $c_{H\tilde{W}}$, $c_{H\tilde{W}B}$, and $c_{H\tilde{B}}$ coupling parameters are presented in Table 9. To cover all the Warsaw basis coupling parameters, three independent fits to the data were performed with a different choice of four independent couplings in each. A summary of the constraints on the SMEFT Higgs and Warsaw basis coupling parameters is presented in Fig. 12.

Finally, the expected and observed f_{a3}^{ggH} likelihood scans are shown in Fig. 13. The result is consistent with the expectation for a SM Higgs boson. Excluding the effect of the *CP*-odd HVV anomalous coupling, by fixing f_{a3} to zero, has a negligible effect. For $\left|f_{a3}^{\mathrm{ggH}}\right|$ approaching unity, the observed $-2\Delta \ln \mathcal{L}$ profile values are larger than expected. This is consistent with downward statistical fluctuations in the data for a couple of bins where sensitivity to the a_3 Hgg coupling contribution is enhanced (Fig. 7 upper). The constraint on the anomalous Hgg coupling parameter with the best fit value and allowed 68% CL interval is shown in Table 7.

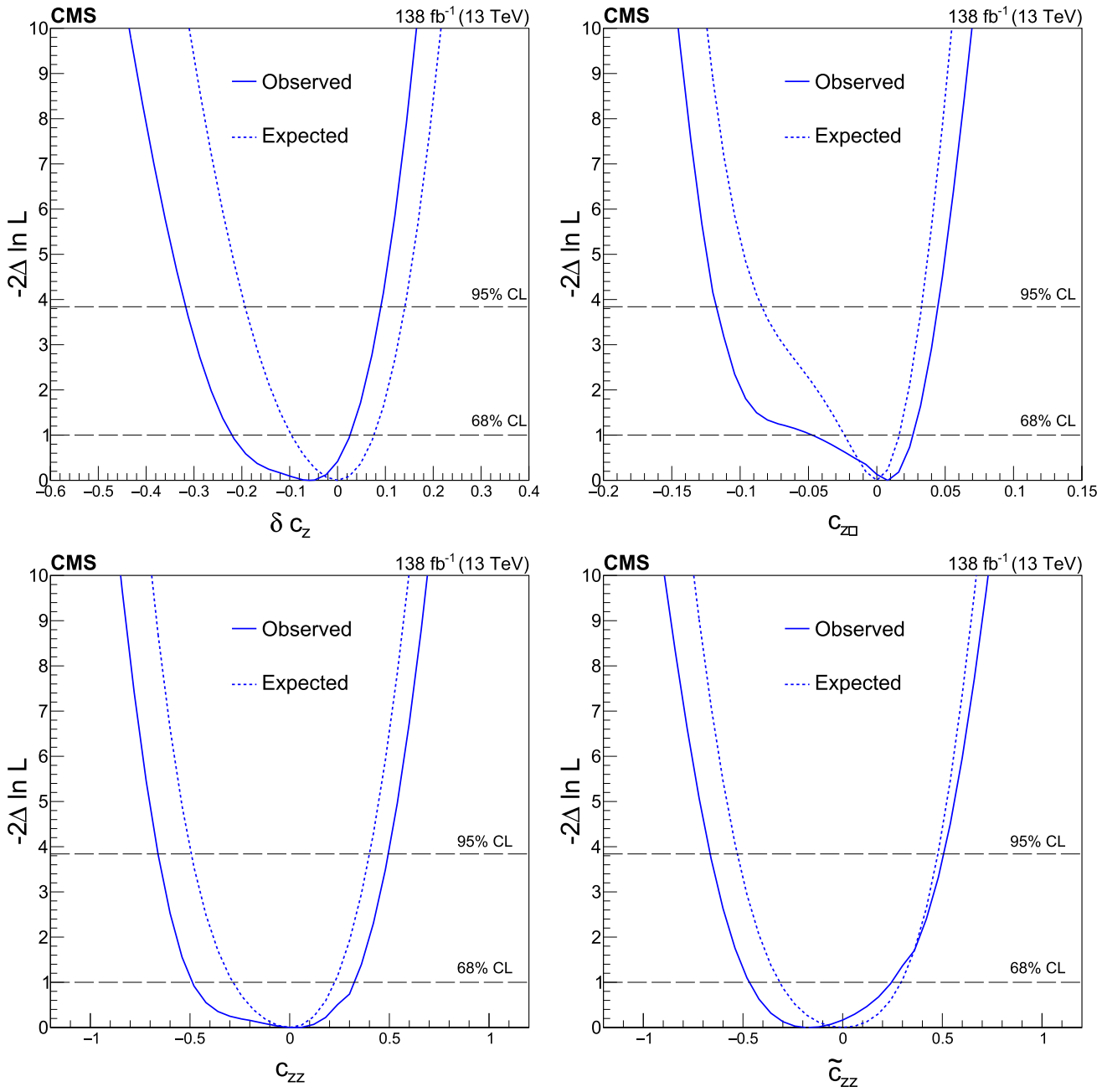

Fig. 11 Expected (dashed) and observed (solid) profiled likelihood on the δc_z (upper left), $c_{z\Box}$ (upper right), c_{zz} (lower left), and $\tilde{c}_{zz}$ (lower right) couplings of the SMEFT Higgs basis. All four couplings are studied simultaneously. The dashed horizontal lines show the 68 and 95% CL regions

Table 8 Summary of constraints on the SMEFT Higgs basis coupling parameters with the best fit values and 68% CL uncertainties. All four couplings are studied simultaneously

Coupling	Observed	Expected
δc_z	$-0.06^{+0.09}_{-0.16}$	$0.00^{+0.08}_{-0.10}$
$c_{z\Box}$	$0.01^{+0.02}_{-0.06}$	$0.00^{+0.02}_{-0.02}$
c_{zz}	$0.03^{+0.30}_{-0.52}$	$0.00^{+0.23}_{-0.29}$
$\tilde{c}_{zz}$	$-0.17^{+0.42}_{-0.30}$	$0.00^{+0.29}_{-0.32}$

Table 9 Summary of constraints on the SMEFT Warsaw basis coupling parameters with the best fit values and 68% CL uncertainties. Only one of c_{HW}, c_{HWB}, and c_{HB} is independent, the same is also true for $c_{H\tilde{W}}$, c_{HWB}, and $c_{H\tilde{B}}$. Three independent fits to the data were performed with a different choice of four independent couplings in each

Coupling	Observed	Expected
$c_{H\Box}$	$-0.76^{+1.43}_{-3.43}$	$0.00^{+1.37}_{-1.84}$
c_{HD}	$-0.12^{+0.93}_{-0.32}$	$0.00^{+0.43}_{-0.30}$
c_{HW}	$0.08^{+0.43}_{-0.87}$	$0.00^{+0.37}_{-0.48}$
c_{HWB}	$0.17^{+0.88}_{-1.79}$	$0.00^{+0.77}_{-0.96}$
c_{HB}	$0.03^{+0.13}_{-0.26}$	$0.00^{+0.11}_{-0.14}$
$c_{H\tilde{W}}$	$-0.26^{+0.67}_{-0.50}$	$0.00^{+0.48}_{-0.52}$
$c_{H\tilde{W}B}$	$-0.54^{+1.37}_{-1.03}$	$0.00^{+0.99}_{-1.07}$
$c_{H\tilde{B}}$	$-0.08^{+0.20}_{-0.15}$	$0.00^{+0.15}_{-0.16}$

11 Summary

This paper presents a study of the anomalous couplings of the Higgs boson (H) with vector bosons, including *CP* violating effects, using its associated production with hadronic jets in gluon fusion, electroweak vector boson fusion, and associated production with a W or Z boson, and its subsequent decay to a pair of W bosons. The results are based on the proton–proton collision data set collected by the CMS detector at the LHC during 2016–2018, corresponding to an integrated luminosity of 138 fb^{-1} at a center-of-mass energy of 13TeV. The analysis targets the different-flavor dilepton ($e\mu$) final state, with kinematic information from associated jets combined using matrix element techniques to increase sensitivity to anomalous effects at the production vertex. Dedicated Monte Carlo simulation and matrix element reweighting provide modeling of all kinematic features in the production and decay of the Higgs boson with full simulation of detector effects. A simultaneous measurement of four Higgs boson

couplings to electroweak vector bosons has been performed in the framework of a standard model effective field theory. All measurements are consistent with the expectations for the standard model Higgs boson and constraints are set on the fractional contribution of the anomalous couplings to the Higgs boson cross section. The most stringent constraints on the HVV anomalous coupling cross section fractions are at the per mille level. These results are in agreement with those obtained in the $H \to ZZ$ and $H \to \tau\tau$ channels, and also significantly surpass those of the previous $H \to WW$ anomalous coupling analysis from the CMS experiment in both scope and precision.

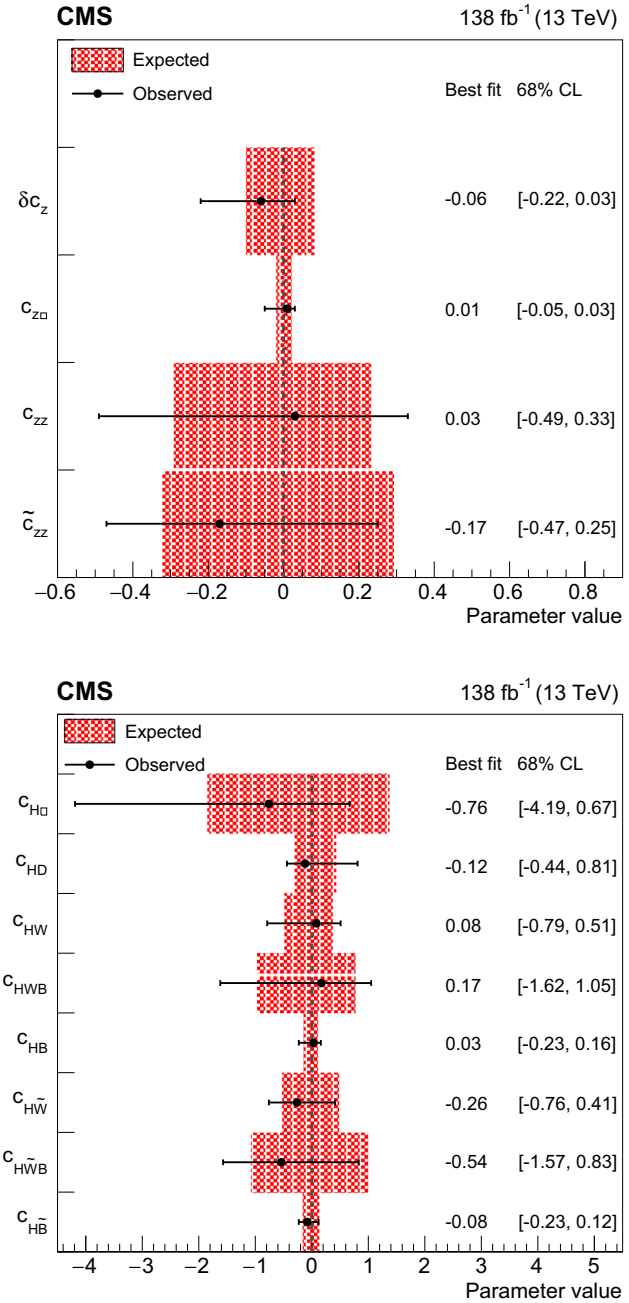

Fig. 12 Summary of constraints on the SMEFT Higgs (upper) and Warsaw (lower) basis coupling parameters with the best fit values and 68% CL uncertainties. For the Warsaw basis, only one of c_{HW} , c_{HWB}, and c_{HB} is independent, the same is also true for $c_{H\tilde{W}}$, c_{HWB}, and $c_{H\tilde{B}}$

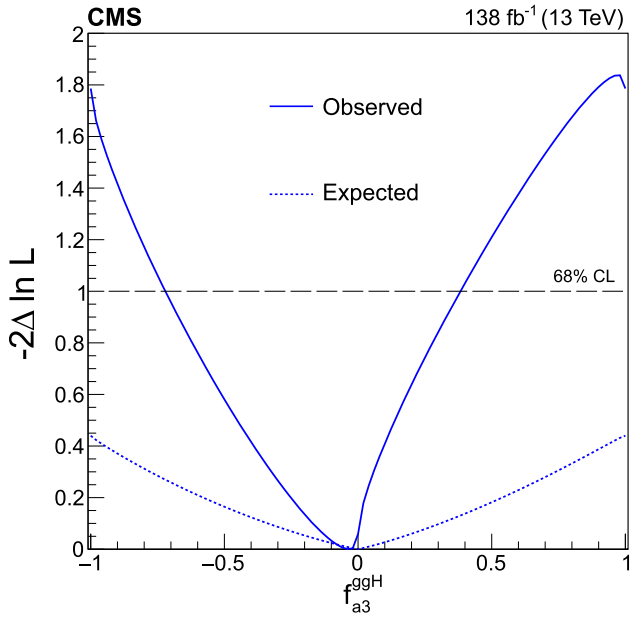

Fig. 13 Expected (dashed) and observed (solid) profiled likelihood on f_{a3}^{ggH}. The signal strength modifiers and the CP-odd HVV anomalous coupling cross section fraction are treated as free parameters. The crossing of the observed likelihood with the dashed horizontal line shows the observed 68% CL region

Acknowledgements We congratulate our colleagues in the CERN accelerator departments for the excellent performance of the LHC and thank the technical and administrative staffs at CERN and at other CMS institutes for their contributions to the success of the CMS effort. In addition, we gratefully acknowledge the computing centers and personnel of the Worldwide LHC Computing Grid and other centers for delivering so effectively the computing infrastructure essential to our analyses. Finally, we acknowledge the enduring support for the construction and operation of the LHC, the CMS detector, and the supporting computing infrastructure provided by the following funding agencies: SC (Armenia), BMBWF and FWF (Austria); FNRS and FWO (Belgium); CNPq, CAPES, FAPERJ, FAPERGS, and FAPESP (Brazil); MES and BNSF (Bulgaria); CERN; CAS, MoST, and NSFC (China); MINCIENCIAS (Colombia); MSES and CSF (Croatia); RIF (Cyprus); SENESCYT (Ecuador); ERC PRG, RVTT3 and MoER TK202 (Estonia); Academy of Finland, MEC, and HIP (Finland); CEA and CNRS/IN2P3 (France); SRNSF (Georgia); BMBF, DFG, and HGF (Germany); GSRI (Greece); NKFIH (Hungary); DAE and DST (India); IPM (Iran); SFI (Ireland); INFN (Italy); MSIP and NRF (Republic of Korea); MES (Latvia); LMTLT (Lithuania); MOE and UM (Malaysia); BUAP, CINVESTAV, CONACYT, LNS, SEP, and UASLP-FAI (Mexico); MOS (Montenegro); MBIE (New Zealand); PAEC (Pakistan); MES and NSC (Poland); FCT (Portugal); MESTD (Serbia); MCIN/AEI and PCTI (Spain); MOSTR (Sri Lanka); Swiss Funding Agencies (Switzerland); MST (Taipei); MHESI and NSTDA (Thailand); TUBITAK and TENMAK (Turkey); NASU (Ukraine); STFC (United Kingdom); DOE and NSF (USA). Rachada-pisek Individuals have received support from the Marie-Curie program and the European Research Council and Horizon 2020 Grant, contract Nos. 675440, 724704, 752730, 758316, 765710, 824093, 101115353, and COST Action CA16108 (European Union); the Leventis Foundation; the Alfred P. Sloan Foundation; the Alexander von Humboldt Foundation; the Science Committee, project no. 22rl-037 (Armenia); the Belgian Federal Science Policy Office; the Fonds pour la Formation à la Recherche dans l'Industrie et dans l'Agriculture (FRIA-Belgium); the Agentschap voor Innovatie door Wetenschap en Technologie (IWT-Belgium); the F.R.S.-FNRS and FWO (Belgium) under the "Excellence of Science – EOS" – be.h project n. 30820817; the Beijing Municipal Science and Technology Commission, No. Z191100007219010 and Fundamental Research Funds for the Central Universities (China); the Ministry of Education, Youth and Sports (MEYS) of the Czech Republic; the Shota Rustaveli National Science Foundation, grant FR-22-985 (Georgia); the Deutsche Forschungsgemeinschaft (DFG), under Germany's Excellence Strategy – EXC 2121 "Quantum Universe" – 390833306, and under project number 400140256 - GRK2497; the Hellenic Foundation for Research and Innovation (HFRI), Project Number 2288 (Greece); the Hungarian Academy of Sciences, the New National Excellence Program - ÚNKP, the NKFIH research grants K 124845, K 124850, K 128713, K 128786, K 129058, K 131991, K 133046, K 138136, K 143460, K 143477, 2020-2.2.1-ED-2021-00181, and TKP2021-NKTA-64 (Hungary); the Council of Science and Industrial Research, India; ICSC – National Research Center for High Performance Computing, Big Data and Quantum Computing, funded by the NextGenerationEU program (Italy); the Latvian Council of Science; the Ministry of Education and Science, project no. 2022/WK/14, and the National Science Center, contracts Opus 2021/41/B/ST2/01369 and 2021/43/B/ST2/01552 (Poland); the Fundação para a Ciência e a Tecnologia, grant CEECIND/01334/2018 (Portugal); the National Priorities Research Program by Qatar National Research Fund; MCIN/AEI/10.13039/501100011033, ERDF "a way of making Europe", and the Programa Estatal de Fomento de la Investigación Científica y Técnica de Excelencia María de Maeztu, grant MDM-2017-0765 and Programa Severo Ochoa del Principado de Asturias (Spain); the Chulalongkorn Academic into Its 2nd Century Project Advancement Project, and the National Science, Research and Innovation Fund via the Program Management Unit for Human Resources and Institutional Development, Research and Innovation, grant B37G660013 (Thailand); the Kavli Foundation; the Nvidia Corporation; the SuperMicro Corporation; the Welch Foundation, contract C-1845; and the Weston Havens Foundation (USA).

Data Availability Statement Data cannot be made available for reasons disclosed in the data availability statement. [Author's comment: Release and preservation of data used by the CMS Collaboration as the basis for publications is guided by the CMS policy as stated in the "CMS data preservation, re-use and open access policy.]

Code Availability Statement This manuscript has no associated code/software. [Author's comment: There is no code availability statement.]

Declarations

Conflict of interest The authors declare that they have no conflict of interest.

Funded by SCOAP[3].

References

1. ATLAS Collaboration, Observation of a new particle in the search for the standard model Higgs boson with the ATLAS detector at the LHC. Phys. Lett. B **716**, 1 (2012). https://doi.org/10.1016/j.physletb.2012.08.020. arXiv:1207.7214
2. C.M.S. Collaboration, Observation of a new boson at a mass of 125 GeV with the CMS experiment at the LHC. Phys. Lett. B **716**, 30 (2012). https://doi.org/10.1016/j.physletb.2012.08.021. arXiv:1207.7235
3. C.M.S. Collaboration, Observation of a new boson with mass near 125 GeV in pp collisions at $\sqrt{s}$ = 7 and 8 TeV. JHEP **06**, 081 (2013). https://doi.org/10.1007/JHEP06(2013)081. arXiv:1303.4571
4. C.M.S. Collaboration, On the mass and spin-parity of the Higgs boson candidate via its decays to Z boson pairs. Phys. Rev. Lett. **110**, 081803 (2013). https://doi.org/10.1103/PhysRevLett.110.081803. arXiv:1212.6639
5. C.M.S. Collaboration, Measurement of the properties of a Higgs boson in the four-lepton final state. Phys. Rev. D **89**, 092007 (2014). https://doi.org/10.1103/PhysRevD.89.092007. arXiv:1312.5353
6. C.M.S. Collaboration, Constraints on the spin-parity and anomalous HVV couplings of the Higgs boson in proton collisions at 7 and 8 TeV. Phys. Rev. D **92**, 012004 (2015). https://doi.org/10.1103/PhysRevD.92.012004. arXiv:1411.3441
7. CMS Collaboration, Limits on the Higgs boson lifetime and width from its decay to four charged leptons. Phys. Rev. D **92**, 072010 (2015). https://doi.org/10.1103/PhysRevD.92.072010. arXiv:1507.06656
8. CMS Collaboration, Combined search for anomalous pseudoscalar HVV couplings in VH production and H → VV decay. Phys. Lett. B **759**, 672 (2016). https://doi.org/10.1016/j.physletb.2016.06.004. arXiv:1602.04305
9. CMS Collaboration, Constraints on anomalous Higgs boson couplings using production and decay information in the four-lepton final state. Phys. Lett. B **775**, 1 (2017). https://doi.org/10.1016/j.physletb.2017.10.021. arXiv:1707.00541
10. CMS Collaboration, Measurements of the Higgs boson width and anomalous HVV couplings from on-shell and off-shell production in the four-lepton final state. Phys. Rev. D **99**, 112003 (2019). https://doi.org/10.1103/PhysRevD.99.112003. arXiv:1901.00174
11. CMS Collaboration, Constraints on anomalous HVV couplings from the production of Higgs bosons decaying to τ lepton pairs. Phys. Rev. D **100**, 112002 (2019). https://doi.org/10.1103/PhysRevD.100.112002. arXiv:1903.06973
12. ATLAS Collaboration, Evidence for the spin-0 nature of the Higgs boson using ATLAS data. Phys. Lett. B **726**, 120 (2013). https://doi.org/10.1016/j.physletb.2013.08.026. arXiv:1307.1432
13. ATLAS Collaboration, Study of the spin and parity of the Higgs boson in diboson decays with the ATLAS detector. Eur. Phys. J. C **75**, 476 (2015). https://doi.org/10.1140/epjc/s10052-015-3685-1. arXiv:1506.05669
14. ATLAS Collaboration, Test of CP invariance in vector-boson fusion production of the Higgs boson using the Optimal Observable method in the ditau decay channel with the ATLAS detector. Eur. Phys. J. C **76**, 658 (2016). https://doi.org/10.1140/epjc/s10052-016-4499-5. arXiv:1602.04516
15. ATLAS Collaboration, Measurement of inclusive and differential cross sections in the H → ZZ^* → 4ℓ decay channel in pp collisions at $\sqrt{s}$ = 13 TeV with the ATLAS detector. JHEP **10**, 132 (2017). https://doi.org/10.1007/JHEP10(2017)132. arXiv:1708.02810
16. ATLAS Collaboration, Measurement of the Higgs boson coupling properties in the H → ZZ^* → 4ℓ decay channel at $\sqrt{s}$ = 13 TeV with the ATLAS detector. JHEP **03**, 095 (2018). https://doi.org/10.1007/JHEP03(2018)095. arXiv:1712.02304
17. ATLAS Collaboration, Measurements of Higgs boson properties in the diphoton decay channel with 36 fb^{-1} of pp collision data at $\sqrt{s}$ = 13 TeV with the ATLAS detector. Phys. Rev. D **98**, 052005 (2018). https://doi.org/10.1103/PhysRevD.98.052005. arXiv:1802.04146
18. ATLAS Collaboration, Test of CP invariance in vector-boson fusion production of the Higgs boson in the H → $\tau\tau$ channel in proton–proton collisions at $\sqrt{s}$ = 13 TeV with the ATLAS detector. Phys. Lett. B **805**, 135426 (2020). https://doi.org/10.1016/j.physletb.2020.135426. arXiv:2002.05315
19. LHC Higgs Cross Section Working Group, Handbook of LHC Higgs cross sections: 4. Deciphering the nature of the Higgs sector. CERN Report CERN-2017-002-M (2016). https://doi.org/10.23731/CYRM-2017-002. arXiv:1610.07922
20. Y. Gao et al., Spin determination of single-produced resonances at hadron colliders. Phys. Rev. D **81**, 075022 (2010). https://doi.org/10.1103/PhysRevD.81.075022. arXiv:1001.3396
21. S. Bolognesi et al., On the spin and parity of a single-produced resonance at the LHC. Phys. Rev. D **86**, 095031 (2012). https://doi.org/10.1103/PhysRevD.86.095031. arXiv:1208.4018
22. I. Anderson et al., Constraining anomalous HVV interactions at proton and lepton colliders. Phys. Rev. D **89**, 035007 (2014). https://doi.org/10.1103/PhysRevD.89.035007. arXiv:1309.4819
23. A.V. Gritsan, R. Röntsch, M. Schulze, M. Xiao, Constraining anomalous Higgs boson couplings to the heavy flavor fermions using matrix element techniques. Phys. Rev. D **94**, 055023 (2016). https://doi.org/10.1103/PhysRevD.94.055023. arXiv:1606.03107
24. A.V. Gritsan et al., New features in the JHU generator framework: constraining Higgs boson properties from on-shell and off-shell production. Phys. Rev. D **102**, 056022 (2020). https://doi.org/10.1103/PhysRevD.102.056022. arXiv:2002.09888
25. CMS Collaboration, Measurements of the Higgs boson production cross section and couplings in the W boson pair decay channel in proton–proton collisions at $\sqrt{s}$ = 13 TeV. Eur. Phys. J. C **83**, 667 (2023). https://doi.org/10.1140/epjc/s10052-023-11632-6. arXiv:2206.09466
26. LHC Higgs Cross Section Working Group, Handbook of LHC Higgs cross sections: 3. Higgs properties: report of the LHC Higgs Cross Section Working Group. CERN Report CERN-2013-004 (2013). https://doi.org/10.5170/CERN-2013-004. arXiv:1307.1347
27. CMS Collaboration, Measurements of $t\bar{t}H$ production and the CP structure of the Yukawa interaction between the Higgs boson and top quark in the diphoton decay channel. Phys. Rev. Lett. **125**, 061801 (2020). https://doi.org/10.1103/PhysRevLett.125.061801. arXiv:2003.10866
28. CMS Collaboration, Constraints on anomalous Higgs boson couplings to vector bosons and fermions in its production and decay using the four-lepton final state. Phys. Rev. D **104**, 052004 (2021). https://doi.org/10.1103/physrevd.104.052004. arXiv:2104.12152
29. HEPData record for this analysis (2024). https://doi.org/10.17182/hepdata.146013
30. B. Grzadkowski, M. Iskrzyński, M. Misiak, J. Rosiek, Dimension-six terms in the standard model Lagrangian. JHEP **10**, 085 (2010). https://doi.org/10.1007/jhep10(2010)085. arXiv:1008.4884
31. J. Davis et al., Constraining anomalous Higgs boson couplings to virtual photons. Phys. Rev. D **105**, 096027 (2022). https://doi.org/10.1103/PhysRevD.105.096027. arXiv:2109.13363

32. A.V. Gritsan et al., New features in the JHU generator framework: constraining Higgs boson properties from on-shell and off-shell production. Phys. Rev. D **102** (2020). https://doi.org/10.1103/physrevd.102.056022
33. C.M.S. Collaboration, The CMS experiment at the CERN LHC. JINST **3**, S08004 (2008). https://doi.org/10.1088/1748-0221/3/08/S08004
34. CMS Collaboration, Performance of electron reconstruction and selection with the CMS detector in proton–proton collisions at $\sqrt{s} = 8$ TeV. JINST **10**, P06005 (2015). https://doi.org/10.1088/1748-0221/10/06/P06005. arXiv:1502.02701
35. CMS Collaboration, Performance of the CMS muon detector and muon reconstruction with proton-proton collisions at $\sqrt{s} = 13$ TeV. JINST **13**, P06015 (2018). https://doi.org/10.1088/1748-0221/13/06/P06015. arXiv:1804.04528
36. CMS Collaboration, Performance of photon reconstruction and identification with the CMS detector in proton–proton collisions at sqrt(s) = 8 TeV. JINST **10**, P08010 (2015). https://doi.org/10.1088/1748-0221/10/08/P08010. arXiv:1502.02702
37. C.M.S. Collaboration, Description and performance of track and primary-vertex reconstruction with the CMS tracker. JINST **9**, P10009 (2014). https://doi.org/10.1088/1748-0221/9/10/P10009. arXiv:1405.6569
38. CMS Collaboration, Particle-flow reconstruction and global event description with the CMS detector. JINST **12**, P10003 (2017). https://doi.org/10.1088/1748-0221/12/10/P10003. arXiv:1706.04965
39. CMS Collaboration, Performance of reconstruction and identification of τ leptons decaying to hadrons and ν_τ in pp collisions at $\sqrt{s} = 13$ TeV. JINST **13**, P10005 (2018). https://doi.org/10.1088/1748-0221/13/10/P10005. arXiv:1809.02816
40. CMS Collaboration, Jet energy scale and resolution in the CMS experiment in pp collisions at 8 TeV. JINST **12**, P02014 (2017). https://doi.org/10.1088/1748-0221/12/02/P02014. arXiv:1607.03663
41. CMS Collaboration, Performance of missing transverse momentum reconstruction in proton–proton collisions at $\sqrt{s} = 13$ TeV using the CMS detector. JINST **14**, P07004 (2019). https://doi.org/10.1088/1748-0221/14/07/P07004. arXiv:1903.06078
42. CMS Collaboration, Performance of the CMS Level-1 trigger in proton–proton collisions at $\sqrt{s} = 13$ TeV. JINST **15**, P10017 (2020). https://doi.org/10.1088/1748-0221/15/10/P10017. arXiv:2006.10165
43. C.M.S. Collaboration, The CMS trigger system. JINST **12**, P01020 (2017). https://doi.org/10.1088/1748-0221/12/01/P01020. arXiv:1609.02366
44. CMS Collaboration, Precision luminosity measurement in proton–proton collisions at $\sqrt{s} = 13$ TeV in 2015 and 2016 at CMS. Eur. Phys. J. C **800**, 81 (2021). https://doi.org/10.1140/epjc/s10052-021-09538-2. arXiv:2104.01927
45. CMS Collaboration, CMS luminosity measurement for the 2017 data-taking period at $\sqrt{s} = 13$ TeV. CMS Physics Analysis Summary CMS-PAS-LUM-17-004 (2017). https://cds.cern.ch/record/2621960
46. CMS Collaboration, CMS luminosity measurement for the 2018 data-taking period at $\sqrt{s} = 13$ TeV. CMS Physics Analysis Summary CMS-PAS-LUM-18-002 (2019). https://cds.cern.ch/record/2676164
47. NNPDF Collaboration, Parton distributions with QED corrections. Nucl. Phys. B **877**, 290 (2013). https://doi.org/10.1016/j.nuclphysb.2013.10.010. arXiv:1308.0598
48. NNPDF Collaboration, Unbiased global determination of parton distributions and their uncertainties at NNLO and at LO. Nucl. Phys. B **855**, 153 (2012). https://doi.org/10.1016/j.nuclphysb.2011.09.024. arXiv:1107.2652
49. NNPDF Collaboration, Parton distributions from high-precision collider data. Eur. Phys. J. C **77**, 663 (2017). https://doi.org/10.1140/epjc/s10052-017-5199-5. arXiv:1706.00428
50. CMS Collaboration, Event generator tunes obtained from underlying event and multiparton scattering measurements. Eur. Phys. J. C **76**, 155 (2016). https://doi.org/10.1140/epjc/s10052-016-3988-x. arXiv:1512.00815
51. CMS Collaboration, Extraction and validation of a new set of CMS PYTHIA8 tunes from underlying-event measurements. Eur. Phys. J. C **80**, 4 (2020). https://doi.org/10.1140/epjc/s10052-019-7499-4. arXiv:1903.12179
52. T. Sjöstrand et al., An introduction to PYTHIA 8.2. Comput. Phys. Commun. **191**, 159 (2015). https://doi.org/10.1016/j.cpc.2015.01.024. arXiv:1410.3012
53. P. Nason, A new method for combining NLO QCD with shower Monte Carlo algorithms. JHEP **11**, 040 (2004). https://doi.org/10.1088/1126-6708/2004/11/040. arXiv:hep-ph/0409146
54. S. Frixione, P. Nason, C. Oleari, Matching NLO QCD computations with parton shower simulations: the POWHEG method. JHEP **11**, 070 (2007). https://doi.org/10.1088/1126-6708/2007/11/070. arXiv:0709.2092
55. S. Alioli, P. Nason, C. Oleari, E. Re, A general framework for implementing NLO calculations in shower Monte Carlo programs: the POWHEG BOX. JHEP **06**, 043 (2010). https://doi.org/10.1007/JHEP06(2010)043. arXiv:1002.2581
56. E. Bagnaschi, G. Degrassi, P. Slavich, A. Vicini, Higgs production via gluon fusion in the POWHEG approach in the SM and in the MSSM. JHEP **02**, 088 (2012). https://doi.org/10.1007/JHEP02(2012)088. arXiv:1111.2854
57. P. Nason, C. Oleari, NLO Higgs boson production via vector-boson fusion matched with shower in POWHEG. JHEP **02**, 037 (2010). https://doi.org/10.1007/JHEP02(2010)037. arXiv:0911.5299
58. G. Luisoni, P. Nason, C. Oleari, F. Tramontano, $HW^{\pm}$/HZ + 0 and 1 jet at NLO with the POWHEG BOX interfaced to GoSam and their merging within MiNLO. JHEP **10**, 083 (2013). https://doi.org/10.1007/JHEP10(2013)083. arXiv:1306.2542
59. H.B. Hartanto, B. Jager, L. Reina, D. Wackeroth, Higgs boson production in association with top quarks in the POWHEG BOX. Phys. Rev. D **91**, 094003 (2015). https://doi.org/10.1103/PhysRevD.91.094003. arXiv:1501.04498
60. K. Hamilton, P. Nason, E. Re, G. Zanderighi, NNLOPS simulation of Higgs boson production. JHEP **10**, 222 (2013). https://doi.org/10.1007/JHEP10(2013)222. arXiv:1309.0017
61. K. Hamilton, P. Nason, G. Zanderighi, Finite quark-mass effects in the NNLOPS POWHEG+MiNLO Higgs generator. JHEP **05**, 140 (2015). https://doi.org/10.1007/JHEP05(2015)140. arXiv:1501.04637
62. N. Berger et al., Simplified template cross sections—stage 1.1 (2019). arXiv:1906.02754
63. R. Frederix, K. Hamilton, Extending the MINLO method. JHEP **05**, 042 (2016). https://doi.org/10.1007/JHEP05(2016)042. arXiv:1512.02663
64. J. Alwall et al., The automated computation of tree-level and next-to-leading order differential cross sections, and their matching to parton shower simulations. JHEP **07**, 079 (2014). https://doi.org/10.1007/JHEP07(2014)079. arXiv:1405.0301
65. CMS Collaboration, A measurement of the Higgs boson mass in the diphoton decay channel. Phys. Lett. B **805**, 135425 (2020). https://doi.org/10.1016/j.physletb.2020.135425. arXiv:2002.06398
66. P. Nason, C. Oleari, M. Rocco, M. Zaro, An interface between the POWHEG BOX and MadGraph5_aMC@NLO. Eur. Phys. J. C **80**, 10 (2020). https://doi.org/10.1140/epjc/s10052-020-08559-7. arXiv:2008.06364

67. P. Nason, G. Zanderighi, W^+W^-, WZ and ZZ production in the POWHEG-BOX-V2. Eur. Phys. J. C **74**, 2702 (2014). https://doi.org/10.1140/epjc/s10052-013-2702-5. arXiv:1311.1365
68. P. Meade, H. Ramani, M. Zeng, Transverse momentum resummation effects in W^+W^- measurements. Phys. Rev. D **90**, 114006 (2014). https://doi.org/10.1103/PhysRevD.90.114006. arXiv:1407.4481
69. P. Jaiswal, T. Okui, Explanation of the WW excess at the LHC by jet-veto resummation. Phys. Rev. D **90**, 073009 (2014). https://doi.org/10.1103/PhysRevD.90.073009. arXiv:1407.4537
70. J.M. Campbell, R.K. Ellis, An update on vector boson pair production at hadron colliders. Phys. Rev. D **60**, 113006 (1999). https://doi.org/10.1103/PhysRevD.60.113006. arXiv:hep-ph/9905386
71. J.M. Campbell, R.K. Ellis, C. Williams, Vector boson pair production at the LHC. JHEP **07**, 018 (2011). https://doi.org/10.1007/JHEP07(2011)018. arXiv:1105.0020
72. J.M. Campbell, R.K. Ellis, W.T. Giele, A multi-threaded version of MCFM. Eur. Phys. J. C **75**, 246 (2015). https://doi.org/10.1140/epjc/s10052-015-3461-2. arXiv:1503.06182
73. F. Caola et al., QCD corrections to vector boson pair production in gluon fusion including interference effects with off-shell Higgs at the LHC. JHEP **07**, 087 (2016). https://doi.org/10.1007/JHEP07(2016)087. arXiv:1605.04610
74. J. Alwall et al., Comparative study of various algorithms for the merging of parton showers and matrix elements in hadronic collisions. Eur. Phys. J. C **53**, 473 (2008). https://doi.org/10.1140/epjc/s10052-007-0490-5. arXiv:0706.2569
75. S. Frixione, P. Nason, G. Ridolfi, A positive-weight next-to-leading-order Monte Carlo for heavy flavour hadroproduction. JHEP **09**, 126 (2007). https://doi.org/10.1088/1126-6708/2007/09/126. arXiv:0707.3088
76. S. Alioli, P. Nason, C. Oleari, E. Re, NLO single-top production matched with shower in POWHEG: s- and t-channel contributions. JHEP **09**, 111 (2009). arXiv:0907.4076. [Erratum: https://doi.org/10.1007/JHEP02(2010)011]
77. E. Re, Single-top Wt-channel production matched with parton showers using the POWHEG method. Eur. Phys. J. C **71**, 1547 (2011). https://doi.org/10.1140/epjc/s10052-011-1547-z. arXiv:1009.2450
78. M. Czakon et al., Top-pair production at the LHC through NNLO QCD and NLO EW. JHEP **10**, 186 (2017). https://doi.org/10.1007/JHEP10(2017)186. arXiv:1705.04105
79. R. Frederix, S. Frixione, Merging meets matching in MC@NLO. JHEP **12**, 061 (2012). https://doi.org/10.1007/JHEP12(2012)061. arXiv:1209.6215
80. GEANT4 Collaboration, GEANT4–a simulation toolkit. Nucl. Instrum. Methods A **506**, 250 (2003). https://doi.org/10.1016/S0168-9002(03)01368-8
81. C.M.S. Collaboration, Muon identification using multivariate techniques in the CMS experiment in proton-proton collisions at $\sqrt{s}$ = 13 TeV. INST **19**, P02031 (2024). https://doi.org/10.1088/1748-0221/19/02/P02031
82. W. Waltenberger, R. Frühwirth, P. Vanlaer, Adaptive vertex fitting. J. Phys. G **34**, N343 (2007). https://doi.org/10.1088/0954-3899/34/12/N01
83. CMS Collaboration, Technical proposal for the Phase-II upgrade of the Compact Muon Solenoid. CMS Technical Proposal CERN-LHCC-2015-010, CMS-TDR-15-02 (2015). http://cds.cern.ch/record/2020886
84. CMS Collaboration, Pileup mitigation at CMS in 13 TeV data. JINST **15**, P09018 (2020). https://doi.org/10.1088/1748-0221/15/09/p09018. arXiv:2003.00503
85. D. Bertolini, P. Harris, M. Low, N. Tran, Pileup per particle identification. JHEP **10**, 059 (2014). https://doi.org/10.1007/JHEP10(2014)059. arXiv:1407.6013
86. J. Thaler, K. Van Tilburg, Identifying boosted objects with N-subjettiness. JHEP **03**, 015 (2011). https://doi.org/10.1007/JHEP03(2011)015. arXiv:1011.2268
87. M. Dasgupta, A. Fregoso, S. Marzani, G.P. Salam, Towards an understanding of jet substructure. JHEP **09**, 029 (2013). https://doi.org/10.1007/JHEP09(2013)029. arXiv:1307.0007
88. J.M. Butterworth, A.R. Davison, M. Rubin, G.P. Salam, Jet substructure as a new Higgs search channel at the LHC. Phys. Rev. Lett. **100**, 242001 (2008). https://doi.org/10.1103/PhysRevLett.100.242001. arXiv:0802.2470
89. A.J. Larkoski, S. Marzani, G. Soyez, J. Thaler, Soft drop. JHEP **05**, 146 (2014). https://doi.org/10.1007/JHEP05(2014)146. arXiv:1402.2657
90. CMS Collaboration, Identification of heavy-flavour jets with the CMS detector in pp collisions at 13 TeV. JINST **13**, P05011 (2018). https://doi.org/10.1088/1748-0221/13/05/P05011. arXiv:1712.07158
91. CMS Collaboration, CMS Phase 1 heavy flavour identification performance and developments. CMS Detector Performance Summary CMS-DP-2020-019 (2017). http://cds.cern.ch/record/2263802
92. CMS Collaboration, Measurements of properties of the Higgs boson decaying to a W boson pair in pp collisions at $\sqrt{s} = 13$ TeV. Phys. Lett. B **791**, 96 (2019). https://doi.org/10.1016/j.physletb.2018.12.073. arXiv:1806.05246
93. C.M.S. Collaboration, Measurements of inclusive W and Z cross sections in pp collisions at $\sqrt{s} = 7$ TeV. JHEP **01**, 080 (2011). https://doi.org/10.1007/JHEP01(2011)080. arXiv:1012.2466
94. CMS Collaboration, An embedding technique to determine $\tau\tau$ backgrounds in proton–proton collision data. JINST **14**, P06032 (2019). https://doi.org/10.1088/1748-0221/14/06/P06032. arXiv:1903.01216
95. C.M.S. Collaboration, Identification techniques for highly boosted W bosons that decay into hadrons. JHEP **12**, 017 (2014). https://doi.org/10.1007/JHEP12(2014)017. arXiv:1410.4227
96. R. Barlow, C. Beeston, Fitting using finite Monte Carlo samples. Comput. Phys. Commun. **77**, 219 (1993). https://doi.org/10.1016/0010-4655(93)90005-W
97. ATLAS Collaboration, Measurement of the inelastic proton–proton cross section at $\sqrt{s} = 13$ TeV with the ATLAS detector at the LHC. Phys. Rev. Lett. **117**, 182002 (2016). https://doi.org/10.1103/PhysRevLett.117.182002. arXiv:1606.02625
98. CMS Collaboration, Measurement of the inelastic proton–proton cross section at $\sqrt{s} = 13$ TeV. JHEP **07**, 161 (2018). https://doi.org/10.1007/JHEP07(2018)161. arXiv:1802.02613
99. G. Passarino, Higgs CAT. Eur. Phys. J. C **74**, 2866 (2014). https://doi.org/10.1140/epjc/s10052-014-2866-7. arXiv:1312.2397
100. C.M.S. Collaboration, Measurement of Higgs boson production and properties in the WW decay channel with leptonic final states. JHEP **01**, 096 (2014). https://doi.org/10.1007/JHEP01(2014)096. arXiv:1312.1129
101. The ATLAS Collaboration, The CMS Collaboration, The LHC Higgs Combination Group, Procedure for the LHC Higgs boson search combination in Summer 2011. Technical Report ATL-PHYS-PUB 2011-11, CMS NOTE 2011/005 (2011). https://cds.cern.ch/record/1379837
102. CMS Collaboration, Combined measurements of Higgs boson couplings in proton–proton collisions at $\sqrt{s} = 13$ TeV. Eur. Phys. J. C **79**, 421 (2019). https://doi.org/10.1140/epjc/s10052-019-6909-y. arXiv:1809.10733
103. S.S. Wilks, The large-sample distribution of the likelihood ratio for testing composite hypotheses. Ann. Math. Stat. **9**, 60 (1938). https://doi.org/10.1214/aoms/1177732360

104. G. Cowan, K. Cranmer, E. Gross, O. Vitells, Asymptotic formulae for likelihood-based tests of new physics. Eur. Phys. J. C **71**, 1554 (2011). https://doi.org/10.1140/epjc/s10052-011-1554-0. arXiv:1007.1727

CMS Collaboration

Yerevan Physics Institute, Yerevan, Armenia
A. Hayrapetyan, A. Tumasyan[1]

Institut für Hochenergiephysik, Vienna, Austria
W. Adam, J. W. Andrejkovic, T. Bergauer, S. Chatterjee, K. Damanakis, M. Dragicevic, P. S. Hussain, M. Jeitler[2], N. Krammer, A. Li, D. Liko, I. Mikulec, J. Schieck[2], R. Schöfbeck, D. Schwarz, M. Sonawane, S. Templ, W. Waltenberger, C.-E. Wulz[2]

Universiteit Antwerpen, Antwerp, Belgium
M. R. Darwish[3], T. Janssen, P. Van Mechelen

Vrije Universiteit Brussel, Brussels, Belgium
E. S. Bols, J. D'Hondt, S. Dansana, A. De Moor, M. Delcourt, H. El Faham, S. Lowette, I. Makarenko, D. Müller, A. R. Sahasransu, S. Tavernier, M. Tytgat[4], G. P. Van Onsem, S. Van Putte, D. Vannerom

Université Libre de Bruxelles, Brussels, Belgium
B. Clerbaux, A. K. Das, G. De Lentdecker, L. Favart, P. Gianneios, D. Hohov, J. Jaramillo, A. Khalilzadeh, K. Lee, M. Mahdavikhorrami, A. Malara, S. Paredes, L. Pétré, N. Postiau, L. Thomas, M. Vanden Bemden, C. Vander Velde, P. Vanlaer

Ghent University, Ghent, Belgium
M. De Coen, D. Dobur, Y. Hong, J. Knolle, L. Lambrecht, G. Mestdach, K. Mota Amarilo, C. Rendón, A. Samalan, K. Skovpen, N. Van Den Bossche, J. van der Linden, L. Wezenbeek

Université Catholique de Louvain, Louvain-la-Neuve, Belgium
A. Benecke, A. Bethani, G. Bruno, C. Caputo, C. Delaere, I. S. Donertas, A. Giammanco, K. Jaffel, Sa. Jain, V. Lemaitre, J. Lidrych, P. Mastrapasqua, K. Mondal, T. T. Tran, S. Wertz

Centro Brasileiro de Pesquisas Fisicas, Rio de Janeiro, Brazil
G. A. Alves, E. Coelho, C. Hensel, T. Menezes De Oliveira, A. Moraes, P. Rebello Teles, M. Soeiro

Universidade do Estado do Rio de Janeiro, Rio de Janeiro, Brazil
W. L. Aldá Júnior, M. Alves Gallo Pereira, M. Barroso Ferreira Filho, H. Brandao Malbouisson, W. Carvalho, J. Chinellato[5], E. M. Da Costa, G. G. Da Silveira[6], D. De Jesus Damiao, S. Fonseca De Souza, R. Gomes De Souza, J. Martins[7], C. Mora Herrera, L. Mundim, H. Nogima, J. P. Pinheiro, A. Santoro, A. Sznajder, M. Thiel, A. Vilela Pereira

Universidade Estadual Paulista, Universidade Federal do ABC, São Paulo, Brazil
C. A. Bernardes[6], L. Calligaris, T. R. Fernandez Perez Tomei, E. M. Gregores, P. G. Mercadante, S. F. Novaes, B. Orzari, Sandra S. Padula

Institute for Nuclear Research and Nuclear Energy, Bulgarian Academy of Sciences, Sofia, Bulgaria
A. Aleksandrov, G. Antchev, R. Hadjiiska, P. Iaydjiev, M. Misheva, M. Shopova, G. Sultanov

University of Sofia, Sofia, Bulgaria
A. Dimitrov, L. Litov, B. Pavlov, P. Petkov, A. Petrov, E. Shumka

Instituto De Alta Investigación, Universidad de Tarapacá, Casilla 7 D, Arica, Chile
S. Keshri, S. Thakur

Beihang University, Beijing, China
T. Cheng, T. Javaid, L. Yuan

Department of Physics, Tsinghua University, Beijing, China
Z. Hu, J. Liu, K. Yi[8,9]

Institute of High Energy Physics, Beijing, China
G. M. Chen[10], H. S. Chen[10], M. Chen[10], F. Iemmi, C. H. Jiang, A. Kapoor[11], H. Liao, Z.-A. Liu[12], R. Sharma[13], J. N. Song[12], J. Tao, C. Wang[10], J. Wang, Z. Wang[10], H. Zhang

State Key Laboratory of Nuclear Physics and Technology, Peking University, Beijing, China
A. Agapitos, Y. Ban, A. Levin, C. Li, Q. Li, Y. Mao, S. J. Qian, X. Sun, D. Wang, H. Yang, L. Zhang, C. Zhou

Sun Yat-Sen University, Guangzhou, China
Z. You

University of Science and Technology of China, Hefei, China
N. Lu

Nanjing Normal University, Nanjing, China
G. Bauer[14]

Institute of Modern Physics and Key Laboratory of Nuclear Physics and Ion-beam Application (MOE)-Fudan University, Shanghai, China
X. Gao[15], D. Leggat, H. Okawa

Zhejiang University, Hangzhou, Zhejiang, China
Z. Lin, C. Lu, M. Xiao

Universidad de Los Andes, Bogotá, Colombia
C. Avila, D. A. Barbosa Trujillo, A. Cabrera, C. Florez, J. Fraga, J. A. Reyes Vega

Universidad de Antioquia, Medellín, Colombia
J. Mejia Guisao, F. Ramirez, M. Rodriguez, J. D. Ruiz Alvarez

Faculty of Electrical Engineering, Mechanical Engineering and Naval Architecture, University of Split, Split, Croatia
D. Giljanovic, N. Godinovic, D. Lelas, A. Sculac

Faculty of Science, University of Split, Split, Croatia
M. Kovac, T. Sculac

Institute Rudjer Boskovic, Zagreb, Croatia
P. Bargassa, V. Brigljevic, B. K. Chitroda, D. Ferencek, S. Mishra, A. Starodumov[16], T. Susa

University of Cyprus, Nicosia, Cyprus
A. Attikis, K. Christoforou, S. Konstantinou, J. Mousa, C. Nicolaou, F. Ptochos, P. A. Razis, H. Rykaczewski, H. Saka, A. Stepennov

Charles University, Prague, Czech Republic
M. Finger, M. Finger Jr., A. Kveton

Escuela Politecnica Nacional, Quito, Ecuador
E. Ayala

Universidad San Francisco de Quito, Quito, Ecuador
E. Carrera Jarrin

Academy of Scientific Research and Technology of the Arab Republic of Egypt, Egyptian Network of High Energy Physics, Cairo, Egypt
S. Elgammal[17], A. Ellithi Kamel[18]

Center for High Energy Physics (CHEP-FU), Fayoum University, El-Fayoum, Egypt
M. A. Mahmoud, Y. Mohammed

National Institute of Chemical Physics and Biophysics, Tallinn, Estonia
K. Ehataht, M. Kadastik, T. Lange, S. Nandan, C. Nielsen, J. Pata, M. Raidal, L. Tani, C. Veelken

Department of Physics, University of Helsinki, Helsinki, Finland
H. Kirschenmann, K. Osterberg, M. Voutilainen

Helsinki Institute of Physics, Helsinki, Finland
S. Bharthuar, E. Brücken, F. Garcia, K. T. S. Kallonen, R. Kinnunen, T. Lampén, K. Lassila-Perini, S. Lehti, T. Lindén, L. Martikainen, M. Myllymäki, M. M. Rantanen, H. Siikonen, E. Tuominen, J. Tuominiemi

Lappeenranta-Lahti University of Technology, Lappeenranta, Finland
P. Luukka, H. Petrow

IRFU, CEA, Université Paris-Saclay, Gif-sur-Yvette, France
M. Besancon, F. Couderc, M. Dejardin, D. Denegri, J. L. Faure, F. Ferri, S. Ganjour, P. Gras, G. Hamel de Monchenault, V. Lohezic, J. Malcles, J. Rander, A. Rosowsky, M. Ö. Sahin, A. Savoy-Navarro[19], P. Simkina, M. Titov, M. Tornago

Laboratoire Leprince-Ringuet, CNRS/IN2P3, Ecole Polytechnique, Institut Polytechnique de Paris, Palaiseau, France
C. Baldenegro Barrera, F. Beaudette, A. Buchot Perraguin, P. Busson, A. Cappati, C. Charlot, M. Chiusi, F. Damas, O. Davignon, A. De Wit, B. A. Fontana Santos Alves, S. Ghosh, A. Gilbert, R. Granier de Cassagnac, A. Hakimi, B. Harikrishnan, L. Kalipoliti, G. Liu, J. Motta, M. Nguyen, C. Ochando, L. Portales, R. Salerno, J. B. Sauvan, Y. Sirois, A. Tarabini, E. Vernazza, A. Zabi, A. Zghiche

Université de Strasbourg, CNRS, IPHC UMR 7178, Strasbourg, France
J.-L. Agram[20], J. Andrea, D. Apparu, D. Bloch, J.-M. Brom, E. C. Chabert, C. Collard, S. Falke, U. Goerlach, C. Grimault, R. Haeberle, A.-C. Le Bihan, M. Meena, G. Saha, M. A. Sessini, P. Van Hove

Institut de Physique des 2 Infinis de Lyon (IP2I), Villeurbanne, France
S. Beauceron, B. Blancon, G. Boudoul, N. Chanon, J. Choi, D. Contardo, P. Depasse, C. Dozen[21], H. El Mamouni, J. Fay, S. Gascon, M. Gouzevitch, C. Greenberg, G. Grenier, B. Ille, I. B. Laktineh, M. Lethuillier, L. Mirabito, S. Perries, A. Purohit, M. Vander Donckt, P. Verdier, J. Xiao

Georgian Technical University, Tbilisi, Georgia
G. Adamov, I. Lomidze, Z. Tsamalaidze[16]

I. Physikalisches Institut, RWTH Aachen University, Aachen, Germany
V. Botta, L. Feld, K. Klein, M. Lipinski, D. Meuser, A. Pauls, N. Röwert, M. Teroerde

RWTH Aachen University, III. Physikalisches Institut A, Aachen, Germany
S. Diekmann, A. Dodonova, N. Eich, D. Eliseev, F. Engelke, J. Erdmann, M. Erdmann, P. Fackeldey, B. Fischer, T. Hebbeker, K. Hoepfner, F. Ivone, A. Jung, M. Y. Lee, L. Mastrolorenzo, F. Mausolf, M. Merschmeyer, A. Meyer, S. Mukherjee, D. Noll, F. Nowotny, A. Pozdnyakov, Y. Rath, W. Redjeb, F. Rehm, H. Reithler, U. Sarkar, V. Sarkisovi, A. Schmidt, A. Sharma, J. L. Spah, A. Stein, F. Torres Da Silva De Araujo[22], L. Vigilante, S. Wiedenbeck, S. Zaleski

RWTH Aachen University, III. Physikalisches Institut B, Aachen, Germany
C. Dziwok, G. Flügge, W. Haj Ahmad[23], T. Kress, A. Nowack, O. Pooth, A. Stahl, T. Ziemons, A. Zotz

Deutsches Elektronen-Synchrotron, Hamburg, Germany
H. Aarup Petersen, M. Aldaya Martin, J. Alimena, S. Amoroso, Y. An, S. Baxter, M. Bayatmakou, H. Becerril Gonzalez, O. Behnke, A. Belvedere, S. Bhattacharya, F. Blekman[24], K. Borras[25], A. Campbell, A. Cardini, C. Cheng, F. Colombina, S. Consuegra Rodríguez, G. Correia Silva, M. De Silva, G. Eckerlin, D. Eckstein, L. I. Estevez Banos, O. Filatov, E. Gallo[24], A. Geiser, A. Giraldi, G. Greau, V. Guglielmi, M. Guthoff, A. Hinzmann, A. Jafari[26], L. Jeppe, N. Z. Jomhari, B. Kaech, M. Kasemann,

C. Kleinwort, R. Kogler, M. Komm, D. Krücker, W. Lange, D. Leyva Pernia, K. Lipka[27], W. Lohmann[28], R. Mankel, I.-A. Melzer-Pellmann, M. Mendizabal Morentin, A. B. Meyer, G. Milella, A. Mussgiller, L. P. Nair, A. Nürnberg, Y. Otarid, J. Park, D. Pérez Adán, E. Ranken, A. Raspereza, B. Ribeiro Lopes, J. Rübenach, A. Saggio, M. Scham[25,29], S. Schnake[25], P. Schütze, C. Schwanenberger[24], D. Selivanova, K. Sharko, M. Shchedrolosiev, R. E. Sosa Ricardo, D. Stafford, F. Vazzoler, A. Ventura Barroso, R. Walsh, Q. Wang, Y. Wen, K. Wichmann, L. Wiens[25], C. Wissing, Y. Yang, A. Zimermmane Castro Santos

University of Hamburg, Hamburg, Germany
A. Albrecht, S. Albrecht, M. Antonello, S. Bein, L. Benato, S. Bollweg, M. Bonanomi, P. Connor, M. Eich, K. El Morabit, Y. Fischer, A. Fröhlich, C. Garbers, E. Garutti, A. Grohsjean, M. Hajheidari, J. Haller, H. R. Jabusch, G. Kasieczka, P. Keicher, R. Klanner, W. Korcari, T. Kramer, V. Kutzner, F. Labe, J. Lange, A. Lobanov, C. Matthies, A. Mehta, L. Moureaux, M. Mrowietz, A. Nigamova, Y. Nissan, A. Paasch, K. J. Pena Rodriguez, T. Quadfasel, B. Raciti, M. Rieger, D. Savoiu, J. Schindler, P. Schleper, M. Schröder, J. Schwandt, M. Sommerhalder, H. Stadie, G. Steinbrück, A. Tews, M. Wolf

Karlsruher Institut fuer Technologie, Karlsruhe, Germany
S. Brommer, M. Burkart, E. Butz, T. Chwalek, A. Dierlamm, A. Droll, N. Faltermann, M. Giffels, A. Gottmann, F. Hartmann[30], R. Hofsaess, M. Horzela, U. Husemann, J. Kieseler, M. Klute, R. Koppenhöfer, J. M. Lawhorn, M. Link, A. Lintuluoto, S. Maier, S. Mitra, M. Mormile, Th. Müller, M. Neukum, M. Oh, M. Presilla, G. Quast, K. Rabbertz, B. Regnery, N. Shadskiy, I. Shvetsov, H. J. Simonis, M. Toms, N. Trevisani, R. Ulrich, R. F. Von Cube, M. Wassmer, S. Wieland, F. Wittig, R. Wolf, X. Zuo

Institute of Nuclear and Particle Physics (INPP), NCSR Demokritos, Agia Paraskevi, Greece
G. Anagnostou, G. Daskalakis, A. Kyriakis, A. Papadopoulos[30], A. Stakia

National and Kapodistrian University of Athens, Athens, Greece
P. Kontaxakis, G. Melachroinos, A. Panagiotou, I. Papavergou, I. Paraskevas, N. Saoulidou, K. Theofilatos, E. Tziaferi, K. Vellidis, I. Zisopoulos

National Technical University of Athens, Athens, Greece
G. Bakas, T. Chatzistavrou, G. Karapostoli, K. Kousouris, I. Papakrivopoulos, E. Siamarkou, G. Tsipolitis, A. Zacharopoulou

University of Ioánnina, Ioannina, Greece
K. Adamidis, I. Bestintzanos, I. Evangelou, C. Foudas, C. Kamtsikis, P. Katsoulis, P. Kokkas, P. G. Kosmoglou Kioseoglou, N. Manthos, I. Papadopoulos, J. Strologas

HUN-REN Wigner Research Centre for Physics, Budapest, Hungary
M. Bartók[31], C. Hajdu, D. Horvath[32,33], K. Márton, F. Sikler, V. Veszpremi

MTA-ELTE Lendület CMS Particle and Nuclear Physics Group, Eötvös Loránd University, Budapest, Hungary
M. Csanád, K. Farkas, M. M. A. Gadallah[34], Á. Kadlecsik, P. Major, K. Mandal, G. Pásztor, A. J. Rádl[35], G. I. Veres

Faculty of Informatics, University of Debrecen, Debrecen, Hungary
P. Raics, B. Ujvari, G. Zilizi

Institute of Nuclear Research ATOMKI, Debrecen, Hungary
G. Bencze, S. Czellar, J. Molnar, Z. Szillasi

MATE Institute of Technology, Karoly Robert Campus, Gyongyos, Hungary
T. Csorgo[35], F. Nemes[35], T. Novak

Panjab University, Chandigarh, India
J. Babbar, S. Bansal, S. B. Beri, V. Bhatnagar, G. Chaudhary, S. Chauhan, N. Dhingra[36], A. Kaur, A. Kaur, H. Kaur, M. Kaur, S. Kumar, K. Sandeep, T. Sheokand, J. B. Singh, A. Singla

University of Delhi, Delhi, India
A. Ahmed, A. Bhardwaj, A. Chhetri, B. C. Choudhary, A. Kumar, A. Kumar, M. Naimuddin, K. Ranjan, S. Saumya

Saha Institute of Nuclear Physics, HBNI, Kolkata, India
S. Baradia, S. Barman[37], S. Bhattacharya, S. Dutta, S. Dutta, S. Sarkar

Indian Institute of Technology Madras, Chennai, India
M. M. Ameen, P. K. Behera, S. C. Behera, S. Chatterjee, P. Jana, P. Kalbhor, J. R. Komaragiri[38], D. Kumar[38], L. Panwar[38], P. R. Pujahari, N. R. Saha, A. Sharma, A. K. Sikdar, S. Verma

Tata Institute of Fundamental Research-A, Mumbai, India
S. Dugad, M. Kumar, G. B. Mohanty, P. Suryadevara

Tata Institute of Fundamental Research-B, Mumbai, India
A. Bala, S. Banerjee, R. M. Chatterjee, R. K. Dewanjee[39], M. Guchait, Sh. Jain, A. Jaiswal, S. Karmakar, S. Kumar, G. Majumder, K. Mazumdar, S. Parolia, A. Thachayath

National Institute of Science Education and Research, An OCC of Homi Bhabha National Institute, Bhubaneswar, Odisha, India
S. Bahinipati[40], C. Kar, D. Maity[41], P. Mal, T. Mishra, V. K. Muraleedharan Nair Bindhu[41], K. Naskar[41], A. Nayak[41], P. Sadangi, P. Saha, S. K. Swain, S. Varghese[41], D. Vats[41]

Indian Institute of Science Education and Research (IISER), Pune, India
S. Acharya[42], A. Alpana, S. Dube, B. Gomber[42], B. Kansal, A. Laha, B. Sahu[42], S. Sharma, K. Y. Vaish

Isfahan University of Technology, Isfahan, Iran
H. Bakhshiansohi[43], E. Khazaie[44], M. Zeinali[45]

Institute for Research in Fundamental Sciences (IPM), Tehran, Iran
S. Chenarani[46], S. M. Etesami, M. Khakzad, M. Mohammadi Najafabadi

University College Dublin, Dublin, Ireland
M. Grunewald

INFN Sezione di Bari[a], Università di Bari[b], Politecnico di Bari[c], Bari, Italy
M. Abbrescia[a,b], R. Aly[a,c,47], A. Colaleo[a,b], D. Creanza[a,c], B. D'Anzi[a,b], N. De Filippis[a,c], M. De Palma[a,b], A. Di Florio[a,c], W. Elmetenawee[a,b,47], L. Fiore[a], G. Iaselli[a,c], M. Louka[a,b], G. Maggi[a,c], M. Maggi[a], I. Margjeka[a,b], V. Mastrapasqua[a,b], S. My[a,b], S. Nuzzo[a,b], A. Pellecchia[a,b], A. Pompili[a,b], G. Pugliese[a,c], R. Radogna[a], G. Ramirez-Sanchez[a,c], D. Ramos[a], A. Ranieri[a], L. Silvestris[a], F. M. Simone[a,b], Ü. Sözbilir[a], A. Stamerra[a], R. Venditti[a], P. Verwilligen[a], A. Zaza[a,b]

INFN Sezione di Bologna[a], Università di Bologna[b], Bologna, Italy
G. Abbiendi[a], C. Battilana[a,b], D. Bonacorsi[a,b], L. Borgonovi[a], R. Campanini[a,b], P. Capiluppi[a,b], A. Castro[a,b], F. R. Cavallo[a], M. Cuffiani[a,b], G. M. Dallavalle[a], T. Diotalevi[a,b], F. Fabbri[a], A. Fanfani[a,b], D. Fasanella[a,b], P. Giacomelli[a], L. Giommi[a,b], C. Grandi[a], L. Guiducci[a,b], S. Lo Meo[a,48], L. Lunerti[a,b], G. Masetti[a], F. L. Navarria[a,b], A. Perrotta[a], F. Primavera[a,b], A. M. Rossi[a,b], T. Rovelli[a,b], G. P. Siroli[a,b]

INFN Sezione di Catania[a], Università di Catania[b], Catania, Italy
S. Costa[a,b,49], A. Di Mattia[a], R. Potenza[a,b], A. Tricomi[a,b,49], C. Tuve[a,b]

INFN Sezione di Firenze[a], Università di Firenze[b], Florence, Italy
P. Assiouras[a], G. Barbagli[a], G. Bardelli[a,b], B. Camaiani[a,b], A. Cassese[a], R. Ceccarelli[a], V. Ciulli[a,b], C. Civinini[a], R. D'Alessandro[a,b], E. Focardi[a,b], T. Kello[a], G. Latino[a,b], P. Lenzi[a,b], M. Lizzo[a], M. Meschini[a], S. Paoletti[a], A. Papanastassiou[a,b], G. Sguazzoni[a], L. Viliani[a]

INFN Laboratori Nazionali di Frascati, Frascati, Italy
L. Benussi, S. Bianco, S. Meola[50], D. Piccolo

INFN Sezione di Genova[a], Università di Genova[b], Genoa, Italy
P. Chatagnon[a], F. Ferro[a], E. Robutti[a], S. Tosi[a,b]

INFN Sezione di Milano-Bicocca[a], Università di Milano-Bicocca[b], Milan, Italy
A. Benaglia[a], G. Boldrini[a,b], F. Brivio[a], F. Cetorelli[a], F. De Guio[a,b], M. E. Dinardo[a,b], P. Dini[a], S. Gennai[a], R. Gerosa[a,b], A. Ghezzi[a,b], P. Govoni[a,b], L. Guzzi[a], M. T. Lucchini[a,b], M. Malberti[a], S. Malvezzi[a], A. Massironi[a], D. Menasce[a], L. Moroni[a], M. Paganoni[a,b], D. Pedrini[a], B. S. Pinolini[a], S. Ragazzi[a,b], T. Tabarelli de Fatis[a,b], D. Zuolo[a]

INFN Sezione di Napoli[a], Università di Napoli 'Federico II'[b], Naples, Italy; Università della Basilicata[c], Potenza, Italy; Scuola Superiore Meridionale (SSM)[d], Naples, Italy
S. Buontempo[a], A. Cagnotta[a,b], F. Carnevali[a,b], N. Cavallo[a,c], F. Fabozzi[a,c], A. O. M. Iorio[a,b], L. Lista[a,b,51], P. Paolucci[a,30], B. Rossi[a], C. Sciacca[a,b]

INFN Sezione di Padova[a], Università di Padova[b], Padova, Italy; Università di Trento[c], Trento, Italy
R. Ardino[a], P. Azzi[a], N. Bacchetta[a,52], D. Bisello[a,b], P. Bortignon[a], A. Bragagnolo[a,b], R. Carlin[a,b], P. Checchia[a], T. Dorigo[a], F. Gasparini[a,b], U. Gasparini[a,b], F. Gonella[a], E. Lusiani[a], M. Margoni[a,b], F. Marini[a], M. Migliorini[a,b], J. Pazzini[a,b], P. Ronchese[a,b], R. Rossin[a,b], F. Simonetto[a,b], G. Strong[a], M. Tosi[a,b], A. Triossi[a,b], S. Ventura[a], H. Yarar[a,b], M. Zanetti[a,b], P. Zotto[a,b], A. Zucchetta[a,b], G. Zumerle[a,b]

INFN Sezione di Pavia[a], Università di Pavia[b], Pavia, Italy
S. Abu Zeid[a,53], C. Aimè[a,b], A. Braghieri[a], S. Calzaferri[a], D. Fiorina[a], P. Montagna[a,b], V. Re[a], C. Riccardi[a,b], P. Salvini[a], I. Vai[a,b], P. Vitulo[a,b]

INFN Sezione di Perugia[a], Università di Perugia[b], Perugia, Italy
S. Ajmal[a,b], G. M. Bilei[a], D. Ciangottini[a,b], L. Fanò[a,b], M. Magherini, G. Mantovani[a,b], V. Mariani[a,b], M. Menichelli[a], F. Moscatelli[a,54], A. Rossi[a,b], A. Santocchia[a,b], D. Spiga[a], T. Tedeschi[a,b]

INFN Sezione di Pisa[a], Università di Pisa[b], Scuola Normale Superiore di Pisa[c], Pisa, Italy; Università di Siena[d], Siena, Italy
P. Asenov[a,b], P. Azzurri[a], G. Bagliesi[a], R. Bhattacharya[a], L. Bianchini[a,b], T. Boccali[a], E. Bossini[a], D. Bruschini[a,c], R. Castaldi[a], M. A. Ciocci[a,b], M. Cipriani[a,b], V. D'Amante[a,d], R. Dell'Orso[a], S. Donato[a], A. Giassi[a], F. Ligabue[a,c], D. Matos Figueiredo[a], A. Messineo[a,b], M. Musich[a,b], F. Palla[a], A. Rizzi[a,b], G. Rolandi[a,c], S. Roy Chowdhury[a], T. Sarkar[a], A. Scribano[a], P. Spagnolo[a], R. Tenchini[a], G. Tonelli[a,b], N. Turini[a,d], A. Venturi[a], P. G. Verdini[a]

INFN Sezione di Roma[a], Sapienza Università di Roma[b], Rome, Italy
P. Barria[a], M. Campana[a,b], F. Cavallari[a], L. Cunqueiro Mendez[a,b], D. Del Re[a,b], E. Di Marco[a], M. Diemoz[a], F. Errico[a,b], E. Longo[a,b], P. Meridiani[a], J. Mijuskovic[a,b], G. Organtini[a,b], F. Pandolfi[a], R. Paramatti[a,b], C. Quaranta[a,b], S. Rahatlou[a,b], C. Rovelli[a], F. Santanastasio[a,b], L. Soffi[a]

INFN Sezione di Torino[a], Università di Torino[b], Turin, Italy; Università del Piemonte Orientale[c], Novara, Italy
N. Amapane[a,b], R. Arcidiacono[a,c], S. Argiro[a,b], M. Arneodo[a,c], N. Bartosik[a], R. Bellan[a,b], A. Bellora[a,b], C. Biino[a], C. Borca[a,b], N. Cartiglia[a], M. Costa[a,b], R. Covarelli[a,b], N. Demaria[a], L. Finco[a], M. Grippo[a,b], B. Kiani[a,b], F. Legger[a], F. Luongo[a,b], C. Mariotti[a], L. Markovic[a,b], S. Maselli[a], A. Mecca[a,b], E. Migliore[a,b], M. Monteno[a], R. Mulargia[a], M. M. Obertino[a,b], G. Ortona[a], L. Pacher[a,b], N. Pastrone[a], M. Pelliccioni[a], M. Ruspa[a,c], F. Siviero[a,b], V. Sola[a,b], A. Solano[a,b], A. Staiano[a], C. Tarricone[a,b], D. Trocino[a], G. Umoret[a,b], E. Vlasov[a,b]

INFN Sezione di Trieste[a], Università di Trieste[b], Trieste, Italy
S. Belforte[a], V. Candelise[a,b], M. Casarsa[a], F. Cossutti[a], K. De Leo[a,b], G. Della Ricca[a,b]

Kyungpook National University, Daegu, Korea
S. Dogra, J. Hong, C. Huh, B. Kim, D. H. Kim, J. Kim, H. Lee, S. W. Lee, C. S. Moon, Y. D. Oh, M. S. Ryu, S. Sekmen, Y. C. Yang

Department of Mathematics and Physics, GWNU, Gangneung, Korea
M. S. Kim

Institute for Universe and Elementary Particles, Chonnam National University, Kwangju, Korea
G. Bak, P. Gwak, H. Kim, D. H. Moon

Hanyang University, Seoul, Korea
E. Asilar, D. Kim, T. J. Kim, J. A. Merlin

Korea University, Seoul, Korea
S. Choi, S. Han, B. Hong, K. Lee, K. S. Lee, S. Lee, J. Park, S. K. Park, J. Yoo

Department of Physics, Kyung Hee University, Seoul, Korea
J. Goh, S. Yang

Sejong University, Seoul, Korea
H. S. Kim, Y. Kim, S. Lee

Seoul National University, Seoul, Korea
J. Almond, J. H. Bhyun, J. Choi, W. Jun, J. Kim, S. Ko, H. Kwon, H. Lee, J. Lee, J. Lee, B. H. Oh, S. B. Oh, H. Seo, U. K. Yang, I. Yoon

University of Seoul, Seoul, Korea
W. Jang, D. Y. Kang, Y. Kang, S. Kim, B. Ko, J. S. H. Lee, Y. Lee, I. C. Park, Y. Roh, I. J. Watson

Department of Physics, Yonsei University, Seoul, Korea
S. Ha, H. D. Yoo

Sungkyunkwan University, Suwon, Korea
M. Choi, M. R. Kim, H. Lee, Y. Lee, I. Yu

College of Engineering and Technology, American University of the Middle East (AUM), Dasman, Kuwait
T. Beyrouthy, Y. Maghrbi

Riga Technical University, Riga, Latvia
K. Dreimanis, A. Gaile, G. Pikurs, A. Potrebko, M. Seidel, V. Veckalns[55]

University of Latvia (LU), Riga, Latvia
N. R. Strautnieks

Vilnius University, Vilnius, Lithuania
M. Ambrozas, A. Juodagalvis, A. Rinkevicius, G. Tamulaitis

National Centre for Particle Physics, Universiti Malaya, Kuala Lumpur, Malaysia
N. Bin Norjoharuddeen, I. Yusuff[56], Z. Zolkapli

Universidad de Sonora (UNISON), Hermosillo, Mexico
J. F. Benitez, A. Castaneda Hernandez, H. A. Encinas Acosta, L. G. Gallegos Maríñez, M. León Coello, J. A. Murillo Quijada, A. Sehrawat, L. Valencia Palomo

Centro de Investigacion y de Estudios Avanzados del IPN, Mexico City, Mexico
G. Ayala, H. Castilla-Valdez, H. Crotte Ledesma, E. De La Cruz-Burelo, I. Heredia-De La Cruz[57], R. Lopez-Fernandez, C. A. Mondragon Herrera, A. Sánchez Hernández

Universidad Iberoamericana, Mexico City, Mexico
C. Oropeza Barrera, M. Ramírez García

Benemerita Universidad Autonoma de Puebla, Puebla, Mexico
I. Bautista, I. Pedraza, H. A. Salazar Ibarguen, C. Uribe Estrada

University of Montenegro, Podgorica, Montenegro
I. Bubanja, N. Raicevic

University of Canterbury, Christchurch, New Zealand
P. H. Butler

National Centre for Physics, Quaid-I-Azam University, Islamabad, Pakistan
A. Ahmad, M. I. Asghar, A. Awais, M. I. M. Awan, H. R. Hoorani, W. A. Khan

Faculty of Computer Science, Electronics and Telecommunications, AGH University of Krakow, Kraków, Poland
V. Avati, L. Grzanka, M. Malawski

National Centre for Nuclear Research, Swierk, Poland
H. Bialkowska, M. Bluj, B. Boimska, M. Górski, M. Kazana, M. Szleper, P. Zalewski

Institute of Experimental Physics, Faculty of Physics, University of Warsaw, Warsaw, Poland
K. Bunkowski, K. Doroba, A. Kalinowski, M. Konecki, J. Krolikowski, A. Muhammad

Warsaw University of Technology, Warsaw, Poland
K. Pozniak, W. Zabolotny

Laboratório de Instrumentação e Física Experimental de Partículas, Lisbon, Portugal
M. Araujo, D. Bastos, C. Beirão Da Cruz E Silva, A. Boletti, M. Bozzo, T. Camporesi, G. Da Molin, P. Faccioli, M. Gallinaro, J. Hollar, N. Leonardo, T. Niknejad, A. Petrilli, M. Pisano, J. Seixas, J. Varela, J. W. Wulff

Faculty of Physics, University of Belgrade, Belgrade, Serbia
P. Adzic, P. Milenovic

VINCA Institute of Nuclear Sciences, University of Belgrade, Belgrade, Serbia
M. Dordevic, J. Milosevic, V. Rekovic

Centro de Investigaciones Energéticas Medioambientales y Tecnológicas (CIEMAT), Madrid, Spain
M. Aguilar-Benitez, J. Alcaraz Maestre, Cristina F. Bedoya, M. Cepeda, M. Cerrada, N. Colino, B. De La Cruz, A. Delgado Peris, A. Escalante Del Valle, D. Fernández Del Val, J. P. Fernández Ramos, J. Flix, M. C. Fouz, O. Gonzalez Lopez, S. Goy Lopez, J. M. Hernandez, M. I. Josa, D. Moran, C. M. Morcillo Perez, Á. Navarro Tobar, C. Perez Dengra, A. Pérez-Calero Yzquierdo, J. Puerta Pelayo, I. Redondo, D. D. Redondo Ferrero, L. Romero, S. Sánchez Navas, L. Urda Gómez, J. Vazquez Escobar, C. Willmott

Universidad Autónoma de Madrid, Madrid, Spain
J. F. de Trocóniz

Instituto Universitario de Ciencias y Tecnologías Espaciales de Asturias (ICTEA), Universidad de Oviedo, Oviedo, Spain
B. Alvarez Gonzalez, J. Cuevas, J. Fernandez Menendez, S. Folgueras, I. Gonzalez Caballero, J. R. González Fernández, E. Palencia Cortezon, C. Ramón Álvarez, V. Rodríguez Bouza, A. Soto Rodríguez, A. Trapote, C. Vico Villalba, P. Vischia

Instituto de Física de Cantabria (IFCA), CSIC-Universidad de Cantabria, Santander, Spain
S. Bhowmik, S. Blanco Fernández, J. A. Brochero Cifuentes, I. J. Cabrillo, A. Calderon, J. Duarte Campderros, M. Fernandez, G. Gomez, C. Lasaosa García, C. Martinez Rivero, P. Martinez Ruiz del Arbol, F. Matorras, P. Matorras Cuevas, E. Navarrete Ramos, J. Piedra Gomez, L. Scodellaro, I. Vila, J. M. Vizan Garcia

University of Colombo, Colombo, Sri Lanka
M. K. Jayananda, B. Kailasapathy[58], D. U. J. Sonnadara, D. D. C. Wickramarathna

Department of Physics, University of Ruhuna, Matara, Sri Lanka
W. G. D. Dharmaratna[59], K. Liyanage, N. Perera, N. Wickramage

CERN, European Organization for Nuclear Research, Geneva, Switzerland
D. Abbaneo, C. Amendola, E. Auffray, G. Auzinger, J. Baechler, D. Barney, A. Bermúdez Martínez, M. Bianco, B. Bilin, A. A. Bin Anuar, A. Bocci, C. Botta, E. Brondolin, C. Caillol, G. Cerminara, N. Chernyavskaya, D. d'Enterria, A. Dabrowski, A. David, A. De Roeck, M. M. Defranchis, M. Deile, M. Dobson, L. Forthomme, G. Franzoni, W. Funk, S. Giani, D. Gigi, K. Gill, F. Glege, L. Gouskos, M. Haranko, J. Hegeman, B. Huber, V. Innocente, T. James, P. Janot, S. Laurila, P. Lecoq, E. Leutgeb, C. Lourenço, B. Maier, L. Malgeri, M. Mannelli, A. C. Marini, M. Matthewman, F. Meijers, S. Mersi, E. Meschi, V. Milosevic, F. Monti, F. Moortgat, M. Mulders, I. Neutelings, S. Orfanelli, F. Pantaleo, G. Petrucciani, A. Pfeiffer, M. Pierini, D. Piparo, H. Qu, D. Rabady, G. Reales Gutiérrez, M. Rovere, H. Sakulin, S. Scarfi, C. Schwick, M. Selvaggi, A. Sharma, K. Shchelina, P. Silva, P. Sphicas[60], A. G. Stahl Leiton, A. Steen, S. Summers, D. Treille, P. Tropea, A. Tsirou, D. Walter, J. Wanczyk[61], J. Wang, S. Wuchterl, P. Zehetner, P. Zejdl, W. D. Zeuner

Paul Scherrer Institut, Villigen, Switzerland
T. Bevilacqua[62], L. Caminada[62], A. Ebrahimi, W. Erdmann, R. Horisberger, Q. Ingram, H. C. Kaestli, D. Kotlinski, C. Lange, M. Missiroli[62], L. Noehte[62], T. Rohe

ETH Zurich-Institute for Particle Physics and Astrophysics (IPA), Zurich, Switzerland
T. K. Aarrestad, K. Androsov[61], M. Backhaus, A. Calandri, C. Cazzaniga, K. Datta, A. De Cosa, G. Dissertori, M. Dittmar, M. Donegà, F. Eble, M. Galli, K. Gedia, F. Glessgen, C. Grab, D. Hits, W. Lustermann, A.-M. Lyon, R. A. Manzoni, M. Marchegiani, L. Marchese, C. Martin Perez, A. Mascellani[61], F. Nessi-Tedaldi, F. Pauss, V. Perovic, S. Pigazzini, C. Reissel, T. Reitenspiess, B. Ristic, F. Riti, D. Ruini, R. Seidita, J. Steggemann[61], D. Valsecchi, R. Wallny, C. Amsler[63]

Universität Zürich, Zurich, Switzerland
P. Bärtschi, D. Brzhechko, M. F. Canelli, K. Cormier, J. K. Heikkilä, M. Huwiler, W. Jin, A. Jofrehei, B. Kilminster, S. Leontsinis, S. P. Liechti, A. Macchiolo, P. Meiring, U. Molinatti, A. Reimers, P. Robmann, S. Sanchez Cruz, M. Senger, Y. Takahashi, R. Tramontano

National Central University, Chung-Li, Taiwan
C. Adloff[64], D. Bhowmik, C. M. Kuo, W. Lin, P. K. Rout, P. C. Tiwari[38], S. S. Yu

National Taiwan University (NTU), Taipei, Taiwan
L. Ceard, Y. Chao, K. F. Chen, P. S. Chen, Z. G. Chen, A. De Iorio, W.-S. Hou, T. H. Hsu, Y. W. Kao, R. Khurana, G. Kole, Y. Y. Li, R.-S. Lu, E. Paganis, X. F. Su, J. Thomas-Wilsker, L. S. Tsai, H. Y. Wu, E. Yazgan

High Energy Physics Research Unit, Department of Physics, Faculty of Science, Chulalongkorn University, Bangkok, Thailand
C. Asawatangtrakuldee, N. Srimanobhas, V. Wachirapusitanand

Physics Department, Science and Art Faculty, Çukurova University, Adana, Turkey
D. Agyel, F. Boran, Z. S. Demiroglu, F. Dolek, I. Dumanoglu[65], E. Eskut, Y. Guler[66], E. Gurpinar Guler[66], C. Isik, O. Kara, A. Kayis Topaksu, U. Kiminsu, G. Onengut, K. Ozdemir[67], A. Polatoz, B. Tali[68], U. G. Tok, S. Turkcapar, E. Uslan, I. S. Zorbakir

Physics Department, Middle East Technical University, Ankara, Turkey
M. Yalvac[69]

Bogazici University, Istanbul, Turkey
B. Akgun, I. O. Atakisi, E. Gülmez, M. Kaya[70], O. Kaya[71], S. Tekten[72]

Istanbul Technical University, Istanbul, Turkey
A. Cakir, K. Cankocak[65,73], Y. Komurcu, S. Sen[74]

Istanbul University, Istanbul, Turkey
O. Aydilek, S. Cerci[68], V. Epshteyn, B. Hacisahinoglu, I. Hos[75], B. Kaynak, S. Ozkorucuklu, O. Potok, H. Sert, C. Simsek, C. Zorbilmez

Yildiz Technical University, Istanbul, Turkey
B. Isildak[76], D. Sunar Cerci[68]

Institute for Scintillation Materials of National Academy of Science of Ukraine, Kharkiv, Ukraine
A. Boyaryntsev, B. Grynyov

National Science Centre, Kharkiv Institute of Physics and Technology, Kharkiv, Ukraine
L. Levchuk

University of Bristol, Bristol, UK
D. Anthony, J. J. Brooke, A. Bundock, F. Bury, E. Clement, D. Cussans, H. Flacher, M. Glowacki, J. Goldstein, H. F. Heath, L. Kreczko, S. Paramesvaran, S. Seif El Nasr-Storey, V. J. Smith, N. Stylianou[77], K. Walkingshaw Pass, R. White

Rutherford Appleton Laboratory, Didcot, UK
A. H. Ball, K. W. Bell, A. Belyaev[78], C. Brew, R. M. Brown, D. J. A. Cockerill, C. Cooke, K. V. Ellis, K. Harder, S. Harper, M.-L. Holmberg[79], J. Linacre, K. Manolopoulos, D. M. Newbold, E. Olaiya, D. Petyt, T. Reis, G. Salvi, T. Schuh, C. H. Shepherd-Themistocleous, I. R. Tomalin, T. Williams

Imperial College, London, UK
R. Bainbridge, P. Bloch, C. E. Brown, O. Buchmuller, V. Cacchio, C. A. Carrillo Montoya, G. S. Chahal[80], D. Colling, J. S. Dancu, I. Das, P. Dauncey, G. Davies, J. Davies, M. Della Negra, S. Fayer, G. Fedi, G. Hall, M. H. Hassanshahi, A. Howard, G. Iles, M. Knight, J. Langford, J. León Holgado, L. Lyons, A.-M. Magnan, S. Malik, M. Mieskolainen, J. Nash[81], M. Pesaresi, B. C. Radburn-Smith, A. Richards, A. Rose, K. Savva, C. Seez, R. Shukla, A. Tapper, K. Uchida, G. P. Uttley, L. H. Vage, T. Virdee[30], M. Vojinovic, N. Wardle, D. Winterbottom

Brunel University, Uxbridge, UK
K. Coldham, J. E. Cole, A. Khan, P. Kyberd, I. D. Reid

Baylor University, Waco, TX, USA
S. Abdullin, A. Brinkerhoff, B. Caraway, J. Dittmann, K. Hatakeyama, J. Hiltbrand, B. McMaster, M. Saunders, S. Sawant, C. Sutantawibul, J. Wilson

Catholic University of America, Washington, DC, USA
R. Bartek, A. Dominguez, C. Huerta Escamilla, A. E. Simsek, R. Uniyal, A. M. Vargas Hernandez

The University of Alabama, Tuscaloosa, AL, USA
B. Bam, R. Chudasama, S. I. Cooper, S. V. Gleyzer, C. U. Perez, P. Rumerio[82], E. Usai, R. Yi

Boston University, Boston, MA, USA
A. Akpinar, D. Arcaro, C. Cosby, Z. Demiragli, C. Erice, C. Fangmeier, C. Fernandez Madrazo, E. Fontanesi, D. Gastler, F. Golf, S. Jeon, I. Reed, J. Rohlf, K. Salyer, D. Sperka, D. Spitzbart, I. Suarez, A. Tsatsos, S. Yuan, A. G. Zecchinelli

Brown University, Providence, RI, USA
G. Benelli, X. Coubez[25], D. Cutts, M. Hadley, U. Heintz, J. M. Hogan[83], T. Kwon, G. Landsberg, K. T. Lau, D. Li, J. Luo, S. Mondal, M. Narain†, N. Pervan, S. Sagir[84], F. Simpson, M. Stamenkovic, W. Y. Wong, X. Yan, W. Zhang

University of California, Davis, Davis, CA, USA
S. Abbott, J. Bonilla, C. Brainerd, R. Breedon, M. Calderon De La Barca Sanchez, M. Chertok, M. Citron, J. Conway, P. T. Cox, R. Erbacher, F. Jensen, O. Kukral, G. Mocellin, M. Mulhearn, D. Pellett, W. Wei, Y. Yao, F. Zhang

University of California, Los Angeles, CA, USA
M. Bachtis, R. Cousins, A. Datta, G. Flores Avila, J. Hauser, M. Ignatenko, M. A. Iqbal, T. Lam, E. Manca, A. Nunez Del Prado, D. Saltzberg, V. Valuev

University of California, Riverside, Riverside, CA, USA
R. Clare, J. W. Gary, M. Gordon, G. Hanson, W. Si, S. Wimpenny[†]

University of California, San Diego, La Jolla, CA, USA
J. G. Branson, S. Cittolin, S. Cooperstein, D. Diaz, J. Duarte, L. Giannini, J. Guiang, R. Kansal, V. Krutelyov, R. Lee, J. Letts, M. Masciovecchio, F. Mokhtar, S. Mukherjee, M. Pieri, M. Quinnan, B. V. Sathia Narayanan, V. Sharma, M. Tadel, E. Vourliotis, F. Würthwein, Y. Xiang, A. Yagil

Department of Physics, University of California, Santa Barbara, Santa Barbara, CA, USA
A. Barzdukas, L. Brennan, C. Campagnari, A. Dorsett, J. Incandela, J. Kim, A. J. Li, P. Masterson, H. Mei, J. Richman, U. Sarica, R. Schmitz, F. Setti, J. Sheplock, D. Stuart, T.Á. Vámi, S. Wang

California Institute of Technology, Pasadena, CA, USA
A. Bornheim, O. Cerri, A. Latorre, J. Mao, H. B. Newman, M. Spiropulu, J. R. Vlimant, C. Wang, S. Xie, R. Y. Zhu

Carnegie Mellon University, Pittsburgh, PA, USA
J. Alison, S. An, M. B. Andrews, P. Bryant, M. Cremonesi, V. Dutta, T. Ferguson, A. Harilal, C. Liu, T. Mudholkar, S. Murthy, P. Palit, M. Paulini, A. Roberts, A. Sanchez, W. Terrill

University of Colorado Boulder, Boulder, CO, USA
J. P. Cumalat, W. T. Ford, A. Hart, A. Hassani, G. Karathanasis, E. MacDonald, N. Manganelli, A. Perloff, C. Savard, N. Schonbeck, K. Stenson, K. A. Ulmer, S. R. Wagner, N. Zipper

Cornell University, Ithaca, NY, USA
J. Alexander, S. Bright-Thonney, X. Chen, D. J. Cranshaw, J. Fan, X. Fan, D. Gadkari, S. Hogan, P. Kotamnives, J. Monroy, M. Oshiro, J. R. Patterson, J. Reichert, M. Reid, A. Ryd, J. Thom, P. Wittich, R. Zou

Fermi National Accelerator Laboratory, Batavia, IL, USA
M. Albrow, M. Alyari, O. Amram, G. Apollinari, A. Apresyan, L. A. T. Bauerdick, D. Berry, J. Berryhill, P. C. Bhat, K. Burkett, J. N. Butler, A. Canepa, G. B. Cerati, H. W. K. Cheung, F. Chlebana, G. Cummings, J. Dickinson, I. Dutta, V. D. Elvira, Y. Feng, J. Freeman, A. Gandrakota, Z. Gecse, L. Gray, D. Green, A. Grummer, S. Grünendahl, D. Guerrero, O. Gutsche, R. M. Harris, R. Heller, T. C. Herwig, J. Hirschauer, L. Horyn, B. Jayatilaka, S. Jindariani, M. Johnson, U. Joshi, T. Klijnsma, B. Klima, K. H. M. Kwok, S. Lammel, D. Lincoln, R. Lipton, T. Liu, C. Madrid, K. Maeshima, C. Mantilla, D. Mason, P. McBride, P. Merkel, S. Mrenna, S. Nahn, J. Ngadiuba, D. Noonan, V. Papadimitriou, N. Pastika, K. Pedro, C. Pena[85], F. Ravera, A. Reinsvold Hall[86], L. Ristori, E. Sexton-Kennedy, N. Smith, A. Soha, L. Spiegel, S. Stoynev, J. Strait, L. Taylor, S. Tkaczyk, N. V. Tran, L. Uplegger, E. W. Vaandering, I. Zoi

University of Florida, Gainesville, FL, USA
C. Aruta, P. Avery, D. Bourilkov, L. Cadamuro, P. Chang, V. Cherepanov, R. D. Field, E. Koenig, M. Kolosova, J. Konigsberg, A. Korytov, K. H. Lo, K. Matchev, N. Menendez, G. Mitselmakher, K. Mohrman, A. Muthirakalayil Madhu, N. Rawal, D. Rosenzweig, S. Rosenzweig, K. Shi, J. Wang

Florida State University, Tallahassee, FL, USA
T. Adams, A. Al Kadhim, A. Askew, S. Bower, R. Habibullah, V. Hagopian, R. Hashmi, R. S. Kim, S. Kim, T. Kolberg, G. Martinez, H. Prosper, P. R. Prova, M. Wulansatiti, R. Yohay, J. Zhang

Florida Institute of Technology, Melbourne, FL, USA
B. Alsufyani, M. M. Baarmand, S. Butalla, T. Elkafrawy[53], M. Hohlmann, R. Kumar Verma, M. Rahmani, E. Yanes

University of Illinois Chicago, Chicago, USA
M. R. Adams, A. Baty, C. Bennett, R. Cavanaugh, R. Escobar Franco, O. Evdokimov, C. E. Gerber, D. J. Hofman, J. H. Lee, D. S. Lemos, A. H. Merrit, C. Mills, S. Nanda, G. Oh, B. Ozek, D. Pilipovic, R. Pradhan, T. Roy, S. Rudrabhatla, M. B. Tonjes, N. Varelas, Z. Ye, J. Yoo

The University of Iowa, Iowa City, IA, USA
M. Alhusseini, D. Blend, K. Dilsiz[87], L. Emediato, G. Karaman, O. K. Köseyan, J.-P. Merlo, A. Mestvirishvili[88], J. Nachtman, O. Neogi, H. Ogul[89], Y. Onel, A. Penzo, C. Snyder, E. Tiras[90]

Johns Hopkins University, Baltimore, MD, USA
B. Blumenfeld, L. Corcodilos, J. Davis, A. V. Gritsan, L. Kang, S. Kyriacou, P. Maksimovic, M. Roguljic, J. Roskes, S. Sekhar, M. Swartz

The University of Kansas, Lawrence, KS, USA
A. Abreu, L. F. Alcerro Alcerro, J. Anguiano, P. Baringer, A. Bean, Z. Flowers, D. Grove, J. King, G. Krintiras, M. Lazarovits, C. Le Mahieu, C. Lindsey, J. Marquez, N. Minafra, M. Murray, M. Nickel, M. Pitt, S. Popescu[91], C. Rogan, C. Royon, R. Salvatico, S. Sanders, C. Smith, Q. Wang, G. Wilson

Kansas State University, Manhattan, KS, USA
B. Allmond, A. Ivanov, K. Kaadze, A. Kalogeropoulos, D. Kim, Y. Maravin, K. Nam, J. Natoli, D. Roy, G. Sorrentino

Lawrence Livermore National Laboratory, Livermore, CA, USA
F. Rebassoo, D. Wright

University of Maryland, College Park, MD, USA
A. Baden, A. Belloni, Y. M. Chen, S. C. Eno, N. J. Hadley, S. Jabeen, R. G. Kellogg, T. Koeth, Y. Lai, S. Lascio, A. C. Mignerey, S. Nabili, C. Palmer, C. Papageorgakis, M. M. Paranjpe, L. Wang

Massachusetts Institute of Technology, Cambridge, MA, USA
J. Bendavid, I. A. Cali, M. D'Alfonso, J. Eysermans, C. Freer, G. Gomez-Ceballos, M. Goncharov, G. Grosso, P. Harris, D. Hoang, D. Kovalskyi, J. Krupa, L. Lavezzo, Y.-J. Lee, K. Long, C. Mironov, A. Novak, C. Paus, D. Rankin, C. Roland, G. Roland, S. Rothman, G. S. F. Stephans, Z. Wang, B. Wyslouch, T. J. Yang

University of Minnesota, Minneapolis, MN, USA
B. Crossman, B. M. Joshi, C. Kapsiak, M. Krohn, D. Mahon, J. Mans, B. Marzocchi, S. Pandey, M. Revering, R. Rusack, R. Saradhy, N. Schroeder, N. Strobbe, M. A. Wadud

University of Mississippi, Oxford, MS, USA
L. M. Cremaldi

University of Nebraska-Lincoln, Lincoln, NE, USA
K. Bloom, D. R. Claes, G. Haza, J. Hossain, C. Joo, I. Kravchenko, J. E. Siado, W. Tabb, A. Vagnerini, A. Wightman, F. Yan, D. Yu

State University of New York at Buffalo, Buffalo, NY, USA
H. Bandyopadhyay, L. Hay, I. Iashvili, A. Kharchilava, M. Morris, D. Nguyen, S. Rappoccio, H. Rejeb Sfar, A. Williams

Northeastern University, Boston, MA, USA
G. Alverson, E. Barberis, J. Dervan, Y. Haddad, Y. Han, A. Krishna, J. Li, M. Lu, G. Madigan, R. Mccarthy, D. M. Morse, V. Nguyen, T. Orimoto, A. Parker, L. Skinnari, A. Tishelman-Charny, B. Wang, D. Wood

Northwestern University, Evanston, IL, USA
S. Bhattacharya, J. Bueghly, Z. Chen, S. Dittmer, K. A. Hahn, Y. Liu, Y. Miao, D. G. Monk, M. H. Schmitt, A. Taliercio, M. Velasco

University of Notre Dame, Notre Dame, IN, USA
G. Agarwal, R. Band, R. Bucci, S. Castells, A. Das, R. Goldouzian, M. Hildreth, K. W. Ho, K. Hurtado Anampa, T. Ivanov, C. Jessop, K. Lannon, J. Lawrence, N. Loukas, L. Lutton, J. Mariano, N. Marinelli, I. Mcalister, T. McCauley, C. Mcgrady, C. Moore, Y. Musienko[16], H. Nelson, M. Osherson, A. Piccinelli, R. Ruchti, A. Townsend, Y. Wan, M. Wayne, H. Yockey, M. Zarucki, L. Zygala

The Ohio State University, Columbus, OH, USA
A. Basnet, B. Bylsma, M. Carrigan, L. S. Durkin, C. Hill, M. Joyce, M. Nunez Ornelas, K. Wei, B. L. Winer, B. R. Yates

Princeton University, Princeton, NJ, USA
F. M. Addesa, H. Bouchamaoui, P. Das, G. Dezoort, P. Elmer, A. Frankenthal, B. Greenberg, N. Haubrich, G. Kopp, S. Kwan, D. Lange, A. Loeliger, D. Marlow, I. Ojalvo, J. Olsen, A. Shevelev, D. Stickland, C. Tully

University of Puerto Rico, Mayagüez, PR, USA
S. Malik

Purdue University, West Lafayette, IN, USA
A. S. Bakshi, V. E. Barnes, S. Chandra, R. Chawla, S. Das, A. Gu, L. Gutay, M. Jones, A. W. Jung, D. Kondratyev, A. M. Koshy, M. Liu, G. Negro, N. Neumeister, G. Paspalaki, S. Piperov, V. Scheurer, J. F. Schulte, M. Stojanovic, J. Thieman, A. K. Virdi, F. Wang, W. Xie

Purdue University Northwest, Hammond, IN, USA
J. Dolen, N. Parashar, A. Pathak

Rice University, Houston, TX, USA
D. Acosta, T. Carnahan, K. M. Ecklund, P. J. Fernández Manteca, S. Freed, P. Gardner, F. J. M. Geurts, W. Li, O. Miguel Colin, B. P. Padley, R. Redjimi, J. Rotter, E. Yigitbasi, Y. Zhang

University of Rochester, Rochester, NY, USA
A. Bodek, P. de Barbaro, R. Demina, J. L. Dulemba, A. Garcia-Bellido, O. Hindrichs, A. Khukhunaishvili, N. Parmar, P. Parygin[92], E. Popova[92], R. Taus

The Rockefeller University, New York, NY, USA
K. Goulianos

Rutgers, The State University of New Jersey, Piscataway, NJ, USA
B. Chiarito, J. P. Chou, Y. Gershtein, E. Halkiadakis, M. Heindl, D. Jaroslawski, O. Karacheban[28], I. Laflotte, A. Lath, R. Montalvo, K. Nash, H. Routray, S. Salur, S. Schnetzer, S. Somalwar, R. Stone, S. A. Thayil, S. Thomas, J. Vora, H. Wang

University of Tennessee, Knoxville, TN, USA
H. Acharya, D. Ally, A. G. Delannoy, S. Fiorendi, S. Higginbotham, T. Holmes, A. R. Kanuganti, N. Karunarathna, L. Lee, E. Nibigira, S. Spanier

Texas A&M University, College Station, TX, USA
D. Aebi, M. Ahmad, O. Bouhali[93], R. Eusebi, J. Gilmore, T. Huang, T. Kamon[94], H. Kim, S. Luo, R. Mueller, D. Overton, D. Rathjens, A. Safonov

Texas Tech University, Lubbock, TX, USA
N. Akchurin, J. Damgov, V. Hegde, A. Hussain, Y. Kazhykarim, K. Lamichhane, S. W. Lee, A. Mankel, T. Peltola, I. Volobouev, A. Whitbeck

Vanderbilt University, Nashville, TN, USA
E. Appelt, Y. Chen, S. Greene, A. Gurrola, W. Johns, R. Kunnawalkam Elayavalli, A. Melo, F. Romeo, P. Sheldon, S. Tuo, J. Velkovska, J. Viinikainen

University of Virginia, Charlottesville, VA, USA
B. Cardwell, B. Cox, J. Hakala, R. Hirosky, A. Ledovskoy, C. Neu, C. E. Perez Lara

Wayne State University, Detroit, MI, USA
P. E. Karchin

University of Wisconsin-Madison, Madison, WI, USA
A. Aravind, S. Banerjee, K. Black, T. Bose, S. Dasu, I. De Bruyn, P. Everaerts, C. Galloni, H. He,

M. Herndon, A. Herve, C. K. Koraka, A. Lanaro, R. Loveless, J. Madhusudanan Sreekala, A. Mallampalli, A. Mohammadi, S. Mondal, G. Parida, D. Pinna, A. Savin, V. Shang, V. Sharma, W. H. Smith, D. Teague, H. F. Tsoi, W. Vetens, A. Warden

Authors Affiliated with an Institute or an International Laboratory Covered by a Cooperation Agreement with CERN, Geneva, Switzerland

S. Afanasiev, V. Andreev, Yu. Andreev, T. Aushev, M. Azarkin, A. Babaev, A. Belyaev, V. Blinov[95], E. Boos, V. Borshch, D. Budkouski, V. Chekhovsky, R. Chistov[95], M. Danilov[95], A. Dermenev, T. Dimova[95], D. Druzhkin[96], M. Dubinin[85], L. Dudko, A. Ershov, G. Gavrilov, V. Gavrilov, S. Gninenko, V. Golovtcov, N. Golubev, I. Golutvin, I. Gorbunov, A. Gribushin, Y. Ivanov, V. Kachanov, V. Karjavine, A. Karneyeu, V. Kim[95], M. Kirakosyan, D. Kirpichnikov, M. Kirsanov, V. Klyukhin, O. Kodolova[97], V. Korenkov, A. Kozyrev[95], N. Krasnikov, A. Lanev, P. Levchenko[98], N. Lychkovskaya, V. Makarenko, A. Malakhov, V. Matveev[95], V. Murzin, A. Nikitenko[97,99], S. Obraztsov, V. Oreshkin, V. Palichik, V. Perelygin, S. Petrushanko, S. Polikarpov[95], V. Popov, O. Radchenko[95], M. Savina, V. Savrin, V. Shalaev, S. Shmatov, S. Shulha, Y. Skovpen[95], S. Slabospitskii, V. Smirnov, A. Snigirev, D. Sosnov, V. Sulimov, E. Tcherniaev, A. Terkulov, O. Teryaev, I. Tlisova, A. Toropin, L. Uvarov, A. Uzunian, A. Vorobyev†, N. Voytishin, B. S. Yuldashev[100], A. Zarubin, I. Zhizhin, A. Zhokin

† **Deceased**

1: Also at Yerevan State University, Yerevan, Armenia
2: Also at TU Wien, Vienna, Austria
3: Also at Institute of Basic and Applied Sciences, Faculty of Engineering, Arab Academy for Science, Technology and Maritime Transport, Alexandria, Egypt
4: Also at Ghent University, Ghent, Belgium
5: Also at Universidade Estadual de Campinas, Campinas, Brazil
6: Also at Federal University of Rio Grande do Sul, Porto Alegre, Brazil
7: Also at UFMS, Nova Andradina, Brazil
8: Also at Nanjing Normal University, Nanjing, China
9: Now at The University of Iowa, Iowa City, IA, USA
10: Also at University of Chinese Academy of Sciences, Beijing, China
11: Also at China Center of Advanced Science and Technology, Beijing, China
12: Also at University of Chinese Academy of Sciences, Beijing, China
13: Also at China Spallation Neutron Source, Dongguan, Guangdong, China
14: Now at Henan Normal University, Xinxiang, China
15: Also at Université Libre de Bruxelles, Brussels, Belgium
16: Also at an Institute or an International Laboratory Covered by a Cooperation Agreement with CERN, Geneva, Switzerland
17: Now at British University in Egypt, Cairo, Egypt
18: Now at Cairo University, Cairo, Egypt
19: Also at Purdue University, West Lafayette, IN, USA
20: Also at Université de Haute Alsace, Mulhouse, France
21: Also at Department of Physics, Tsinghua University, Beijing, China
22: Also at The University of the State of Amazonas, Manaus, Brazil
23: Also at Erzincan Binali Yildirim University, Erzincan, Turkey
24: Also at University of Hamburg, Hamburg, Germany
25: Also at III. Physikalisches Institut A, RWTH Aachen University, Aachen, Germany
26: Also at Isfahan University of Technology, Isfahan, Iran
27: Also at Bergische University Wuppertal (BUW), Wuppertal, Germany
28: Also at Brandenburg University of Technology, Cottbus, Germany
29: Also at Forschungszentrum Jülich, Jülich, Germany
30: Also at CERN, European Organization for Nuclear Research, Geneva, Switzerland
31: Also at Institute of Physics, University of Debrecen, Debrecen, Hungary

32: Also at Institute of Nuclear Research ATOMKI, Debrecen, Hungary
33: Now at Universitatea Babes-Bolyai-Facultatea de Fizica, Cluj-Napoca, Romania
34: Also at Physics Department, Faculty of Science, Assiut University, Asyût, Egypt
35: Also at HUN-REN Wigner Research Centre for Physics, Budapest, Hungary
36: Also at Punjab Agricultural University, Ludhiana, India
37: Also at University of Visva-Bharati, Santiniketan, India
38: Also at Indian Institute of Science (IISc), Bangalore, India
39: Also at Birla Institute of Technology, Mesra, Mesra, India
40: Also at IIT Bhubaneswar, Bhubaneswar, India
41: Also at Institute of Physics, Bhubaneswar, India
42: Also at University of Hyderabad, Hyderabad, India
43: Also at Deutsches Elektronen-Synchrotron, Hamburg, Germany
44: Also at Department of Physics, Isfahan University of Technology, Isfahan, Iran
45: Also at Sharif University of Technology, Tehran, Iran
46: Also at Department of Physics, University of Science and Technology of Mazandaran, Behshahr, Iran
47: Also at Helwan University, Cairo, Egypt
48: Also at Italian National Agency for New Technologies, Energy and Sustainable Economic Development, Bologna, Italy
49: Also at Centro Siciliano di Fisica Nucleare e di Struttura Della Materia, Catania, Italy
50: Also at Università degli Studi Guglielmo Marconi, Rome, Italy
51: Also at Scuola Superiore Meridionale, Università di Napoli 'Federico II', Naples, Italy
52: Also at Fermi National Accelerator Laboratory, Batavia, IL, USA
53: Also at Ain Shams University, Cairo, Egypt
54: Also at Consiglio Nazionale delle Ricerche-Istituto Officina dei Materiali, Perugia, Italy
55: Also at Riga Technical University, Riga, Latvia
56: Also at Department of Applied Physics, Faculty of Science and Technology, Universiti Kebangsaan Malaysia, Bangi, Malaysia
57: Also at Consejo Nacional de Ciencia y Tecnología, Mexico City, Mexico
58: Also at Trincomalee Campus, Eastern University, Sri Lanka, Nilaveli, Sri Lanka
59: Also at Saegis Campus, Nugegoda, Sri Lanka
60: Also at National and Kapodistrian University of Athens, Athens, Greece
61: Also at Ecole Polytechnique Fédérale Lausanne, Lausanne, Switzerland
62: Also at Universität Zürich, Zurich, Switzerland
63: Also at Stefan Meyer Institute for Subatomic Physics, Vienna, Austria
64: Also at Laboratoire d'Annecy-le-Vieux de Physique des Particules, IN2P3-CNRS, Annecy-le-Vieux, France
65: Also at Near East University, Research Center of Experimental Health Science, Mersin, Turkey
66: Also at Konya Technical University, Konya, Turkey
67: Also at Izmir Bakircay University, Izmir, Turkey
68: Also at Adiyaman University, Adiyaman, Turkey
69: Also at Bozok Universitetesi Rektörlügü, Yozgat, Turkey
70: Also at Marmara University, Istanbul, Turkey
71: Also at Milli Savunma University, Istanbul, Turkey
72: Also at Kafkas University, Kars, Turkey
73: Now at Istanbul Okan University, Istanbul, Turkey
74: Also at Hacettepe University, Ankara, Turkey
75: Also at Faculty of Engineering, Istanbul University-Cerrahpasa, Istanbul, Turkey
76: Also at Yildiz Technical University, Istanbul, Turkey
77: Also at Vrije Universiteit Brussel, Brussels, Belgium
78: Also at School of Physics and Astronomy, University of Southampton, Southampton, UK
79: Also at University of Bristol, Bristol, UK
80: Also at IPPP Durham University, Durham, UK
81: Also at Faculty of Science, Monash University, Clayton, Australia
82: Also at Università di Torino, Turin, Italy
83: Also at Bethel University, St. Paul, MN, USA

84: Also at Karamanoğlu Mehmetbey University, Karaman, Turkey
85: Also at California Institute of Technology, Pasadena, CA, USA
86: Also at United States Naval Academy, Annapolis, MD, USA
87: Also at Bingol University, Bingol, Turkey
88: Also at Georgian Technical University, Tbilisi, Georgia
89: Also at Sinop University, Sinop, Turkey
90: Also at Erciyes University, Kayseri, Turkey
91: Also at Horia Hulubei National Institute of Physics and Nuclear Engineering (IFIN-HH), Bucharest, Romania
92: Now at an Institute or an International Laboratory Covered by a Cooperation Agreement with CERN, Geneva, Switzerland
93: Also at Texas A&M University at Qatar, Doha, Qatar
94: Also at Kyungpook National University, Daegu, Korea
95: Also at Another Institute or International Laboratory Covered by a Cooperation Agreement with CERN, Geneva, Switzerland
96: Also at Universiteit Antwerpen, Antwerp, Belgium
97: Also at Yerevan Physics Institute, Yerevan, Armenia
98: Also at Northeastern University, Boston, MA, USA
99: Also at Imperial College, London, UK
100: Also at Institute of Nuclear Physics of the Uzbekistan Academy of Sciences, Tashkent, Uzbekistan